University of Alberta

Investigation of the role of PITX2 in ocular expression pathways and human disease

by

Marcela Hermina Strungaru

A thesis submitted to the Faculty of Graduate Studies and Research
in partial fulfillment of the requirements for the degree of

Doctor in Philosophy

Medical Sciences-Medical Genetics

Fall 2010

Edmonton, Alberta

Examining Committee

Michael A Walter, Medical Genetics

Ordan Lehmann, Medical Genetics

Andrew J. Waskiewicz, Biological Sciences

Sarah Hughes**,** Medical Genetics

William K. Stell, Cell Biology and Anatomy, University of Calgary

Dedication

I dedicate this thesis to my son, Daniel Adrian Strungaru, my husband, Nicolae Strungaru, and my grandparents, Elena and Eugeniu Tindeche.

Abstract

The overall goal of my work has been to gain a better understanding of Axenfeld-Rieger Syndrome (ARS), a human autosomal dominantly inherited mal-development of the anterior segment of the eye that is associated with glaucoma. By studying rare genetic causes of this complex disease we are gaining insight into the initial steps that ultimately lead to blindness. To achieve the goal of better understanding ARS, my research project had two parts.

In the first part, I performed a retrospective clinical study in which I analyzed the glaucoma-related clinical presentation of ARS patients with *FOXC1* and *PITX2* defects. This study showed a good genotype-phenotype correlation which may be important for the physician in dealing with ARS patients. Patients with *FOXC1* mutations had the mildest prognosis in glaucoma development, while patients with *PITX2* defects and patients with *FOXC1* duplication had a more severe prognosis in glaucoma development than patients with *FOXC1* mutations. I tried to determine the best treatment for glaucoma in these patients. Unfortunately, in this study, current medical therapies did not successfully lower intraocular pressure or prevent progression of glaucoma in ARS patients with *FOXC1* or *PITX2* alterations. This clinical study also provided useful diagnostic criteria to identify the gene responsible for ARS.

The second part of the project was to study the gene regulatory pathways of the PITX2 gene, mutations of which cause ARS. PITX2 is a transcription factor that regulates the expression of genes in the eye. The discovery of direct downstream targets of PITX2 is necessary for understanding the genetic

mechanisms underlying complex, highly regulated processes such as development and underlying heritable human disorders. To find direct target genes of PITX2, I have used a recently developed method: the hormone receptor (HR)-inducible expression system for transcription factors coupled microarray analysis. The results obtained using this method have involved PITX2 in control of cellular stress. Recent investigations have suggested significant roles for cellular stress in glaucoma pathology. Understanding the control of these key aspects of cell function will have profound implications for understanding and treating the glaucoma that is the most clinically serious consequence of mutations of PITX2.

Acknowledgements

I would like to express my gratitude to the entire laboratory of Dr. Michael Walter for their support and assistance during my graduate years. In particular, I would like to thank Dr. Michael Walter. I could not have imagined having a better supervisor and mentor for my PhD. My interest in Medical Genetics, Ocular Genetics and research in general strongly developed during my PhD years thanks to Dr. Michael Walter. I would also like to thank Tim Footz for providing assistance with all types of technical problems - at all times. Special thanks to Farideh Mirzayans and Sofia Lungin for their kind help, guidance, support and encouragement throughout my study. Thanks to Dr. Ian MacDonald, Dr. Ordan Lehmann and Dr. Yves Sauvé for their advice, help and critical comments.

I must mention my wonderful little angel, Daniel Strungaru, who was born during my graduate studies. His smile always helped me to go through any difficulty and he brought me a lot of joy for the last two years. I am forever grateful to my husband for his understanding, endless patience and encouragement when it was most required. He has always supported my dreams and aspiration. I would also like to thank my parents, grandparents and my sister for their support and understanding through my entire life.

Table of Contents

List of tables

Table **Page**

Chapter 4

Chapter 5

Chapter 6

List of figures

Figures **Page**

Chapter 1

Chapter 2

Chapter 3

Chapter 4

Chapter 5

Chapter 6

Abbreviations

AA- Axenfeld anomaly

ACG-Angle-closure glaucoma

ALX4- Aristaless-like 4

ANF/NPPA-Atrial natriuretic factor

ARM-Axenfeld- Rieger Malformation

AS-Axenfeld Syndrome

β-Beta

BLAST-Basic Local Alignment Search Tool

BMP-Bone morphogenic protein

BMP2K- Bone morphogenic protein 2- inducible kinase

Bp-Base pairs of DNA

BS-Binding Sites

BSA-Bovine Serum Albumin

cDNA-Complementary DNA

CDR-Cup/Disc ratio

ChIP-Chromatin-immunoprecipitation

CHX- cyclohexamide

CMV-Cytomegalovirus

CYP1B1-cytochrome P4501B1

Da-Dalton

DACH- Dachshund homolog

D-CHIP-DNA-Chip Analyzer

DLL4-Delta-like protein 4 Precursor (Drosophila Delta homolog 4)

DLX2-Distal-less homeobox 2

DMEM-Dulbecco's modified Eagle's medium

DNA- Deoxyribonucleic acid

dNTP-Deoxynucleotide triphosphate nucleotides

DPP-Decapentaplegic

DTT-Dithiothreitol

DVL-Dishevelled

EDTA-Ethylenediaminetetraacetic acid

EGTA-Ethylene glycol tetraacetic acid

ERK- Extracellular signal-regulated kinases

ETC- Electron Transport Chain

FAD, FADH2- Flavin Adenine Dinucleotide and its reduced form

FGF19-Fibroblast growth factor 19

FGFR4- Fibroblast growth factor receptor 4

FHD-Forkhead domain

FISH-Fluorescence in situ hybridization

FMN, FMNH2- Flavin Mononucleotide and its reduced form

FOX-Forkhead

FOXC1- Forkhead box C1 gene (formally called FKHL7)

FOXO1A

FVT-1- Follicular variant translocation protein 1

GI-Gastrointestinal

GR- growth retardation

GSH-Reduced glutathione

GSSH-Oxidized glutathione

HCEC-Human Corneal Endothelium Cells

HD-Homeodomain

HDLB-High Density Lipoprotein Binding Protein/ vigilin

HEPES-4-(2-hydroxyethyl)-1-piperazineethanesulfonic acid

hPR-LBD-Human progesterone hormone receptor

HR-Hormone

HRP-Horseradish peroxidase

HSP90-Heat Sock Protein 90

HT-Hypertelorism

HTM-Human trabecular meshwork

H_2O_2-Hydrogen peroxide

IGD-Iridogoniodysgenesis

IH-Iris hypoplasia

IOP-Intraocular pressure

IP-Immunoprecipitation

JOAG-Juvenile-onset POAG

Kb-Kilobase

KCl-Potassium chloride

KDa-Kilodalton

LTBP2- Latent-transforming growth factor beta-binding protein 2 Precursor

MAD-Mothers against Decapentaplegic

MAP-Mitogen-potein

MAPK-Mitogen-activated protein kinase

MSX2- Muscle segment homeobox gene 2

MYOC-Myocilin

NaCl-Sodium chloride

NaDC3-Sodium/dicarboxylate cotransporter

NAD^+-Nicotinamide Adenine Dinucleotide

NADH-The reduced form of NAD^+

NADPH-Phosphate form of NADH

NCBI-National Center for Biotechnology Information

NEB-New England Biolabs

NPCE-Non-Pigmented Ciliary Epithelial

NTG-Normal tension glaucoma

OAG-Open-angle glaucoma

OAR-Orthopedia, Aristaless, and Rax

OD-Right eye

OH·-Hydroxyl radical

oligo d(T)-Oligomeric deoxyribonucleotide

OPTN-Optineurin

OS-Left eye

O^-_2·-Superoxide anion

PARP2-Poly (ADP-ribose) polymerase family, member 2

PAS-Peripheral anterior synechiae

PAX6-Paired box protein Pax-6

PBS-Phosphate buffered saline

PCR-Polymerase chain reaction

PDC-Pyruvate dehydrogenase complex

PDK-Pyruvate dehydrogenase kinase

PDP-Pyruvate dehydrogenase phosphatase

PE-Posterior embryotoxon

PGE2-Prostaglandin E2

PIP-Percent identity plotPITX2-Pituitary homeobox 2 gene

PLOD2-Pro-collagen lysyl hydroxylase

PMSF-Phenylmethanesulfonylfluoride

POAG-Primary open angle glaucoma

PRG-Progesterone binding domain

RA-Rieger anomaly

RGCs-Retinal ganglion cells

RNA-Ribonucleic acid

ROS-Reactive oxygen species

RS-Rieger Syndrome

RT-PCR-Reverse transcriptase polymerase chain reaction

SDS-Sodium Dodecyl Sulfate

SDS-PAGE-Sodium dodecyl sulfate polyacrylamide gel electrophoresis

SSC-Sodium Chloride, sodium citrate

siRNA-Small interfering RNA

SLC13A3-Solute carrier family 13 (sodium-dependent dicarboxylate transporter) member 3

SIX-1-Sine oculis homeobox (Drosophila) homolog 1

STI1-Stress-induced-phosphoprotein 1

TBX1-T-box transcription factor

TCA-Tricarboxylic Acid Cycle

TGF-β-transforming growth factor β

TIGR-Trabecular meshwork inducible glucocorticoid response

TK-Thymidine kinase

TM-Trabecular meshwork

VA-Visual acuity

VEGF-Vascular endothelial growth factor

UV-Ultraviolet

WDR36-WD repeat domain 36

WNT-Wingless

WT-Wild type

Chapter one: Introduction

This chapter contains some arguments presented in:

Strungaru MH, Dinu I, Walter MA. Genotype-Phenotype correlations in Axenfeld-Rieger MalformationAxenfeld-Rieger and glaucoma patients with FOXC1 and PITX2 mutations. *Investigative Ophthalmology & Visual Science*. 2007 [1]

Glaucoma

Epidemiology

The modern concept of glaucoma dates back to the mid-19th century when glaucoma was recognized as a distinct group of ocular disorders. However, glaucoma has been documented since the times of Hippocrates (460-377 BC), Celsus (1st century AD), and Galen (130-201 AD) [2, 3]. In Hippocrates's writing, it appears as "glaucosis", but this term was applied to a larger group of blinding conditions. The association between the elevated intraocular pressure and glaucoma is found in 10th century Arabian writings [2].

Glaucoma is the second leading cause of blindness throughout the world, after cataract and it is followed by age-related macular degeneration. In 2004, the World Health Organization reported that 37 million people worldwide were blind in 2002, from which 82% of people were 50 years or older. Glaucoma accounts for 12.3% of global blindness (behind cataracts at 47.8% of global blindness) [2, 4, 5]. There are several reasons why glaucoma is now the second leading cause of blindness. One important reason is the population growing older. It was reported that the world population aged 50 and older has increased by 30% since 1990 [5]. Another reason is the decreasing rate of trachoma. In 1995, trachoma was documented the second leading cause of blindness worthwide, before glaucoma. In 2002, trachoma has decreased significantly as a cause of blindness, and is now in seventh position (trachoma accounts for 3.6% of global blindness) due to the Global Elimination of Trachoma Project and a better access to health care and information.

Glaucoma is defined by the American Optometric Association (AOA) as "a group of ocular diseases with various causes that ultimately is associated with a progressive optic neuropathy leading to vision function loss" [4]. Glaucomatous optic neuropathy is associated with a progressive loss of the visual fields, which can lead to total, irreversible blindness if the condition is not diagnosed and treated properly.

Overview of Aqueous Humor

The diagnosis and the management of glaucoma deal primarily with the consequences of elevated intraocular pressure [2, 4]. Therefore, it is important to be familiar with the physiological factors that control intraocular pressure (IOP) and the dynamics of aqueous humor. In simple terms, IOP is a function of the rate at which aqueous humor is produced in the eye (inflow) and the rate at which it leaves the eye (outflow). When inflow is the same as outflow, a steady-state exists and the pressure remains constant. When there is an imbalance, the result is either hypotony or more often glaucoma. The two main structures important to aqueous humor dynamics are the ciliary body, the site of aqueous humor production, and the limbal region, which includes the trabecular meshwork, the principal site of aqueous humor outflow [2, 4] (Figure 1). Aqueous humor appears to be formed from plasma within the capillary network of the ciliary processes. The various constituents of aqueous humor traverse the three tissue layers of the ciliary processes (the capillary wall, stroma and epithelia) to reach the posterior chamber by a combination of three mechanisms: ultrafiltration, secretion and diffusion [2,

4]. Ultrafiltration is the passive movement of substances regulated by the osmotic and hydrostatic pressure gradients, while diffusion is the passive movement of substances regulated by the concentration gradient; both mechanisms contribute to a very small portion of the aqueous humor formation. The active secretion of ions by the nonpigmented layer of ciliary epithelium accounts for 80% to 90% of the total aqueous humor formation [2, 4]. Sodium transport appears to be the principal mechanism for water movement. In this way, aqueous humor enters the posterior chamber, between the iris and lens, flows through the pupil into the anterior chamber angle and leaves the eye via structures in the anterior chamber angle, primarily through the trabecular meshwork and Schlemm's canal [6, 7]. Aqueous humor passes from Schlemm's canal into the blood system in the episcleral veins (Figure 1-1).

Risk factors

The characteristic optic neuropathy which is the common denominator of the glaucoma group of disorders derives from various risk factors including increased intraocular pressure (IOP). Although elevated IOP is clearly the most frequent causative risk factor for the atrophy of the optic nerve, it is not the only factor. Other risk factors which contribute to glaucoma development are age, race, family history, corneal thickness, refractive error (such as myopic eye), previous ocular trauma, topical steroid use on eyes and systemic diseases such as hypertension and ischemic heart disease [4, 8, 9].

Figure 1-1. Normal aqueous humor outflow and iridocorneal angle structure

(A) Most aqueous humor flow is through the trabecular meshwork *(large arrow)* and a small fraction is through uveoscleral routes *(small arrow)*. Each pathway is drained by the eye's venous circulation. Taken from [10].

(B) Histological sections of the peripheral part of the anterior chamber taken from: http://education.vetmed.vt.edu/curriculum/vm8054/EYE/AQUEOUS.HTM.

(C) A three-dimensional representation of the trabecular meshwork taken from: http://education.vetmed.vt.edu/curriculum/vm8054/EYE/AQUEOUS.HTM.

A

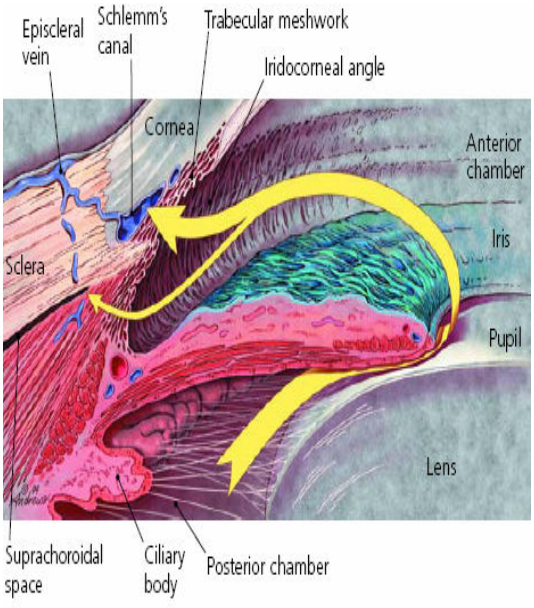
Episcleral vein
Schlemm's canal
Trabecular meshwork
Iridocorneal angle
Cornea
Anterior chamber
Iris
Sclera
Pupil
Lens
Suprachoroidal space
Ciliary body
Posterior chamber

B

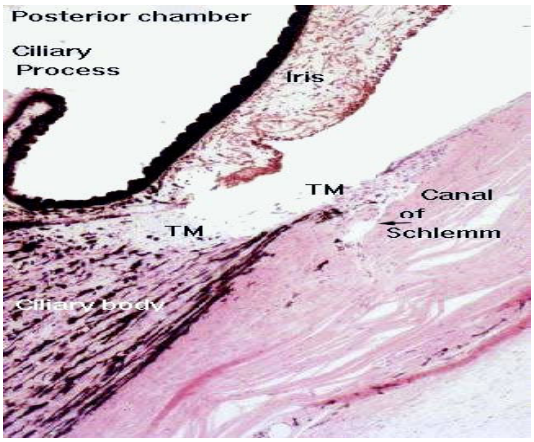
Posterior chamber
Ciliary Process
Iris
TM
Canal of Schlemm
TM
Ciliary body

C

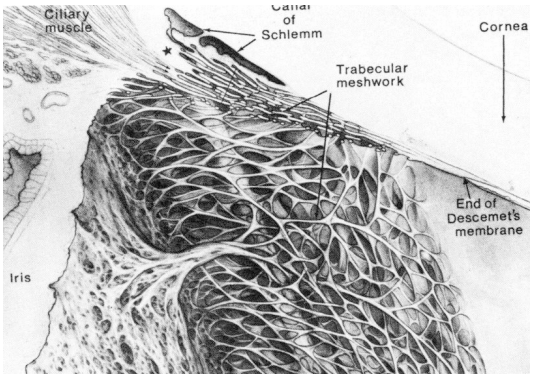
Ciliary muscle
Canal of Schlemm
Cornea
Trabecular meshwork
End of Descemet's membrane
Iris

Classification and Genetics

There are several systems by which glaucoma may be classified. The most common are based on *etiology*, that is, the underlying disorder that leads to an alteration in aqueous humor dynamics, and *mechanism*, that is, the alteration of the anterior chamber angle which leads to an elevated IOP. Based on the *etiology*, the glaucomas have been classified into the *primary* and *secondary* glaucomas. The primary glaucomas are typically bilateral and probably have a genetic basis. In contrast, the secondary glaucomas have predisposing ocular or systemic events, may be unilateral or bilateral, and some may have a genetic basis, whereas others are acquired. However, this classification is becoming increasingly inadequate, as modern knowledge of the mechanism underlying the pathophysiology of the glaucomas is expanding. Based on the *mechanism*, the glaucomas can be divided into three groups: open-angle glaucoma, angle-closure glaucoma and congenital glaucoma. Open-angle glaucoma (OAG) and angle-closure glaucoma (ACG) are defined based on the angular width of the anterior chamber as assessed with goniolens, narrowing of the angle resulting in ACG. Currently, the classification of glaucoma is based on the way patients present to the physicians, or phenotypes. However, now that a number of genes have been identified, the hope of being able to reclassify these disorders based on genetic causes, or genotypes is being realized. The field of genetics is becoming more important in understanding molecular mechanisms and pathways. Since 1842 when a heritable form of primary open angle glaucoma (POAG) was described for the first time (Benedict) [11], a number of genetic loci have been reported and a smaller number of genes

have been identified. Glaucoma may be inherited as an autosomal-dominant, autosomal-recessive or as a complex multifactorial trait. Genetic loci associated with different forms of glaucoma have different chromosomal locations as shown in Table 1-1. These loci have been group into three categories: GLC1, GLC2 and GLC3, which correspond to primary open angle glaucoma (POAG), primary closed angle glaucoma (PCAG) and congenital glaucoma, respectively. For each locus identified, it is given an alphabetical letter after the GLC prefix.

Primary open angle glaucoma (POAG)

POAG occurs most frequently, accounting for more than 50% of all forms of the disease and affecting approximately 2% of the world's population over 40 years old. POAG does not usually have a typical mendelian inheritance. POAG is a complex disorder resulting from the interactions of multiple genetic factors with the environment. According to age of onset, POAG is divided into juvenile-onset POAG (JOAG) and adult-onset POAG. POAG is genetically heterogeneous, which links to at least 20 genetic loci [12-23] (Table 1-1). There are currently 11 chromosomal loci assigned with GLC nomenclature (*GLC1A* to *GLC1K)*, from which only 3 of them (*GLC1A*, *GLC1J* and *GLC1K*) contribute to JOAG, while the others contribute to adult-onset POAG [12, 13]. Three loci, discussed below, have been characterized so far: *GLC1A* (*myocilin*, *MYOC*) [14], *GLC1E* (*optineurin*, *OPTN*) [15] and *GLC1G* (*WD repeat domain 36*, *WDR36*) [16].

GLC1A (myocilin, MYOC)

The first gene identified in 1997 for open-angle glaucoma was the myocilin gene (*MYOC*) or formally called *trabecular meshwork inducible glucocorticoid response (TIGR)* [17] localized on chromosome 1q24. It is expressed in the trabecular meshwork (TM), the ciliary body and the retina; however it is also expressed in many extraocular tissues, suggesting that it may not have an eye-specific function [18, 19]. Approximately 3-5% of patients with adult-onset POAG and 20% with early-onset POAG have defects in *MYOC* gene [20, 21]. *MYOC* mutations in European and American populations have a prevalence of approximately 4% in adult onset POAG and over 10% in JOAG [21, 22], whereas the prevalence of *MYOC* mutations is 1.1%–1.8% in Chinese POAG patients [23]. To date more than 70 disease-associated mutations in MYOC have been identified [19, 24], with the Gln368STOP being the most common known glaucoma causing mutation worldwide [21]. Other common *MYOC* mutations are Thr377Met [21] and Pro370Leu, the last one causing severe juvenile-onset POAG [25]. Some mutations are more common in early-onset POAG, while others are associated with adult-onset disease. It has been suggested that glaucoma is more severe in patients with mutations in both *MYOC* and *CYP1B1* genes [26]. Most of *MYOC* mutations are found in the third exon of the gene which encodes the olfactomedin domain, this domain participating in extracellular processes [21]. The role of the normal protein in the outflow pathway is not well known. The normal protein is detected in extracellular matrix being secreted from the cell; however it seems that myocilin is not needed for the normal aqueous humor outflow [27-30].

Mutant myocilin appears to be misfolded and aggregated into the cell, suggesting that disease-causing mutants may be toxic to the trabecular meshwork cells or may prevent the secretion of other proteins that are important for the normal function of the outflow pathway [30].

GLC1E (*optineurin*, *OPTN*)

The second POAG gene identified was the *optineurin* (*OPTN*), "optic neuropathy-inducing" gene at the GLC1E locus [31], located on the short ARS of chromosome 10. *OPTN* may have important roles in exocytosis, Golgi ribbon formation and tumor necrosis factor-α (TNF-α) apoptotic pathways [32, 33]. It is believed that optineurin protects the optic nerve against apoptosis mediated through TNF-α and mutation of this protein decreases the threshold for retinal ganglion cells apoptosis in patients with glaucoma. Mutations in *OPTN* were originally reported to account for approximately 16.7% of familial POAG from normal tension glaucoma (NTG), and 12% of sporadic patients with POAG [31]. However, two studies in Caucasians [34, 35] and one study in Japanese [36] reported no *OPTN* causative mutations in POAG patients. The most common *OPTN* disease-causing variant is Glu50Lys [31]; individuals with this mutation develop aggressive NTG with a lower age of onset.

Table 1-1. Reported genetic loci for Glaucoma

Locus name	Chromosomal location	Gene identified	Condition	Inheritance Pattern	References
GLC1A	1q21–q31	*MYOC*	Early and adult-onset POAG	Early-onset; AD Adult-onset; complex	[12]
GLC1B	2cen–q13	-	Adult-onset POAG	AD	[37]
GLC1C	3q21–q24	-	Adult-onset POAG	AD	[38]
GLC1D	8q23	-	Adult-onset POAG	AD	[39]
GLC1E	10p15–p14	*OPTN*	Adult-onset POAG; low-tension glaucoma	AD	[40]
GLC1F	7q35–q36	-	Adult-onset POAG	AD	[41]
GLC1G	5q22.1	*WDR36*	Adult-onset POAG	AD, complex	[16]
GLC1H	2p16.3–p15	-			
GLC1I	15q11–q13	-	Adult-onset POAG	Complex	[42]
GLC1J	9q22	-	Early-onset POAG	AD	[13]
GLC1K	20p12	-	Early-onset POAG	AD	[13]
GLC3A	2p21	*CYP1B1*	Congenital glaucoma	AR	[43]
GLC3B	1p36	-	Congenital glaucoma	AR	[44]
GLC3C	14q24.2-q24.3	*LTBP2*	Congenital glaucoma	AR	[45, 46]
Pending	14q11	-	Adult-onset POAG	Complex	[47]
-	4q25	*PITX2*	Axenfeld-Rieger Syndrome	AD	[48]
-	6p25	*FOXC1*	Axenfeld-Rieger Syndrome	AD	[49]
-	13q14	-	Axenfeld-Rieger Syndrome	AD	[50]
-	16q24	-	Axenfeld-Rieger Syndrome	AD	[51]
	7q35-q36	*GPDS1*	Pigment dispersion syndrome	AD	
	11p13	*PAX6*	Aniridia	AD	
	9q34	*LMX1B*	Glaucoma associated with nail-patella syndrome	AD	
	11p	*NNO1*	Nanophthalmos	AD	
	11q12	*VMD2*	Nanophthalmos	AD	
	11q23	MFRP	Nanophthalmos	AR	

AD- Autosomal Dominant

AR- Autosomal Recessive

GLC1G (*WD repeat domain 36*, *WDR36*)

The most recently identified gene for POAG is WDR36, mapping to the 5q22 locus [16]. The prevalence of *WDR36* variations was found between 1.6% and 17% of patients with POAG [16, 52]. However, the involvement of *WDR36* as a causative gene in glaucoma is disputed, since some studies of families with POAG mapped to the same region on chromosome 5, but have failed to identify genetic variants in WDR36 [53-55]. *WDR36* is a gene with 23 exons, which encodes a 951 amino acid protein, and is expressed in lens, iris, sclera, ciliary muscles, ciliary body, trabecular meshwork, retina and optic nerve. *WDR36* is involved in ribosomal RNA and interacts with p53 stress response pathway [56]. A recent work in yeast showed that the human- derived sequence variants in *UTP21*, the yeast homologue of *WDR36*, presented an affected phenotype only in the presence of stress-inducible *STI1* (Stress-inducible protein 1) mutated background [57]. The authors of this paper suggested that variations in *WDR36* predispose to glaucoma; patients with *WDR36* variations develop glaucoma only in certain genetic context such as mutations of *STI1* or due to *WDR36*-environment interactions [57].

Primary closed angle glaucoma (POAG)

Primary closed angle glaucoma is much less common than POAG and no genetic component has been discovered yet.

Primary congenital glaucoma (PCG)

Numerous developmental disorders associated with anomalies of the anterior chamber angle can lead to elevated IOP. The initial event is in most cases a genetic defect, although some may be acquired from an intrauterine insult. PCG is the most severe form of glaucoma, the age of onset being before the age of three. The anatomical defect is in trabecular meshwork, trabeculodysgenesis, and causes increased IOP, corneal edema, photophobia, excessive tearing, and enlargement of the cornea and opacity of the cornea. Three loci have been mapped for primary congenital glaucoma (PCG): GLC3A, GLC3B and GLC3C (Table 1-1).

GLC3A (*cytochrome P4501B1*, *CYP1B1*)

CYP1B1 is believed to play a role in the secretion of aqueous humor and in the development and regulation of outflow facility of the trabecular meshwork [58]. Mutations in this gene increased IOP by interference with normal function of the trabecular meshwork. Mutations in *CYP1B1* were found in 48% of French PCG patients [59] but only 20% of Japanese patients [60]. The Human Gene Mutation reported more than 100 mutations in *CYP1B1.*

GLC3C (*latent transforming growth factor beta binding protein 2, LTBP2*)

The gene associated with GLC3C, *LTBP2,* has been recently identified [45, 46]. The latent TGF-beta binding protein 2 encoded by *LTBP2* is localized to the extracellular matrix proteins at the ciliary process [45]. LTBP2 contains multiple epidermal growth factor (EGF)-like domains and transforming growth factor beta

binding domains. The amino terminal of LTBP2 binds fibulin 5, while the carboxyl terminal of LTBP2 binds fibrillin 1. Mutations in fibrillin 1 causes Marfan syndrome characterized by skeletal, cardiovascular and ocular defects (ectopic lenses and glaucoma) [61]. The function of LTBP2 is not known, however it is believed that mutations in this gene affect the elasticity of the ciliary body and trabecular meshwork resulting in increased resistance of aqueous fluid outflow causing glaucoma.

Secondary glaucoma and *LOXL1 (lysyl oxidase like 1)*

Most of secondary glaucomas are diagnosed when a potential etiology such as ocular disease, orbital disease or corticosteroid usage could be identified. One of the most common causes of secondary glaucoma is exfoliation syndrome. The name of exfoliation syndrome comes from the abnormal accumulation of exfoliative material in the anterior segment of the eye. The deposits of exfoliative material can cause obstruction of aqueous flow and damage to the trabecular meshwork leading to glaucoma. The prognosis of glaucoma caused by exfoliation syndrome is worse than that of POAG due to higher IOP and greater resistance to medical and surgical treatment. Worldwide, exfoliation syndrome accounts for 10-20% of glaucoma [62], being common in individuals over 60 years of age. A recent genome wide study [63] identified *LOXL1* to be associated with exfoliation syndrome. *LOXL1* encodes for a protein with catalytic properties. LOXL1 binds and catalyzes tropoelastine and fibulin 5. Alterations in *LOXL1* may affect the catalytic activity and the interaction with tropoelastine and fibulin 5, resulting in

accumulation of elastin fibers in the anterior segment of the eye, increased resistance in aqueous flow and glaucoma.

The Axenfeld–Rieger malformation, discussed below, is one of several congenital maldevelopments of the anterior segment of the eye that are associated with glaucoma.

Clinical presentation of Axenfeld-Rieger Syndrome (ARS)

Axenfeld–Rieger malformation (ARS) is a rare autosomal dominant disorder that affects anterior eye structures derived from the periocular mesenchyme [64, 65]. In 1920 [66], Axenfeld reported a patient with a white line in the posterior portion of the cornea to which iris tissue was adherent and he named this "posterior embryotoxon of the cornea". In 1934, Rieger [67] described two patients that had similar manifestations adding marked iris stroma and congenital pupillary abnormalities. In 1935, Rieger called this condition as "dysgenesis mesodermalis corneae et iridis". The similarity of anterior segment angle defects described by Axenfeld and Rieger had led to the suggestion that these diseases are part of the same group of disorders. In the past, Axenfeld-Rieger disorders were divided into four groups: Axenfeld *anomaly* (AA), Axenfeld *Syndrome* (AS), Rieger *anomaly* (RA) and Rieger *Syndrome* (RS). Initially, Axenfeld *anomaly* was diagnosed when a patient presented with posterior embryotoxon and peripheral anterior adhesions, while Axenfeld *syndrome* was diagnosed when the patient presented systemic defects in addition to Axenfeld anomaly. Rieger

anomaly was diagnosed when a patient presented with posterior embryotoxon, peripheral anterior adhesions, iris hypoplasia, corectopia and polycoria, while Rieger *syndrome* was diagnosed when the patient presented systemic defects in addition to Rieger anomaly. Patients with ARS may present with ocular features (Figure 1-2) which can occur with or without non-ocular features (Figure 1-3). Because ocular and systemic defects overlap among the four groups of disorders and the four groups of disorders are caused by mutations of the same genes, in 2000, the Axenfeld-Rieger group of disorders was recognized as one entity as Axenfeld-Rieger Syndrome (ARS) [68].

Ocular features of ARS

The diagnosis of ARS refers to a heterogeneous constellation of dominantly inherited ocular findings, including anomalies of the anterior chamber angle and aqueous drainage structures. The eyes of an affected individual can appear with a variety of defects (Figure 1-2). Schwalbe's line (the termination of Descemet's membrane, a basement membrane of the trabecular meshwork) is prominently visible in slit-lamp examination as a white or yellowish ring lining the iris of the eye. This feature is called posterior embryotoxon (PE) and up to 15% of the normal population may have milder forms [69]. The angle tissue in the affected patients is abnormal and can include iridocorneal adhesions (peripheral anterior synechiae-PAS). The iris can be hypoplastic (iris hypoplasia-IH) and often disrupted such as corectopia (eccentric pupil) or polycoria (iris tears). Some patients may present with iridogoniodysgenesis (IGD) which is iris hypoplasia

and goniodysgenesis with excess tissue in the angle and anomalous angle vascularity. The corneal endothelium and Descemet's membrane may also be absent in affected eyes. The corneal stroma is sometimes centrally opaque perhaps due to edema associated with the permeability of the endothelial barrier. The changes in eye morphogenesis in ARS are highly penetrant and my study described in Chapter 2 showed that ARS is associated with an approximately 75% risk of developing glaucoma in patients with FOXC1 and PITX2 defects [70]. Glaucoma, which can lead to blindness, is the most important consequence of ARS [71, 72]. Glaucoma in ARS patients can develop in infancy, but more usually in adolescence or early adulthood. In rare cases, glaucoma has been observed after middle age. As a result, patients with ARS remain at risk for developing glaucoma throughout their lives.

Figure 1-2. Ocular characteristics of patients with Axenfeld-Rieger Syndrome [70]. Adapted from [1].

(**A)** Left eye of a patient with *FOXC1* duplication shows marked iris stroma hypoplasia with exposure of the sphincter muscle.

(**B)** Right eye of a patient with *FOXC1* mutation shows marked iris stroma hypoplasia with exposure of the sphincter muscle (generously provided by Dr. Elise Héon).

(**C)** Left eye of a patient with *PITX2* mutation shows displaced pupil, iris atrophy, polycoria, prominent and displaced Schwalbe's line (posterior embryotoxon).

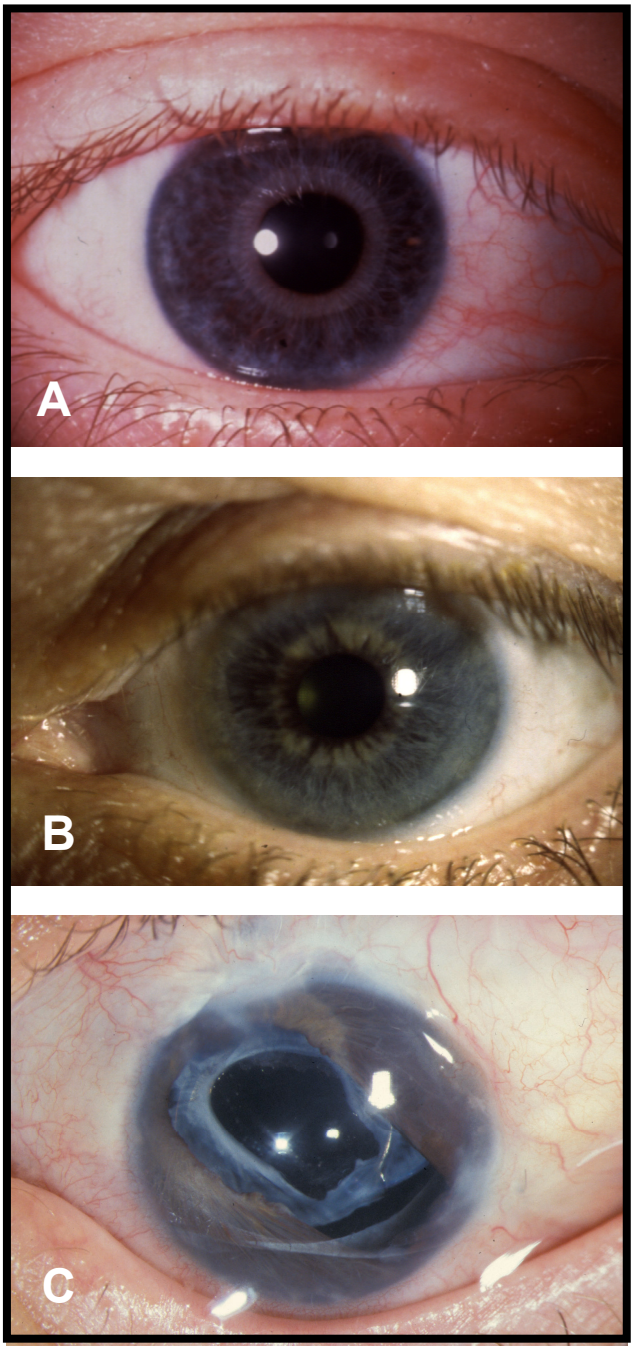
A
B
C

Systemic features of ARS

ARS patients may also present with systemic malformations seen with incomplete penetrance and variable expressivity. Non-ocular features typically include facial, dental and umbilical defects. ARS patients may have a flat midface due to maxillary hypoplasia. Dental abnormalities usually include fewer (hypodontia) or smaller (microdontia) teeth than normal with a complete lack of teeth (anodontia) being the most serious dental manifestation. The umbilical feature is often failure of the involution of the periumbilical skin. In severe cases, patients are dead at birth from gastrointestinal (GI) defects such as omphalocele and failure of the abdominal wall to close. In rare cases, ARS patients may also have pituitary defects such as empty sella syndrome and growth hormone deficiencies resulting in growth retardation (GR). Hypertelorism, sensory hearing loss and congenital heart defects (atrial and ventricular cardiac septal defects, outflow tract abnormalities) are other systemic manifestations of ARS.

Genetic etiology of ARS

ARS is genetically heterogeneous. Genetic linkage analysis has revealed five loci associated with ARS: the pituitary homeobox 2 gene (*PITX2*) located at 4q25, the forkhead box C1 gene (*FOXC1*, formally called *FKHL7*) located at 6p25 and two unidentified genes at 13q14 and 16q24 [48-50, 73-76]. ARS due to deletion of the paired-box transcription factor *PAX6* has been reported in a single case [76, 77]. For 60% of patients with ARS, the causative mutation is unknown [76, 78] (Mirzayans F, Walter MA, unpublished observations).

Figure 1-3. Systemic malformations found in patients with Axenfeld-Rieger Syndrome

(A) (B) Small, misshapen and absent teeth in an ARS patient, as previously published in [79, 80].

(**C) (D)** Excessive periumbilical skin, as previously published in [79, 80].

(E) Maxilla poorly developed with flattened midface in an ARS patient, as previously published in [80].

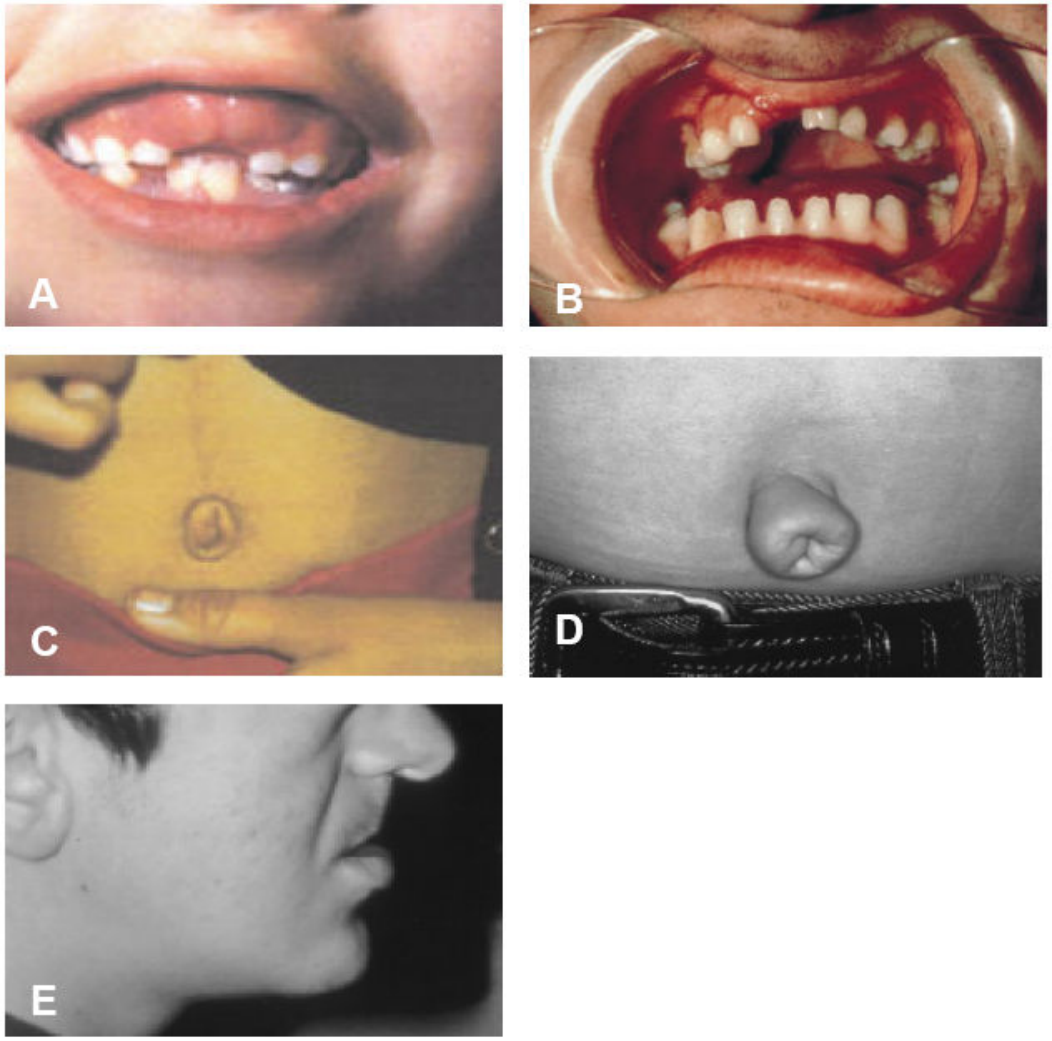
A
B
C
D
E

Forkhead box C1 gene (*FOXC1)*

FOXC1 structure

In 1994, Pierrou et *al.* [81] reported the cloning of seven human forkhead orthologues from a craniofacial cDNA library, one of them being *FREAC-3* (now called *FOXC1*). In 1998 [49, 74], *FOXC1* was shown to cause anterior segment dysgenesis. All members of the Forkhead gene family have a conserved, 110-residue forkhead domain that it is responsible for DNA binding, localization to the nucleus and protein-protein interaction [82]. FOX proteins are key regulators of diverse cellular functions including the development of many organ systems, energy homeostasis and oncogenesis [83-85]. *FOXC1* gene of 1.6 kb long contains one exon and encodes a protein of 553 amino acids. Transactivation function requires two activation domains and the activity of these domains are attenuated by a central domain (215-366), the inhibitory domain [86]. The inhibitory domain also appears to be a target for inhibitory phosphorylation by protein kinases such as p44/42 ERK, implying that FOXC1 may be susceptible to regulation via mitogen-potein kinase (MAP kinase) pathways [86, 87].

Disease- causing defects of FOXC1

The most common defects of the *FOXC1* locus which produce AR phenotypes are point mutations, however segmental and telomeric chromosome rearrangements involving 6p25 are also present [88-90]. The intragenic mutations of *FOXC1* include 23 missense mutations, six nonsense mutations and 17 deletion/ insertions/ duplication. All the missense mutations, except one, are

within FHD and were shown to affect in variable degree the nuclear localization, DNA- binding and transactivation function of the protein [49, 74, 75, 88, 91-99]. Chromosomal rearrangements involving FOXC1 mutations and producing a spectrum of anterior segment disorder phenotypes are balanced translocation [74], interstitial or telomeric deletions and interstitial duplications of the 6p25 [89, 92]. These findings taken together suggest both lower and upper thresholds for the appropriate level of FOXC1 activity *in vivo* [88, 90]. However, amounts of FOXC1 activity do not correlate with the severity of the anterior segment dysgenesis.

Foxc1 mice phenotype

Heterozygous and homozygous null mutants mice of *Foxc1* were generated either from a targeted allele ($Foxc1^{+/-}$ and $Foxc1^{-/-}$ respectively) or the spontaneous mutation congenital hydrocephalus ($Foxc1^{ch/+}$ and $Foxc1^{ch/ch}$ respectively). The heterozygote *Foxc1* mice have anterior segment abnormalities similar to those observed in patients; however the IOP was not elevated [100]. These mice presented with failure of the formation of the anterior eye segment, iris hypoplasia, thickening of the corneal epithelium, absence of corneal endothelium and open eyelids. The homozygous *Foxc1* mice die pre- and perinatally with cardiovascular, ocular, severe skeletal defects and hemorrhagic hydrocephalus [101].

FOXC1 target genes

In the past years, several different target genes directly regulated by FOXC1 have been identified. *TBX1*, a T-box transcription factor, was the first direct *in vivo* target of FOXC1 to be described [102]. *FGF19*, fibroblast growth factor 19, was also shown to be a direct target of FOXC1 [103]. FGF19 is secreted into the aqueous humour where it signals through FGFR4 tyrosine kinase, to alter MAPK phosphorylation in the cornea. Recently it has been reported that FOXC1 regulates the expression of *FOXO1A* [104]. *FOXO1A* is an important protein in cellular stress response and apoptotic pathways implicating FOXC1 in oxidative stress. FOXC1 also activates the *DLL4* and *HYE2* genes in VEGF- Notch signaling pathway in arterial and venous endothelial cells [105]. FOXC1 has been suggested to regulate expression of the homeobox genes *MSX2* and *ALX4* by mediating BMP signalling [106]. Other genes (*BMP2K*, *DACH*, *FVT-1*, *SIX-1*, *PGE-2* receptor, *BMP7*, *SMAD2*, *TGF-B1*, and *WNT6*) have been shown to be potential targets genes for FOXC1 [107].

Pituitary homeobox 2 gene (*PITX2*)

PITX2 structure and isoforms

The *PITX2* transcription factor was identified for the first time as an ARS causing gene in 1996 [48]. *PITX2* has six alternatively spliced exons which produce four mRNA transcripts (PITX2A-D), however a translation product of PITX2D has never been found [48, 79, 108-111] (Figure 1-4). All four human isoforms share the same C-terminus, whereas they are different at the N-terminus

[112, 113]. The PITX2A-C proteins contain a conserved 60 amino acid homeodomain of the paired-bicoid class that it is responsible for DNA binding, PITX2 localization to the nucleus and protein-protein interaction [82]. PITX2A (271 amino acids) has a short N-terminus preceding the homeodomain, whereas PITX2B (317 amino acids) and PITX2C (324 amino acids) have large, different N-termini. PITX2D has a truncated, non-functional homeodomain [111]. The second conserved region of PITX2 is OAR containing fifteen amino acids [114, 115]. The OAR domain was first identified as a conserved region between the paired-like activators Orthopedia, Aristaless, and Rax. This domain is found near the extreme C-terminus of homeoproteins. PITX2 A is the best studied isoform and recent experiments showed that PITX2A has two activation domains and two inhibitory domains [116]. The first activation domain is located between amino acid 1 and 38 and it is specific to the PITX2A isoform. The second activation domain is at the C- terminus, at residues 160-232 of PITX2A. The inhibitory domains are located at residues 99-159 and 233-271 respectively. The second inhibitory domain contains the OAR. Isoforms A, B, and C are widely expressed in craniofacial and other tissue such as the pituitary and heart. Isoforms A–C have been shown to transactivate different target gene promoters in *vitro*, to varying degrees, suggesting that they have diverged functions [110, 111]. The D isoform neither activates promoters nor binds DNA; instead, it has been proposed to serve as a negative regulator of transactivating activity of the other isoforms [111].

Disease- causing defects of PITX2

The most common defects of the *PITX2* locus which produce AR phenotypes are point mutations; however chromosome rearrangements involving 4q25 have also been described. The chromosome rearrangements found in ARS patients are in the forms of interstitial deletions, microscopic and submicroscopic deletions and translocations involving 4q25 [117-122]. Duplication of a distal region of 4q2 (including 4q25) has been found in one patient with hypoplastic left heart [123] indicating that an increased *PITX2* copy number may also be the cause of AR. Forty one intragenic mutations of *PITX2* have been described to date, which include eighteen missense mutations, four nonsense mutations, five splice-site mutations and fourteen deletions/ duplications [48, 73, 76, 118, 124-129]. Fifteen missense mutations out of eighteen are within the homeodomain. Most of the intragenic mutations are loss-of-function mutations resulting in decreased or no DNA binding, decreased or no transactivation and unstable protein. One PITX2 mutation, Lys88Glu, has a dominant negative effect on the wild-type protein [127, 130]. A single hypermorphic allele of *PITX2* (V45L in the homeodomain) has been identified in ARS, suggesting an upper limit for PITX2 activity in normal ocular development [127]. As a result, tight control of *PITX2* expression is required for normal development of the eye as either too much or too little activity of this transcription factor results in anterior segment defects and glaucoma. A correlation between the dosage of normal PITX2 protein and the severity of the phenotype has also been noted, as a dominant-negative mutation in *PITX2* was shown to result in a more severe ocular developmental phenotype [125, 131].

PITX2 mutations may also cause other anomalies such as Peters anomaly and ring dermoid of the cornea [132, 133].

Pitx2 mice phenotype

During mouse embryogenesis, *Pitx2* is expressed in the tissues and organs affected by ARS such as eye, face and dentition [134]. In the eye, *PITX2* is expressed in the structures of the anterior segment, sclera, ocular vasculature and extraocular muscles [135]. In some studies, heterozygote ($Pitx2^{+/-}$) mice do not show any obvious phenotype [136], in other studies, these mice presented with eye defects, tooth and abdominal wall defects [108, 137]. Homozygous null mutant ($Pitx2^{-/-}$) mice die early during embryogenesis due to heart defects [108, 136, 137]. Besides the heart defects, these mice presented with eye, tooth, pulmonary, abdominal wall, pituitary, mandibular and maxillary defects.

Figure 1-4. Isoforms of PITX2. Top: The four characterized protein isoforms of PITX2 and their transcripts are schematically represented**.** The protein structure of PITX2 shows the homeodomain and OAR domain. The exons that code for the respective proteins are shown below each isoform. Checkered and stippled boxes denote the differences in the N-terminal region of the isoforms. **Bottom:** Genomic organization of the PITX2 gene; intron sizes are shown on the top, and exon sizes are at the bottom. PITX2C and PITX2D RNA is transcribed using an internal promoter shown as a *striped box* flanking exon 4.

The figure is based on [78, 79, 111].

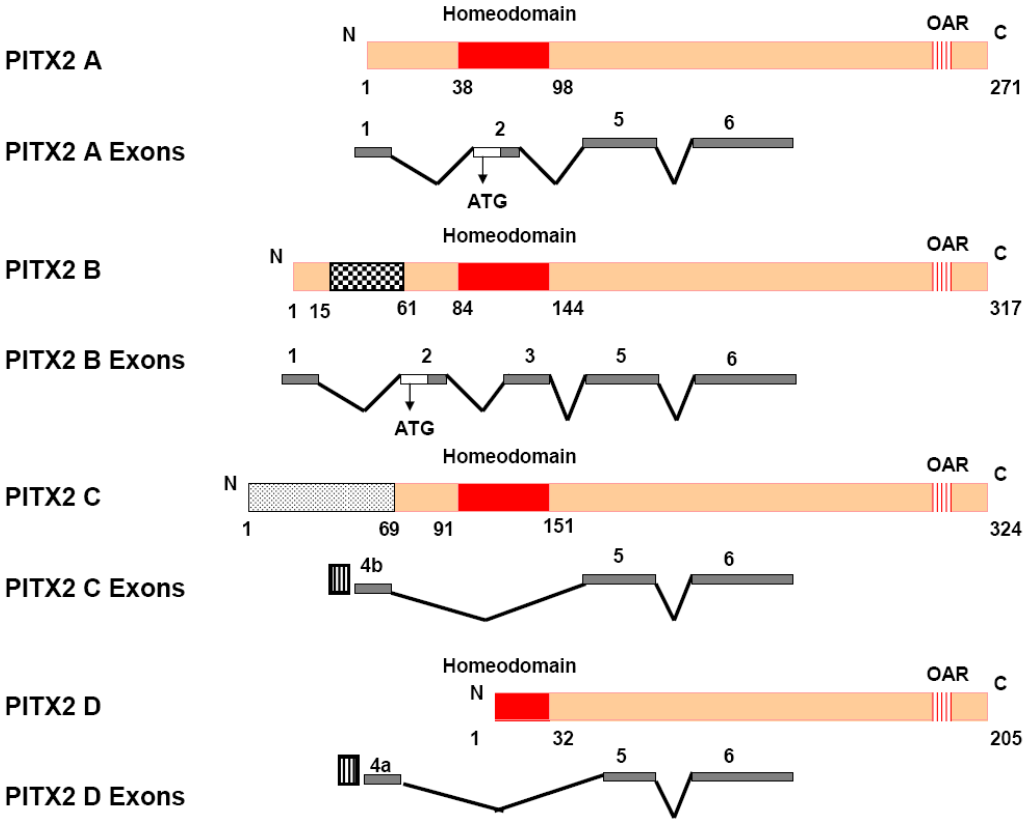
PITX2 A
Homeodomain
N
OAR
C
1
38
98
271
PITX2 A Exons
1
2
5
6
ATG
PITX2 B
Homeodomain
N
OAR
C
1
15
61
84
144
317
PITX2 B Exons
1
2
3
5
6
ATG
PITX2 C
Homeodomain
N
OAR
C
1
69
91
151
324
PITX2 C Exons
4b
5
6
PITX2 D
Homeodomain
N
OAR
C
1
32
205
PITX2 D Exons
4a
5
6


3.8kb
0.5kb
9.2kb
0.2kb
0.9kb
2.5kb
1
2
3
4a
4b
5
6
233bp
56bp
137bp
201bp
558bp
206bp
1258bp

The eye defects include agenesis of the corneal endothelium and stroma, loss of extraocular muscles, and optic nerve abnormalities. When Pitx2 is overexpressed in mouse corneal mesenchyme, the eye phenotype is similar to ARS and consists in corneal opacification, corneal hyperthrophy, irido-corneal adhesions and retinal degeneration [138].

PITX2 target genes

Several different downstream transcriptional target genes have been shown or suggested for PITX2 in different organs, based on a variety of biochemical and genetic experiments (Table 1-2). The most recent gene to be identified as a direct target gene in mouse eye through chromatin immunoprecipitation was *Dkk2* [139]. *Dkk2* encodes an extracellular antagonist of Wnt/ β-catenin signaling and the activation of this gene by Pitx2 is an important event during eye development. In the pituitary, Pitx2 upregulates transcription of the *prolactin* gene, whereas in the heart, transcription of the atrial natriuretic factor (ANF/NPPA) is upregulated by Pitx2 [140]. Another two PITX2 downstream target genes that seem to have relevance to ARS are the transcription factor *distal-less homeobox 2* (*DLX2*) expressed in the tooth and the *pro-collagen lysyl hydroxylase* (*PLOD2*) expressed in the eye. Dysregulation of *DLX2* may explain the tooth phenotypes of ARS patients, and dysregulation of *PLOD* may explain some of the ocular ARS phenotypes. Data from human mutations in *PITX2* and their effect on patient's teeth match the corresponding response of *DLX2* reporter genes in cell culture

[141]. Corneal overexpression of PITX2A is accompanied by a mild downregulation of *PLOD2* [127].

PITX2 and FOXC1 in the same pathway

The PITX2 transcription factor is part of a large network of gene regulation, which is only partially characterized at present. The recent discovery that PITX2 and FOXC1 directly interact to negatively regulate FOXC1 activity [64] provides evidence that at least some portion of the regulatory pathway in the eye of these two genes must be in common. The results of Berry et *al* study suggest that in cells expressing both FOXC1 and PITX2 proteins, PITX2 target genes are expressed, whereas FOXC1 target genes are inhibited by FOXC1-PITX2 complexes (Figure 1-5). When there are PITX2 loss of function mutations, PITX2 target genes expression is reduced, while FOXC1 target genes are inappropriately activated.

The investigation of the downstream and upstream of PITX2 gene pathways is necessary for understanding the development of the eye and also the normal function of the adult eye. Altered regulation of these pathways may have significant impact on the development and progression of glaucoma which is the most important clinical consequence of *PITX2* defects.

Table 1-2. Proposed PITX2 target genes

Gene	Name	Cell type/ organ	References
ANFINPPA	Atrial natriuretic factor	Heart	[110]
BMP4	Bone morphogenetic protein 4	Tooth	[142]
CYCD2	Cyclin D2	Pituitary, heart	[143]
DLX2	Distal-less homeobox 2	Tooth	[141]
Dkk2	Dickkopf homolog 2	Eye	[139]
FGF8	Fibroblast growth factor 8	Tooth	[137, 142]
HESX1	Homeobox gene expressed in ESCs	Pituitary	[108]
LHX3	Lim-domain homeobox gene 3	Pituitary	[79]
PRL	Prolactin	Pituitary	[144]
PROP1	Prophet of PIT1	Pituitary	[108, 137]
PLOD1	Pro-collagen lysyl hydroxylase	Eye	[145]
TRIO	Triple functional domain	HeLa cells	[146]

Abbreviations: ESC, embryonic stem cell; PIT1, pituitary-specific transcription factor 1

Figure 1-5. A link between PITX2 and FOXC1 pathways. Top: PITX2 target genes are activated by FOXC1-PITX2 complex, whereas FOXC1 target genes are repressed by the same complex. **Bottom:** Mutations of PITX2 result in no expression of PITX2 target genes and activation of FOXC1 target genes. Figure adapted from [64].

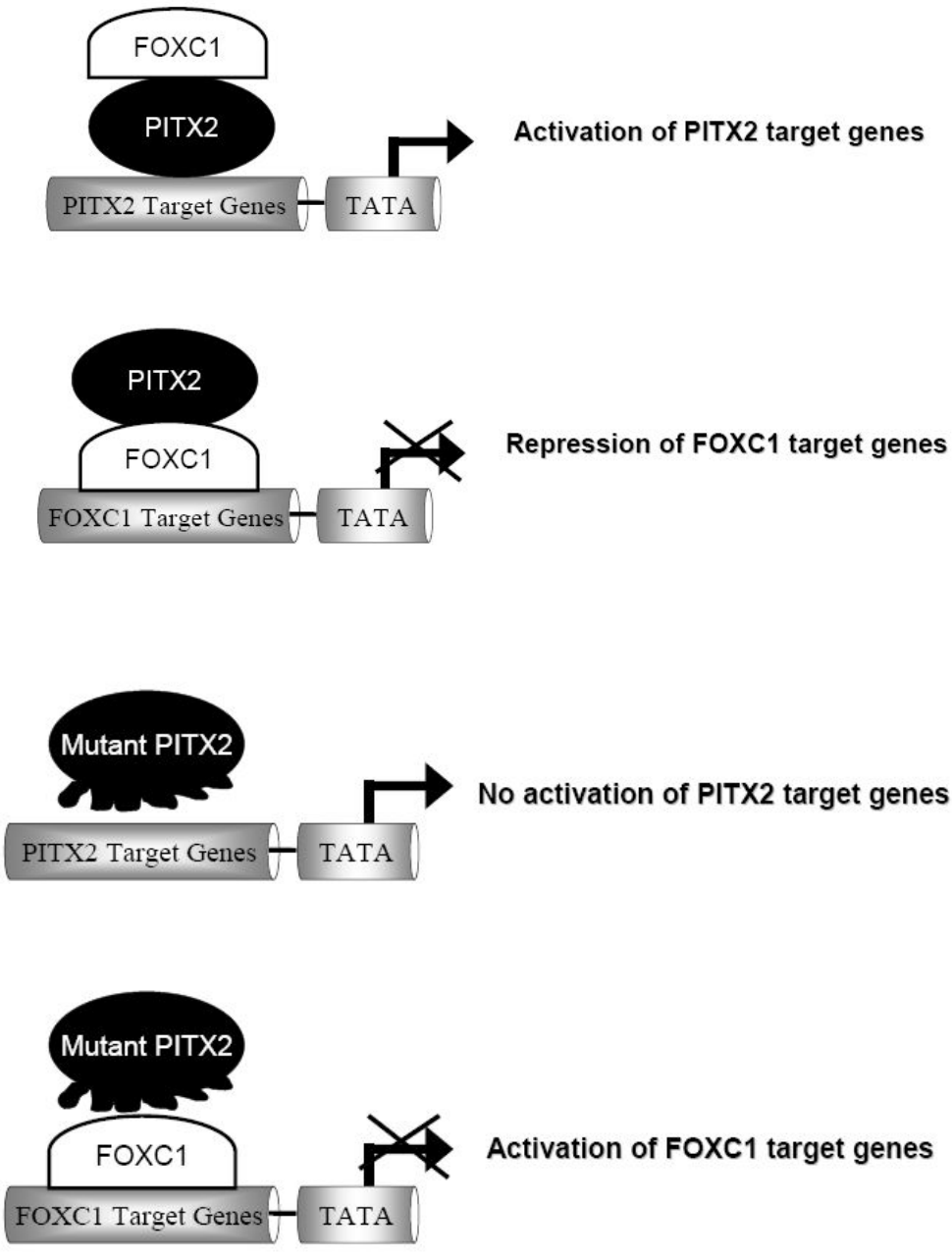
FOXC1
PITX2
PITX2 Target Genes
TATA
Activation of PITX2 target genes
PITX2
FOXC1
FOXC1 Target Genes
TATA
Repression of FOXC1 target genes
Mutant PITX2
PITX2 Target Genes
TATA
No activation of PITX2 target genes
Mutant PITX2
FOXC1
FOXC1 Target Genes
TATA
Activation of FOXC1 target genes

Chapter two:

Genotype-Phenotype correlation in ARS and glaucoma patients with FOXC1 and PITX2 mutations

This chapter contains arguments and text presented in:

Strungaru MH, Dinu I, Walter MA. Genotype-Phenotype correlations in Axenfeld-Rieger Malformation and glaucoma patients with FOXC1 and PITX2 mutations. *Investigative Ophthalmology & Visual Science*. 2007 [1]

Introduction

Axenfeld Rieger Syndrome (ARS) has been studied in detail from both clinical and genetical points of view in the past few years. Several clinical studies have been published [95, 129, 147-149] describing one or two families affected with ARS. For example, Shields et *al* in 1985 [147] presented a family of twelve individuals affected with ARS. This study suggested a 50% glaucoma incidence in affected patients with ARS. However, studies including a large cohort of patients affected with ARS have not been perfomed until now. This chapter describes the results of a retrospective study on the largest cohort of patients with ARS up to date. We included in this study 126 patients diagnosed with ARS in whom our laboratory has previously identified disease-causing genetic defects in either *FOXC1* or *PITX2*. The goals of this study were to gain a better understanding of the ARS-associated glaucoma and insight into the best glaucoma treatment for ARS patients. *FOXC1* and *PITX2* mutations and *PITX2* deletions found in affected patients who participated in this study (Table 2-1) were previously analyzed in our laboratory for their effects on the structure and function of these two transcription factors. In this study, the absolute number of probands and/or different families with ARS was too small for interfamilial comparison of clinical presentation and precluded comparisons between phenotypic parameters and the biochemical analysis of mutations, therefore the absolute number of patients was used in this study.

Table 2-1. Probands/families included in the study and their defects.				
	Probands	**Affected individuals**	**Defect**	**References**
FOXC1 Mutation	Family 1	7	S82T	[49, 92, 97]
FOXC1 Mutation	Family 2	12	Q23Stop	[98]
FOXC1 Mutation	Family 3	2	Δ363C	*
FOXC1 Mutation	Family 4	2	L130F	[150]
FOXC1 Mutation	Family 5	2	L86F	[33]
FOXC1 Mutation	Family 6	3	Δ10bp	[49]
FOXC1 Mutation	Family 7	2	I87M	[49, 92]
FOXC1 Mutation	Patient 1	1	P297S	*
FOXC1 Mutation	Patient 2	1	L86F	[33]
FOXC1 Mutation	Patient 3	1	G165R	[93]
FOXC1 Mutation	Patient 4	1	R169P	[93]
FOXC1 Duplication	Family 8	46	Gene Duplication	[89, 90, 151]
FOXC1 Duplication	Family 9	11	Gene Duplication	[89, 90]
PITX2 Mutation	Family 10	12	R69H	[130, 151]
PITX2 Mutation	Family 11	12	ΔC416FS	[76]
PITX2 Mutation	Patient 5	1	Intron 2, G→T	[76]
PITX2 Mutation	Patient 6	1	ΔG114FS	[76]
PITX2 Deletion	Family 12	6	Gene Deletion [23]	[76]
PITX2 Deletion	Family 13	2	Gene Deletion [23]	[76]
PITX2 Deletion	Patient 7	1	Gene Deletion [23]	[76]

* Unpublished data

Methods

This study adhered to the tenets of the Declaration of Helsinki and was approved by the University of Alberta Ethics Board. Informed consent was obtained from each subject.

Patients

I included in the retrospective study 126 patients diagnosed with ARS and collected complete clincal data from 55 patients, incomplete clinical data from 45 patients, and 26 patients were lost to followup or did not wish to participate in our study (Table 2-2). *PITX2* mutations, *PITX2* deletion and *FOXC1* mutations were identified previously by Mr. Matthew Lines and Mrs. Kathy Kozlowski, graduate students in Dr. Walter's laboratory, by polymerase chain reaction (PCR) sequence analysis. Microsatellite markers were used to map 4q25 microdeletions at a contig scale. Fluorescence in situ hybridization (FISH) was used to identify the *FOXC1* duplications and was performed in the laboratory of Dr. Rosemary Ekong, University College London, London, UK.

Clinical data

Clinical data was collected through the examination of patient records and through clinical questionnaires. The patient records were examined for local patients. For ophthalmologists outside of Edmonton, Alberta, I sent a questionnaire to physicians who referred the patients to us. I obtained information regarding: the incidence of glaucoma among ARS patients, the age of diagnosis

with ARS and with glaucoma, the distribution of ARS/glaucoma in females and males, which ocular/non-ocular malformations were present, if the ARS-associated glaucoma was present in one eye (unilateral disease) or in both eyes (bilateral disease), which glaucoma treatment(s) was used, and if the treatment was successful in managing the ARS-associated glaucoma.

Statistical Analysis

Statistical analyses was performed by Dr. Irina Dinu (Department of Public Health Sciences, University of Alberta). Clinical data were tabulated and compared using statistical analyses. Both eyes were statistically analysed for ophthalmological tests. If no significant difference was found between the two eyes, then the left eye (OS) was chosen for further statistical analysis. Frequencies and cross-tabulations were constructed for categorical variables. For both univariate and bivariate analyses, various tests were used, including asymptotic and exact versions to protect against small counts. The Pearson Chi-square test or Z-test assessed the difference in proportions for the univariate analysis. Two-sided p-values were reported for tests with two-sided hypotheses, and one sided p-values were reported for tests with one-sided hypotheses. Several situations were identified for the bivariate analysis. The Pearson Chi-square test was used to check for a significant relationship between the two variables when both variables were nominal (Chi-square test with corresponding number of degrees of freedom). When one of the variables was nominal, the response was ordinal, and the measurements were done on the same patient (for example, visual acuity

measured for OD and OS of the same patient), the Marginal Homogeneity test was used to assess the difference in responses between the nominal categories. The McNemar test was used to assess the difference in responses between the nominal categories when one of the variables was nominal, the response was binary, and the measurements were done on the same patient (for example, IOP measured for OD and OS of the same patient). The Jonckheere-Terpstra (JT) trend test was used to assess whether there was a monotonic relationship between the two variables when both variables were ordinal. The Generalized Linear Mixed Models and procedure GLIMMIX were used to account for correlations in binary outcomes when patients were coming from the same family. It was not necessary to make adjustments for multiple comparisons because the same patients were not used for two comparisons. Statistical Analysis System and Statistical Package for the Social Sciences were used to run statistical analyses.

Table 2-2. Summary of data situation of patients who participated in the study and the defects found in these patients.

Nr. of patients	Complete info	Incomplete info	No info
126	55	45	26

Defect	Type of defect	Probands	Affected individuals
FOXC1 91 patients	Mutation	11	34
	Duplication	2	57
PITX2 35 patients	Mutation	4	26
	Deletion	3	9

Results

Subjects Demographics

Our laboratory has identified *FOXC1* and *PITX2* alterations in 20 different probands, representing a total of 126 patients with ARS (table 2-2). From these patients, 91 patients were found to have *FOXC1* defects (13 different probands), while 35 have *PITX2* defects (7 different probands). From 91 patients with *FOXC1* defects, 57, representing 2 families, have *FOXC1* gene duplication and 34, representing 7 families and 4 isolated cases, have *FOXC1* mutations. From 35 patients with *PITX2* defects, 26, representing 2 families and 2 isolated cases, have *PITX2* mutations and 9, representing 2 families and 1 isolated case, have *PITX2* gene deletion. There was no significant difference in gender among patients with ARS (p-value > 0.32; 48% females, 52% males).

Clinical features of ARS patients: Ocular and Systemic malformations

Patients with *FOXC1* duplication, *FOXC1* mutations, *PITX2* deletion and *PITX2* mutations were tested for differences in clinical presentation. Patients who participated in this study were usually diagnosed with ARS in childhood (0-15 years, p-value < 0.01). The ocular malformations found in ARS patients are presented in Table 2-3. Notably, patients with *FOXC1* mutations are more likely to have iris hypoplasia, corectopia, peripheral anterior synechiae (PAS) and posterior embryotoxon (PE) than patients with *FOXC1* duplication, while patients with *FOXC1* duplication are more likely to have iridogoniodysgenesis (IGD) than patients with *FOXC1* mutations. Patients with *PITX2* deletion are more likely to

have PE than patients with *PITX2* mutations. Patients with *PITX2* defects (mutations and deletion) are more likely to have corectopia than patients with *FOXC1* defects (mutations and duplication). Overall, patients with *FOXC1* duplications are more likely to have iridogoniodysgenesis (IGD) than patients with *PITX2* defects, while patients with *PITX2* defects are more likely to have iris hypoplasia (IH), corectopia, peripheral anterior synechiae (PAS) and posterior embryotoxon (PE).. No other statistically significant differences in ocular clinical presentation were found. For all ARS patients, irrespective of the type of defect, the disease affects both eyes in all cases (p-value <0.05). The small number of patients with polycoria or "other" ocular malformations (microcornea, macrocornea, dyscoria) for any category of defect precluded statistical analysis for differences in frequencies between the different categories.

The systemic malformations found in ARS patients are presented in Table 2-4. Patients with *FOXC1* mutations are more likely to have systemic malformations than patients with *FOXC1* duplication (p-value <0.0001). Patients with *PITX2* defects are more likely to have systemic malformations than patients with *FOXC1* defects (p-value =0.006). Patients with *PITX2* defects are more likely to have systemic malformations of the teeth, umbilicus, and facies than patients with *FOXC1* defects (p-value <0.04). No other statistically significant differences in non-ocular clinical presentation were found. There were too few patients with heart malformations and hearing loss with *PITX2* mutations and *PITX2* deletion to allow for statistical testing.

Table 2-3. Ocular malformations found in patients with ARS.

Defect	Ocular Malformations							
	Affected individuals	IGD*	IH*	Corectopia*‡	Polycoria	PAS*	PE*†§	Other‖
FOXC1 Mutations	23	5 (22%)	17 (74%)	6 (26%)	0 (0%)	19 (83%)	19 (83%)	3 (13%)
FOXC1 Duplication	25	25 (100%)	7 (28%)	0 (0%)	0 (0%)	3 (12%)	0 (0%)	0 (0%)
Total *FOXC1*	48	30 (63%)	24 (50%)	6 (13%)	0 (0%)	22 (46%)	19 (40%)	3 (6%)
PITX2 Deletion	4	0 (0%)	4 (100%)	2 (50%)	1 (25%)	2 (50%)	3 (75%)	1 (25%)
PITX2 Mutations	17	12 (71%)	11 (65%)	5 (29%)	1 (6%)	6 (35%)	2 (12%)	1 (6%)
Total *PITX2*	21	12 (57%)	15 (71%)	7 (33%)	2 (10%)	8 (38%)	5 (24%)	2 (10%)
All ARS	69	42 (61%)	39 (57%)	13 (19%)	2 (3%)	30 (43%)	24 (35%)	5 (7%)

Iridogoniodysgenesis (IGD), Iris hypoplasia (IH), Peripheral anterior synechiae (PAS) and Posterior embryotoxon (PE)

*Statistically significant difference between patients with FOXC1 duplication and FOXC1 mutations (p-value < 0.003)

†Statistically significant difference between patients with PITX2 deletion and PITX2 mutations (p-value= 0.004)

‡Statistically significant difference between patients with Total FOXC1 and Total PITX2 (p-value= 0.04)

§Statistically significant difference between patients with FOXC1 duplication and Total PITX2 (p-value < 0.02)

‖Other: microcornea, macrocornea, dyscoria

Table 2-4. Systemic malformations found in patients with ARS.

Defect	Systemic Malformation								
	Patients*[†‡]	Dental[†‡]	Umbilical[†]	Heart[†‡]	Facial[‡]	GI	GR	HT	Other[§]
FOXC1 Mutations	16 (67%)	6 (25%)	3 (13%)	3 (13%)	10 (42%)	1 (4%)	3 (13%)	6 (25%)	2 (8%)
FOXC1 Duplications	2 (8%)	0 (0%)	0 (0%)	0 (0%)	0 (0%)	0 (0%)	1 (4%)	0 (0%)	1 (4%)
Total *FOXC1*	18 (37%)	6 (12%)	3 (6%)	3 (6%)	10 (20%)	1 (2%)	4 (8%)	6 (12%)	3 (6%)
PITX2 Deletion	4 (100%)	4 (100%)	1 (25%)	0 (0%)	3 (75%)	0 (0%)	1 (25%)	0 (0%)	0 (0%)
PITX2 Mutations	14 (78%)	11 (61%)	10 (56%)	0 (0%)	12 (67%)	4 (22%)	0 (0%)	0 (0%)	0 (0%)
Total *PITX2*	18 (82%)	15 (68%)	11 (50%)	0 (0%)	15 (68%)	4 (18%)	1 (5%)	0 (0%)	0 (0%)
All ARS	36 (51%)	21 (30%)	14 (20%)	3 (4%)	25 (35%)	5 (7%)	5 (7%)	6 (17%)	3 (4%)

Gastrointestinal defects (GI), Growth Retardation (GR), Hypertelorism (HT)

*Statistically significant difference between patients with FOXC1 duplication and FOXC1 mutations (p-value< 0.0001)

[†]Statistically significant difference between patients with Total FOXC1 and Total PITX2 (p-value< 0.04)

[‡]Statistically significant difference between patients with FOXC1 duplication and Total PITX2 (p-value< 0.025)

[§]Other: hearing loss

Clinical features of ARS patients: Glaucoma

The incidence of glaucoma in ARS patients who participated in this study was 100% (29/29) for patients with duplications of *FOXC1*, 74% (17/23) for patients with mutations of *PITX2* and 75% (71/95) for all patients with ARS. Patients with *FOXC1* duplication are more likely to have an increased incidence of glaucoma than patients with *FOXC1* mutations (p-value < 0.01). Patients with *FOXC1* duplication also are more likely to have an increased incidence of glaucoma than patients with *PITX2* defects (p-value < 0.01). With respect to the age when glaucoma was diagnosed, patients with ARS are more likely to develop glaucoma in adolescence or early adulthood (under 30 years old, p-value < 0.01). However, for patients with *FOXC1* duplication, glaucoma is more likely to develop at early age, in childhood (0-15 years, p-value < 0.01). Patients with *FOXC1* duplication are more likely to develop glaucoma at an earlier age than patients with *PITX2* defects (p-value = 0.01). No other statistically significant differences in the group of age were found.

Factors known to be associated with glaucoma development in the general population were examined, including family history, hypertension, ischemic heart disease, myopic eye, previous ocular trauma and topical steroid use on eyes. Regarding the risk factors, patients with *FOXC1* defects, either mutations or duplication, patients with *PITX2* mutations, total patients with *PITX2* defects and all patients with ARS are more likely to have family history of glaucoma than not to have family history (p-values = 0.00). Due to the small number of patients with *PITX2* deletion included in this study, family history was not found to be a risk

factor for these patients (p-value = 0.70). Patients with *FOXC1* defects are more likely to have family history than patients with *PITX2* defects (p-value = 0.02). For the rest of the risk factors (hypertension, ischemic heart disease, myopic eye, previous ocular trauma and topical steroid use on eyes), patients with ARS and glaucoma are more likely to have at least one risk factor than not to have one (p-value = 0.01).

Ophthalmologic examination of ARS patients with glaucoma

Complete ophthalmic examination information, including visual acuity with refraction, slit-lamp biomicroscopy, applanation tonometry, gonioscopy, dilated fundus examination, and photography, when appropriate, was requested for each patient. Visual acuity (VA) was reported with the best correction in place. VA values were classified in 3 groups: good (20/20-20/40), fair (20/40-20/100) and poor (≤ 20/200, counting fingers, hand motion, light perception or no light perception). VA results of each group of genetic defects are displayed in figure 2-1. Among patients with glaucoma, patients with *FOXC1* mutations have significantly lower visual acuity and are more likely to have lost vision due to glaucoma than those with *FOXC1* duplication (p-value < 0.02). Among patients with glaucoma, patients with *PITX2* defects are more likely to have fair or poor vision and bilateral vision loss than those with *FOXC1* defects (p-value < 0.03).

Figure 2-1. Visual acuity results. Percentage of left eyes of ARS patients (**A)** and ARS patients with glaucoma (**B)** with good (20/20-20/40), fair (20/40-20/100) or poor (≤ 20/200, counting fingers, hand motion, light perception or no light perception) visual acuity (VA) for each type of defect. There were too few patients in the *PITX2* deletion group to apply any statistical tests. *Statistically significant difference, p-value< 0.05.

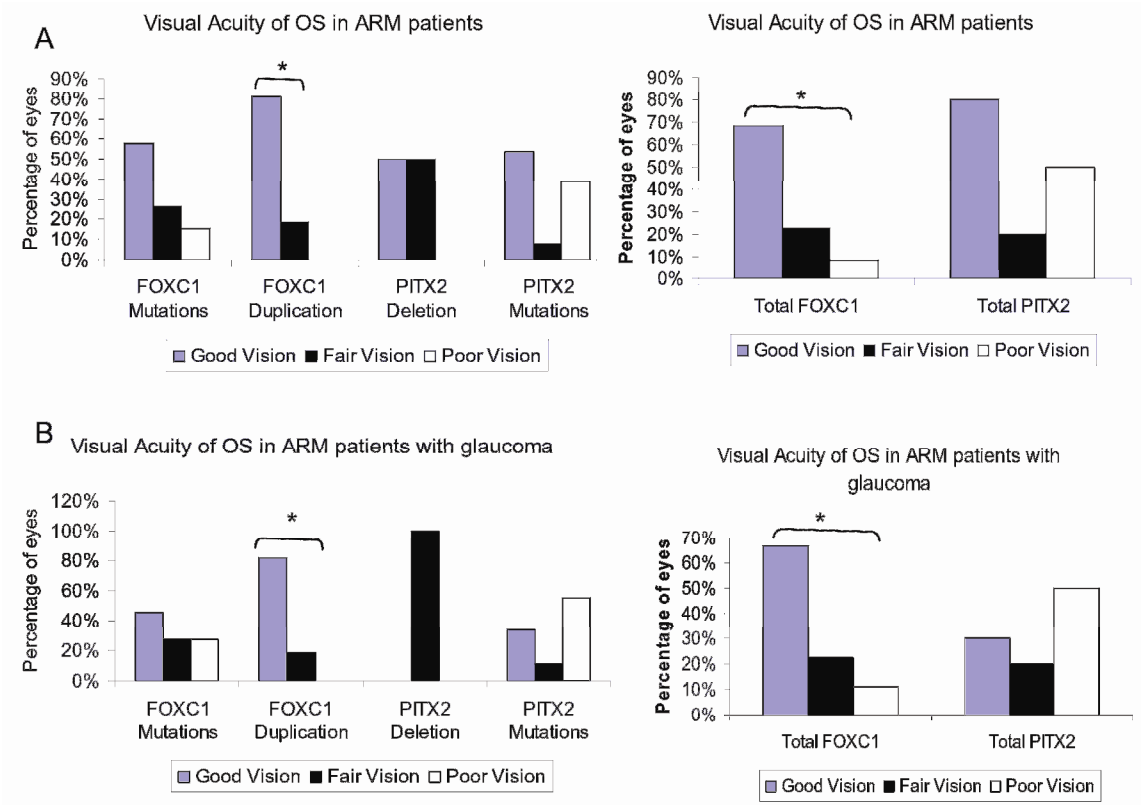
A
Visual Acuity of OS in ARM patients
Percentage of eyes
90%
80%
70%
60%
50%
40%
30%
20%
10%
0%
*
FOXC1 Mutations
FOXC1 Duplication
PITX2 Deletion
PITX2 Mutations
Good Vision
Fair Vision
Poor Vision
Visual Acuity of OS in ARM patients
Percentage of eyes
90%
80%
70%
60%
50%
40%
30%
20%
10%
0%
*
Total FOXC1
Total PITX2
Good Vision
Fair Vision
Poor Vision
B
Visual Acuity of OS in ARM patients with glaucoma
Percentage of eyes
120%
100%
80%
60%
40%
20%
0%
*
FOXC1 Mutations
FOXC1 Duplication
PITX2 Deletion
PITX2 Mutations
Good Vision
Fair Vision
Poor Vision
Visual Acuity of OS in ARM patients with glaucoma
Percentage of eyes
70%
60%
50%
40%
30%
20%
10%
0%
*
Total FOXC1
Total PITX2
Good Vision
Fair Vision
Poor Vision

Visual acuity in glaucoma patients with *PITX2* mutations, in all patients with *PITX2* and in all ARS patients is significantly lower than visual acuity in patients without glaucoma (p-value < 0.03). No other statistically significant differences in visual acuity were found.

The diagnosis of glaucoma was based on the observation of at least two of the following criteria: glaucomatous optic disc damage, glaucomatous visual field defects, or high intraocular pressure (≥ 22 mmHg). Intraocular pressure (IOP) data in this study were collected before applying any treatment. IOP was measured for each eye and scored as either low (< 22mmHg) or high (≥ 22mmHg) pressure. IOP results of each group of genetic defects are displayed in Figure 2-2. The range of IOP in patients with *FOXC1* defects is 15-68 mmHg and in patients with *PITX2* defects is 14-58 mmHg. Patients with *FOXC1* duplication, total *FOXC1*, *PITX2* mutations and all ARS patients are more likely to have an elevated IOP (≥ 22 mmHg) than to have a low IOP (< 21mmHg, figure 2-2). For both eyes, for all categories of patients, independent of the type of defect, elevated IOP (≥ 22 mmHg) is significantly associated with glaucoma (p-value < 0.05). However, there is significant difference in IOP between OS and OD in patients with glaucoma (p-value = 0.031). This difference of IOP in patients with glaucoma might be due to differences in the central corneal thickness between the two eyes.

Figure 2-2. Intraocular pressure measurements. Percentage of left eyes of ARS patients with low intraocular pressure (IOP< 21mmHg) and elevated intraocular pressure (IOP ≥ 22mmHg)) for each type of gene defect. There were too few patients in the *PITX2* deletion group to apply any statistical tests. *Statistically significant difference, p-value< 0.05

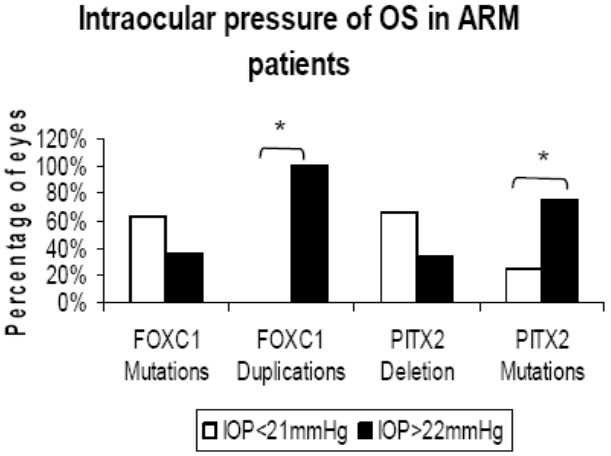
Intraocular pressure of OS in ARM patients
Percentage of eyes
120%
100%
80%
60%
40%
20%
0%
*
*
FOXC1 Mutations
FOXC1 Duplications
PITX2 Deletion
PITX2 Mutations
IOP<21mmHg
IOP>22mmHg

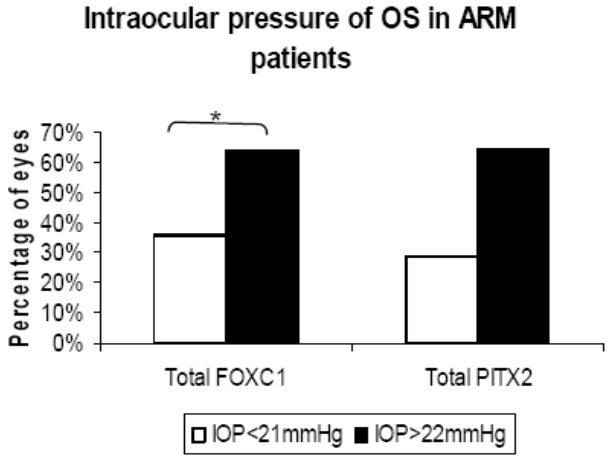
Intraocular pressure of OS in ARM patients
Percentage of eyes
70%
60%
50%
40%
30%
20%
10%
0%
*
Total FOXC1
Total PITX2
IOP<21mmHg
IOP>22mmHg

Figure 2-3. Cup/Disc ratio of ARS patients with glaucoma (red) and ARS patients without glaucoma (green). The mean of the Cup/Disc ratio measurements in ARS patients was statistically higher than the mean of the Cup/Disc ratio measurements in the general population (dotted lines). The means and 95% confidence intervals (solid lines) are displayed for each data set. There were too few patients in the PITX2 deletion group to apply any statistical tests. *Statistically significant difference, p-value< 0.05.

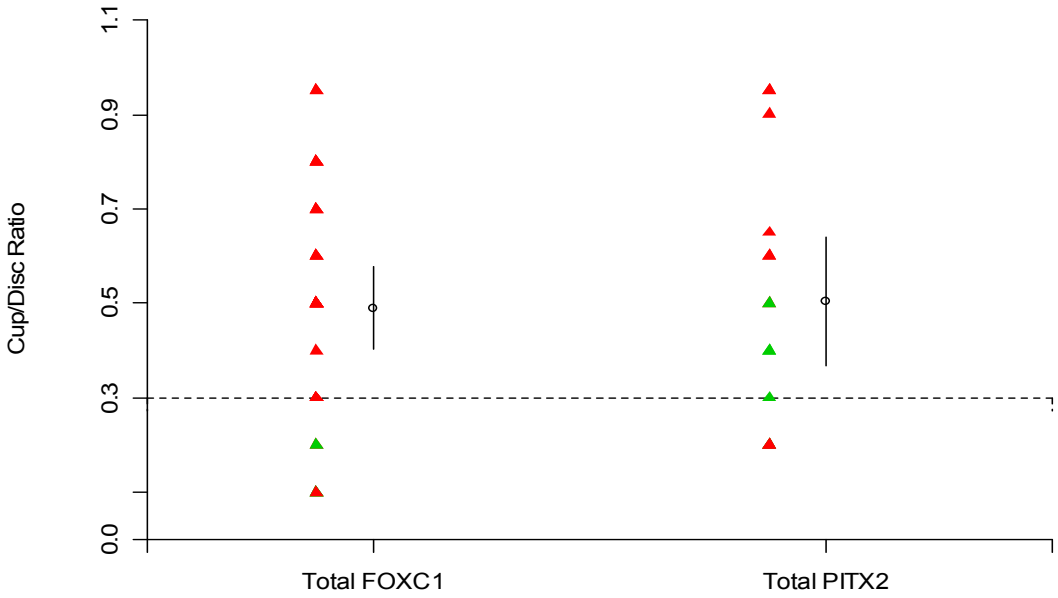
Cup/Disc Ratio
0.0
0.3
0.5
0.7
0.9
1.1
Total FOXC1
Total PITX2

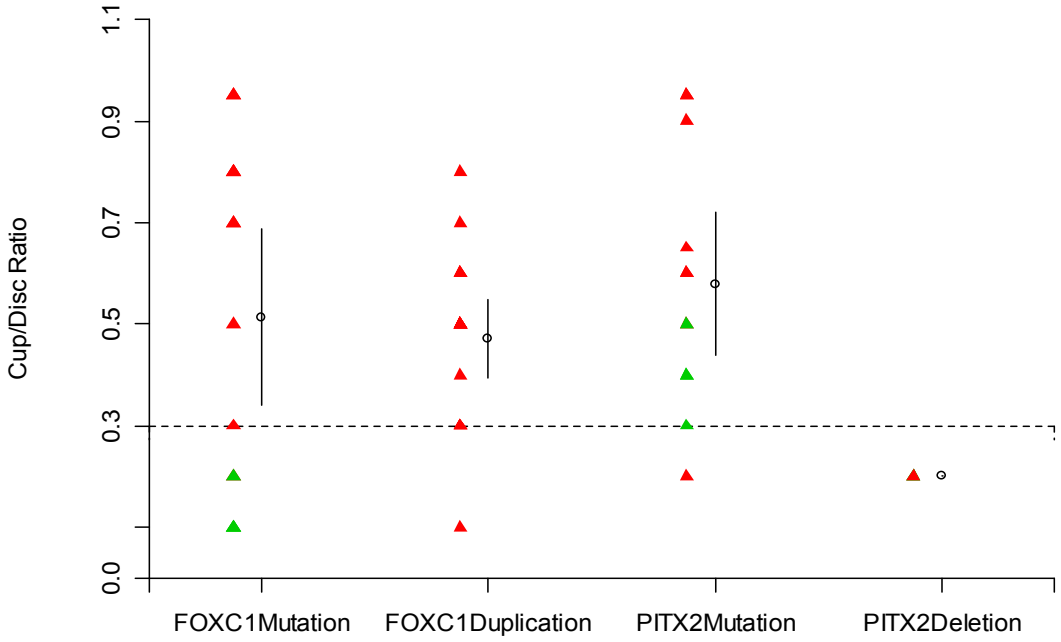
Cup/Disc Ratio
0.0
0.3
0.5
0.7
0.9
1.1
FOXC1Mutation
FOXC1Duplication
PITX2Mutation
PITX2Deletion

Cup/Disc ratio (CDR) measurements are displayed in figure 2-3 in reference to each group of genetic defect. Abnormalities of the optic disc are defined as excavation with the vertical CDR of 0.5 or more and asymmetric disc excavation with a difference in vertical CDR of more than 0.2 between the two eyes. The mean of the vertical CDR measurements in patients with *FOXC1* mutations, *FOXC1* duplication, total *FOXC1* defects, *PITX2* mutations and total *PITX2* is statistically higher than the mean of the vertical CDR measurements in the general population (p-value < 0.05). However these patients do not have a difference in CDR of more than 0.2 between the two eyes (p-value < 0.04). Unfortunately, corneal thickness and visual fields parameters were obtained from too few patients and no statistical test was applied for this information.

Treatment

The only proven method of treatment for glaucoma is reducing the intraocular pressure. There are two ways to lower intraocular pressure: medication and surgical treatment. Medical treatment consists of the use of topical ocular hypotensive drugs, including the following classes of medications: beta-blockers, alpha-2 agonists, carbonic anhydrase inhibitors, prostaglandins, miotics and combination medication. Surgical treatment is an invasive procedure including conventional surgery and laser. Conventional surgery is an incisional procedure such as: trabeculotomy, trabeculectomy with or without adjunctive antifibrosis therapy, glaucoma drainage surgery, or cyclodestructive procedures. Laser surgeries used to treat glaucoma include: laser trabeculoplasty, laser peripheral

iridotomy, laser peripheral iridoplasty and laser cyclophotocoagulation. Congenital glaucoma is primarily a disease requiring surgery, with medical management serving as a temporary measure before surgery or as postoperative adjunctive treatment. Treatment data are displayed in figure 2-4. More than half of total ARS patients received both medical and surgical treatments (57%, 29/51), while 24 % (12/51) patients received only medication, 12% (6/51) patients received only surgical treatment, and 8% (4/51) patients received no treatment. The patients who did not receive treatment were either blind or were being monitored (patients with glaucomatous visual fields defects, but low IOP). Patients with *FOXC1* mutations, total *FOXC1*, and all ARS patients received medication as first treatment (p-value <0.04). Results of treatment were assessed based on the success in reducing IOP and maintaining a good visual acuity. Results were "not successful" when IOP increased after treatment (≥ 22mmHg) or when IOP was < 21mmHg, but with poor VA. Results were "successful" when IOP lowered after treatment (IOP < 21mmHg) and "stable" when IOP was maintained at the same level, without any increase in values. Glaucoma in only 18% of ARS patients responded to medical or surgical (used solely or in combination) treatment. Treatment was not successful in 59% (23/39), successful in 18% (7/39) and stable in 23% (9/39) of the ARS patients who participated in our study. However, no significant differences in the results of treatment were found in patients with either *FOXC1* or *PITX2* defects, independently of the type of defect (p-value > 0.06). For ophthalmologic tests and treatment categories of data, there were too few patients in the *PITX2* deletion group to apply any

statistical tests, or to compare the *PITX2* deletion patients with *PITX2* mutations patients.

Figure 2-4. **Treatment received by patients with ARS**. **A.** Patients with *FOXC1* mutations, *FOXC1* duplication and Total *FOXC1* defects were statistically more likely to have both medical and surgical treatments than not (p-value <0.05). **B.** Patients with *PITX2* mutations were more likely to have multiple surgeries than have one surgery (p-value < 0.05), while patients with *FOXC1* duplication were statistically more likely to not have multiple surgeries than to have them (p-value <0.05). Patients with *PITX2* defects were more likely to have multiple surgeries than patients with *FOXC1* defects (p-value < 0.05). **C.** No statistically significant differences in the results of treatment were found in patients with either *FOXC1* or *PITX2* defects (p-value > 0.06). *-statistically significant

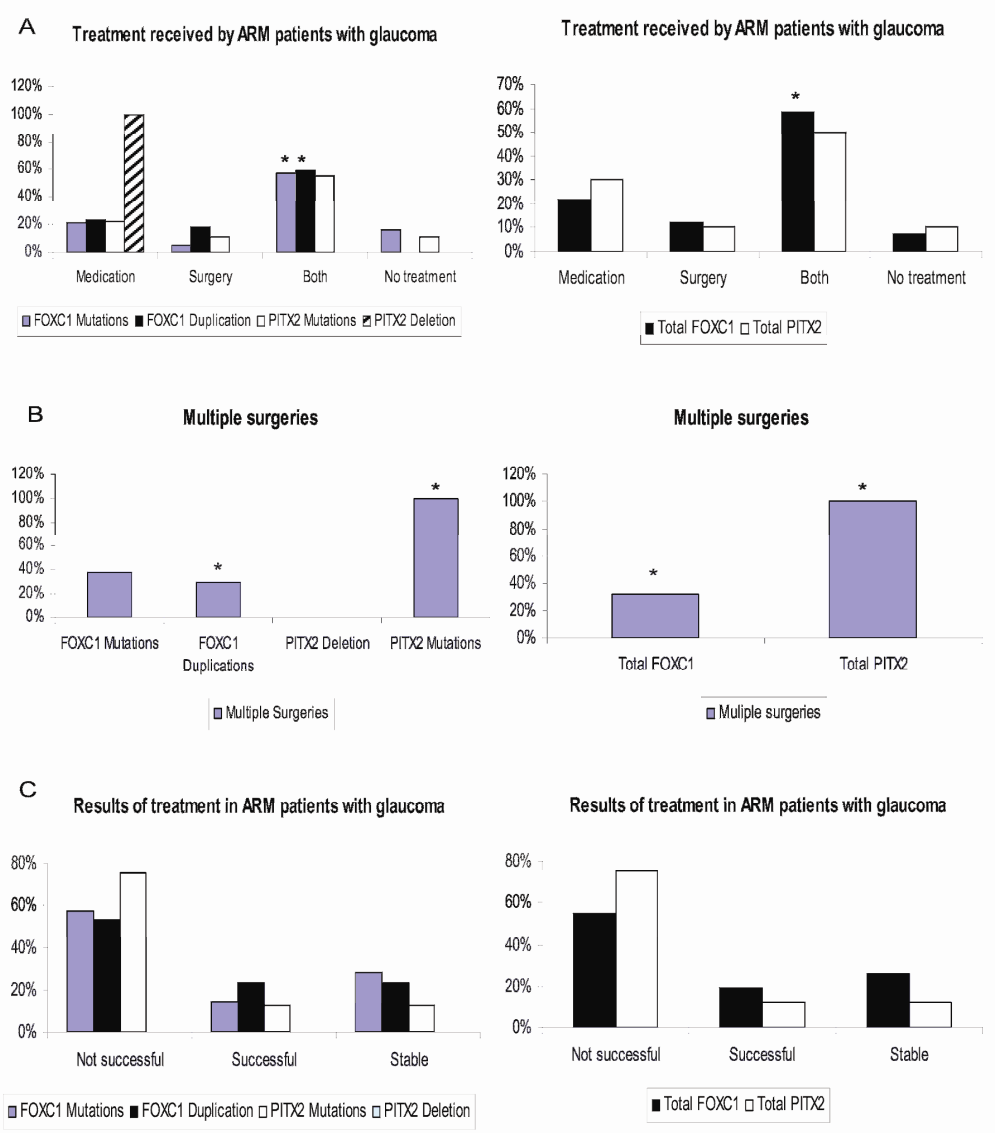
A
Treatment received by ARM patients with glaucoma
120%
100%
80%
60%
40%
20%
0%
Medication
Surgery
Both
No treatment
FOXC1 Mutations
FOXC1 Duplication
PITX2 Mutations
PITX2 Deletion
Treatment received by ARM patients with glaucoma
70%
60%
50%
40%
30%
20%
10%
0%
Medication
Surgery
Both
No treatment
Total FOXC1
Total PITX2
B
Multiple surgeries
120%
100%
80%
60%
40%
20%
0%
FOXC1 Mutations
FOXC1 Duplications
PITX2 Deletion
PITX2 Mutations
Multiple Surgeries
Multiple surgeries
120%
100%
80%
60%
40%
20%
0%
Total FOXC1
Total PITX2
Muliple surgeries
C
Results of treatment in ARM patients with glaucoma
80%
60%
40%
20%
0%
Not successful
Successful
Stable
FOXC1 Mutations
FOXC1 Duplication
PITX2 Mutations
PITX2 Deletion
Results of treatment in ARM patients with glaucoma
80%
60%
40%
20%
0%
Not successful
Successful
Stable
Total FOXC1
Total PITX2

Discussion

In the present study we conducted a retrospective examination of the glaucoma-related clinical presentation of individuals with *PITX2* or *FOXC1* mutations. The investigation included the largest cohort of ARS patients ever investigated. We found that ARS-associated glaucoma is a bilateral disease, equally prevalent in males and females. 75% of total patients with ARS who participated in this study developed glaucoma. This finding is not consistent with previous reports that suggested glaucoma develops in approximately 50% of patients with ARS. This discrepancy could be due to the larger number of patients in our study, the fact that we only included ARS patients with known defects of *PITX2* or *FOXC1*, or a consequence of the high proportion of patients with *FOXC1* duplication in comparison with the proportion of patients with other types of genetic defects included in this study. However, as in the previous reports, glaucoma in these patients develops in adolescence or early adulthood. As discovered in other glaucoma studies, at least one risk factor (any of family history, myopia, hypertension, heart disease, trauma or optical steroids) was found statistically to be associated with the development of glaucoma in ARS patients. In our study, glaucoma in only 18% of patients with either *PITX2* or *FOXC1* genetic defects responded to medical or surgical (used solely or in combination) treatment and more than half of total ARS patients received both treatments. These findings suggest that current medical therapies do not successfully lower intraocular pressure or prevent progression of glaucoma in ARS patients with *FOXC1* or *PITX2* alterations, and that neither medication nor surgery appears to

be effective. However, failure to respond to the surgical treatment might be due to surgical complications such as early fibrosis after trabeculectomy or the presence of modifier genes.

Genotype-Phenotype correlations

Patients with duplication of *FOXC1* typically have IGD malformations and an increased incidence of elevated IOP and of glaucoma (usually childhood-onset) than patients with *FOXC1* mutations. In contrast, patients with mutations of *FOXC1* present with iris hypoplasia, corectopia, peripheral anterior synechiae and posterior embryotoxon. Thus, patients with *FOXC1* mutations appear to have a more diverse clinical presentation than patients with *FOXC1* duplication. The incidence of elevated IOP and glaucoma is lower and glaucoma develops later in life in patients with *FOXC1* mutations than in patients with *FOXC1* duplication. Therefore, on the basis of significant differences of glaucoma incidence and age of onset of glaucoma, we suggest that patients with *FOXC1* duplication have a more severe prognosis for glaucoma development than patients with *FOXC1* mutations (figure 2-5). Interestingly, patients with non-ocular findings appear likely to have *FOXC1* mutations rather than *FOXC1* duplication. This suggests that the eye is particularly sensitive to duplication of *FOXC1*. Due to the small number of patients with *PITX2* deletion, we could not statistically compare patients with *PITX2* mutations and *PITX2* deletion. Patients with *PITX2* defects typically have corectopia, visual acuity in patients with *PITX2* defects is worse than that in patients with *FOXC1* defects. Patients with *PITX2* defects are more

likely to have bilateral vision loss due to glaucoma than patients with *FOXC1* defects. However, no patient with *FOXC1* defects has polycoria; visual acuity in patients with *FOXC1* defects is better, and they are more likely to have unilateral vision loss, than patients with *PITX2* defects. The absence of polycoria in patients with *FOXC1* defects is consistent with results reported in previous studies. Patients with *PITX2* defects required multiple surgeries to achieve the same results of treatment as patients with *FOXC1* defects receiving single/ fewer surgeries. Therefore, glaucoma in patients with *PITX2* defects is more difficult to treat than that in patients with *FOXC1* defects. Patients with non-ocular findings are more likely to have *PITX2* defects rather than *FOXC1* defects. Taken together, on the basis of significant differences in visual acuity, treatment outcome of glaucoma, these results suggest that patients with *PITX2* defects have a more severe prognosis for glaucoma development than patients with *FOXC1* defects (figure 2-5). Taking into consideration the recent finding that *PITX2* inhibits *FOXC1* activity [64], our model predicts that *PITX2* defects might result in both an inability to activate *PITX2* targets and a gain of function activation of *FOXC1* targets. Therefore, the severity of the ocular phenotype in patients with *PITX2* defects might be the simultaneous consequence of *PITX2* haploinsufficiency and a gain-of-function of *FOXC1*. The potential limitations of our study are the absence of sufficient information regarding visual fields and central coreneal thickness to allow statistical testing and the large number of patients coming from a small number of families. These limitations might have some impact on the results presented in this chapter.

Figure 2-5. Severity of prognosis of glaucoma. Patients with *FOXC1* mutations have the mildest prognosis in glaucoma development, while patients with *PITX2* defects and patients with *FOXC1* duplication have more severe prognoses in glaucoma development. Glaucoma progression was defined as advancing of the disease with increasing intraocular pressure, cupping of the optic nerve head, and visual acuity defects despite intensified medical treatment or surgery.

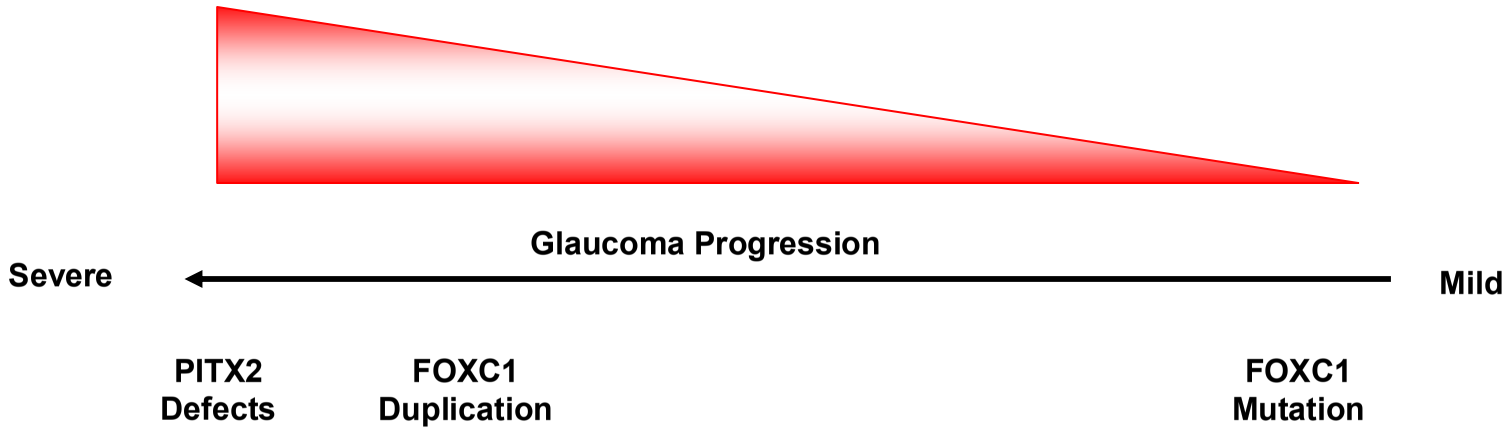
Glaucoma Progression
Severe
Mild
PITX2
Defects
FOXC1
Duplication
FOXC1
Mutation

Chapter three:

Isolation of the genes directly regulated by PITX2 in adult eye tissues using a novel hormone-inducible transcription factor expression system

Introduction

Mutations in two known genes cause Axenfeld- Rieger Malformation (ARS): *PITX2* located at 4q25 and *FOXC1* located at 6p25. Linkage analysis suggested another two loci to be associated with ARS, 13q14 and 16q24; however these disease-causing genes have not been identified [50, 51]. About 60% of the patients with ARS do not have defects of either *PITX2* or *FOXC1* (Mirzayans F, Walter MA, unpublished observations), leaving the potential for discovery of more causative genes for ARS. PITX2 is expressed in the developing eye having key roles for the anterior segment of the eye formation. For example, *Pitx2* knockout mice present with severe ocular dysgenesis features including agenesis of the cornea, abnormal blood vessels, a dysgenic optic nerve and coloboma. [65]. PITX2 also continues to be expressed in adult eye, and recent experiments have shown that Pitx2 is important in the extraocular muscles of mice after birth [152]. Loss of Pitx2 postnatally affected extraocular muscles function making, them more fatigable than wild type mice. These results suggest that genes regulated by PITX2 in adult eye tissues are important for the normal function of the adult eye. We hypothesize that altered regulation and expression of the target genes of PITX2 have key roles in ARS- associated glaucoma.

The goal of the rest of my thesis is to determine and characterize the genes directly regulated by PITX2. To discover direct target genes of PITX2, I have adapted a hormone (HR) inducible expression system coupled with microarray analysis for PITX2. In this system, the ligand-binding domain of the truncated form of human progesterone hormone receptor (hPR-LBD or PRG) is fused with

PITX2 resulting in the formation of a molecule that acts as a steroid hormone receptor. In the absence of the hormone, the HR-transcription factor molecule remains in an inactive form by being complexed with intracellular proteins such as Heat Shock Protein 90 (HSP90). The cells are treated with cycloheximide, a protein synthesis inhibitor, to prevent any other new protein from being form. By adding the hormone, mifepristone, the hormone-inducible construct binds to the ligand and adopts a transcriptionally active form. The RNA is isolated twelve hours postinduction, and gene expression profiles are compared using microarray analysis (Figure 3-1). The microarray-based approach is the most promising high-throughput screening method designed to identify novel target genes. Several technical platforms are available for microarray-based analysis of differential gene expression. Among these, the GeneChip technology has gained interest due to its extensive genetic content, high level of reproducibility and the fact that it is supplied ready for use with no start-up time required. Thus, using a microarray with the hormone-inducible expression system provides a powerful technique for identification of target promoters.

As a proof of principle, Dr. Fred Berry has developed and tested a hormone-inducible expression system for FOXC1 transcription factor which was recently published [104]. Because this method successfully worked for FOXC1, I conducted similar analyses of the PITX2 transcription factor. This chapter describes the results obtained using the hormone-inducible expression system coupled with microarray analysis for PITX2. The genes selected for further analyses had their expression significantly changed in multiple microarrays, were

expressed in the eye tissues, and contained binding motifs of PITX2 in their upstream regions. Furthermore, the genes were validated by an independent method such as northern blot analysis or semi-quantitative reverse transcriptase polymerase chain reaction (RT-PCR).

Figure 3-1. Schematic diagram of the hormone inducible expression coupled with microarray analysis used to identify PITX2 target genes. The hormone responsive construct transfected into the cells encodes a protein which remains in an inactive form while complexed with HSP 90. The cells are pretreated with cycloheximide (CHX) and the hormone, mifepristone, is added to activate the construct. Twelve hours post-induction, the RNA is extracted and gene expression profiles are compared using microarray analysis.

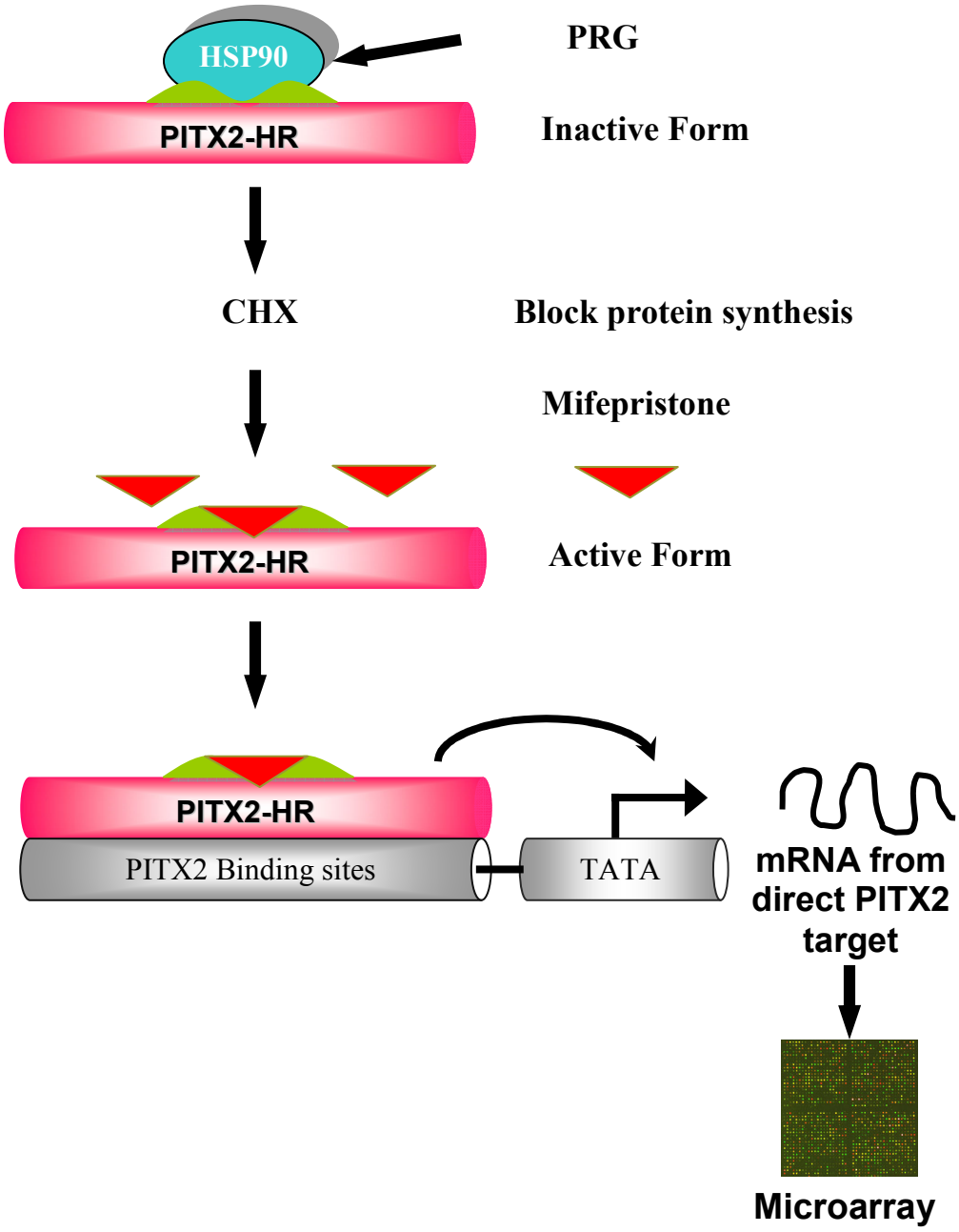
HSP90
PRG
PITX2-HR
Inactive Form
CHX
Block protein synthesis
Mifepristone
PITX2-HR
Active Form
PITX2-HR
PITX2 Binding sites
TATA
mRNA from direct PITX2 target
Microarray

Methods

Where not explicitly stated, the composition of all reagents used in the following procedures is found in Appendix A.

Hormone inducible constructs for PITX2

All constructs used in the procedures described in this chapter were expressed in the vector pcDNA4HisMaxA (Invitrogen).

HR-PITX2 (FOXC1ΔFHD▼ HD PRG)

PCR was used to amplify the homeobox domain (HD) of the wild type PITX2A. The PCR reaction of a total volume of 25µl contained 50ng DNA, 2.5µl 10x ThermoPol New England Biolabs (NEB) buffer, 2.5µl 2mM dNTPs, 0.125µl BSA (20µg/ml), 0.2µl T*aq* (NEB), 10 picomoles of forward and reverse primers (5'-GATCATGGGCCCCAAAGGCAGCGG-3' and 5'-ATGATCCGGACCGGGC TCCCTCTTTCTCCATTTG-3') and was cycled in a thermocycler for 35 cycles, with 67ºC annealing temperature. The PCR products were size-separated on a 1% agarose gel and purified using a QIAgen Gel Extraction kit. The HD fragment was cloned into pGEM T (Promega) vector using the manufacturer's protocol, and then subcloned in-frame into *Apa*I- *Rsr*II sites of pcDNAFOXC1-PRG (provided by Dr. Fred Berry), which is lacking the forkhead domain (FHD). The final construct was sequenced to ensure the integrity of the construct.

PITX2-PRGC

PITX2-PRGC was provided by Tim Footz. The progesterone binding domain (PRG) was inserted between the homeodomain and the C terminus of PITX2. A BstBI site was cloned in PITX2A wt pcDNAHisMax [130] between position 138 and 139 via site-directed mutagenesis. The PRG was PCR-cloned from pSWITCH vector (Invtrogen) and then cloned in-frame into the BstBI site of PITX2A wt.

Cell culture and transfection

Human Non-Pigmented Ciliary Epithelial (NPCE) cells were grown in Dulbecco's modified Eagle's medium (DMEM; Invitrogen, Burlington, ON) supplemented with 10 % heat inactivated fetal calf serum (Gemini Bioproducts, Calabasas, CA). Cells were transfected using Fugene6 transfection reagent (Roche) according to the manufacturer's protocol twenty four hours after the cells were plated. Fugene6 is a highly efficient transfection reagent being composed by a mixture of lipids. For protein expression, 4µg of plasmid DNA and 12µl of Fugene6 were used for a 100mm transfection plate. For luciferase assays, NPCE cells were transfected in 24-well plates using 160ng of PITX2 hormone-inducible construct or empty vector, 60ng of the pGL3- thymidine kinase (TK) promoter reporter plasmid (see below), 20ng of the pCMV beta-galactosidase transfection control plasmid and 3µl of Fugene6 transfection reagent. For RNA extraction, NPCE cells were transfected in 60mm well plates using 2µg PITX2 hormone-inducible construct or empty vector and 6µl of Fugene6 transfection reagent.

pGL3-TK was produced by replacing the SV40 promoter fragment of pGL3-SV40 vector [130] in HindIII and BglII sites with the TK promoter from pRL-TK vector (Promega).

Protein expression

Protein extraction was performed forty-eight hours after transfection to allow optimal expression of the recombinant proteins. The cells were washed three times with phosphate buffered saline (PBS) at room temperature and were collecting by scraping in 1ml PBS. The next steps were performed at 4ºC. A cell pellet was obtained by centrifugation at 3000g for 10 minutes. The supernatant was removed and the pellet was suspended in a lysis buffer containing protease inhibitors (PMSF and PIC). Samples were vortexed briefly and incubated on ice for 45 minutes. The lysates were centrifuged at 13 000g for 5 min at 4°C and assayed for total protein concentration using the Bradford assay. Western-blot analysis was performed using a mouse monoclonal anti-Xpress antibody (Invitrogen) against the pcDNA His/Max4 vector encoded N-terminal Xpress tag.

Transactivation assays

NPCE cells were cultured in 24-well plates at a density of $4x10^4$ cells/plate twenty four hours prior to transfection. Cells were transfected with HR-PITX2, PITX2- PRGC or empty expression vectors along with pGL3-TK and pCMV beta-galactosidase. At 36 hours post transfection, the cells were treated with either mifepristone (10^{-8} M) or 20% ethanol. Cells were harvested after forty eight hours

of incubation and luciferase activity was monitored following the manufacturer's protocol (Promega). Transactivations were performed in triplicates and repeated at least twice for confirmation.

Hormone-inducible expression system

NPCE cells were cultured in 60mm well plates at a density of $1x10^6$ cells/well 24 hours prior to transfection. Cells were transfected with HR-PITX2, PITX2-PRGC or empty expression vector. Once introduced into cells, these constructs remained in inactive form by being complexed with heat shock protein 90 (HSP 90), which binds to the steroid receptor. Cells were treated with cycloheximide (100μg/ml) 36 hours post-transfection to provide an enrichment of mRNA expressed directly in response to the transcription factor activation. Mifepristone (10^{-8} M) was added after one hour of the treatment with cycloheximide. In response to administration of the hormone, the transcription factor binds to the ligand and adopts a transcriptionally active form. RNA extraction was performed 12 hours post-induction.

RNA extraction

RNA extraction was performed twelve hours after induction by washing the cells twice in phosphate buffered saline (PBS), collecting the cells by scraping and lysing the cells in the presence of 1ml Trizol (Invitrogen). Lysates were homogenized by pipetting the lysate several times. The lysate was incubated at room temperature for 5 minutes. After addition of chloroform and vigorously

shaking, the homogenate was incubated at room temperature (2 min) and was then centrifuged (12000g, 15 min, 4°C). The upper aqueous phase was collected in a separate tube and 0.5ml isopropyl alcohol was added. The solution was incubated at room temperature for 10 minutes and then centrifuged (12000g, 10 min, 4°C). The pellet was resuspended in 1 volume of 70% ethanol and the solution was centrifuged (7500g, 5 min, 4°C). Finally, the RNA was resuspended with 50µl RNase-free water.

Microarray analysis

RNA extractions were performed in triplicates and subjected to microarray analysis. The Affymetrix Human Genome U133A microarray chips were hybridized at the Laval University, Quebec. Biotin-labeled cRNA was fragmented according to Affymetrix protocols. The fragmented cRNA from each sample was hybridized to individual Affymetrix U133A gene array chips, the hybridized chips were scanned, and a scaling factor was applied to each chip using the DNA-Chip Analyzer (D-CHIP) software to normalize the mean raw fluorescence intensity for each chip to an average base-line fluorescence level. D-CHIP is a statistical software package used to calculate fold changes between the hormone constructs and the control. Statistically significant differences ($p < 0.05$) in the average normalized fluorescence intensity of each transcript between the hormone-inducible constructs and the empty vector samples were determined. These analyses were done with the gracious help of members of Dr. Vincent Raymond

laboratory (Mr. Élie Deilhes did the microarray analysis and the data was analyzed by Mr. Pascal Belleau, graduate students in Dr. Raymond laboratory).

Computer based *in silico* analyses

The *in silico* tissue expression profile of each gene was determined via an electronic search of Stanford University database (http://genome-www5.stanford.edu/cgi-bin/source/sourceSearch). The search of PITX2 DNA binding motives (TAATCC, GGATTA, GGCTTAG or CTAAGCC) [153-155] on the upstream region of each gene was performed on Stanford University (http://genome-www5.stanford.edu/cgi-bin/source/sourceSearch) and EMBL - EBI -Sanger Institute (http://www.ensembl.org/index.html) websites. The gene functions were determined using GoSurfer software found on GoSurfer website (http://bioinformatics.bioen.uiuc.edu/gosurfer/).

Northern blot analysis

RNA samples were extracted from NPCE cells as described above. 25µg of RNA was denatured in formamide-based denaturing buffer and subjected to electrophoresis through a 1% agarose-formaldehyde gel. RNA was then transferred to positively charged nylon membrane and immobilized by UV crosslinking. The probes were digested from cDNA clones (Open Biosystems, Table 3-1), denatured (95°C sand bath, 5 min and on ice, 5 min) and then labeled with ^{32}P using a Random Primers Labeling Kit (Invitrogen). ExpressHyb solution (Clontech) was used for prehybridization (68°C for one hour) and hybridization (68°C for overnight) prior to washing with 2x SSC, 0.1 % SDS (room temperature

for 45 min) and 0.1 x SSC, 0.1% SDS (50°C for 45 min). Biomax film (Kodak, Rochester, NY) was then exposed to the northern blots for a minimum of 16 hours. Beta-actin was used as a probe to control for RNA loading according to the manufacturer's recommendations (Clontech).

Semi-quantitative reverse transcription–polymerase chain reaction (RT-PCR)

RNA samples were extracted from NPCE cells as described above. Total RNA was used as a substrate for semi-quantitative reverse transcription–polymerase chain reaction (RT-PCR). A standard 20µl reverse transcription recipe contained the following components: 2µg total RNA, 500ng oligo d(T), 0.5mM dNTPs, 1x First Strand Buffer, 0.01M DTT, 40U RNaseOUT, 200U reverse transcriptase (Invitrogen). cDNA specific PCR primers were designed using Integrated DNA Technologies website (http://www.idtdna.com/Home/Home.aspx) or Primer3 Output Program on the Whitehead Institute for Biomedical Research web page (http://www.Genome.wi.mit.edu) and are shown in Table 3-2. Reactions were cycled in a thermocycler for 28 cycles. PCR products were separated using agarose gel electrophoresis and visualized with ethidium bromide. 200ng RNA corresponding to each construct (empty vector, HR-PITX2 or PITX2-PRGC) were used in 25µl PCR as negative controls. Beta-actin was used as "input" control according to the manufacturer's recommendations (Clontech).

Table 3-1.	DNA Probes used in Northern Blot Analysis				
Gene	**Gene Symbol**	**OpenBiosystems Catalog Nr**	**Restriction Sites**	**Vector**	**Product Size (bp)**
Coatomer protein complex, subunit gamma 2	COPG2	MHS1011-74920	EcoRV/SacI	pOTB7	710
High density lipoprotein binding protein (vigilin)	HDLBP	MHS101159883	EcoRI/NotI	pOTB7	500
Kelch-like 3	KLHL3	MHS1010-7295124	BamHI/EcoRV	pBluescriptR	654
Nucleoporin 133kDa	NUP133	MHS1010-58232	NcoI/XbaI	pCMV-Sport6	897
Poly (ADP-ribose) polymerase family, member 2	PARP2	EHS1001-24041	BamHI/EcoRV	pBluescriptR	596
Pyruvate dehydrogenase phosphatase isoenzyme 2	PDP2	EHS1001-5723374	NotI/PstI	pCMV-Sport6	1187
Phosphatidylglycerophosphate synthase 1	PGS1	MHS1011-7509250	AvaI	pOTB7	796
Protein C receptor, endothelial (EPCR)	PROCR	MHS1011-76703	XhoI/XbaI	pOTB7	456
Regulating synaptic membrane exocytosis 4	RIMS4	EHS1001-28668	Bsu36I	pBluescriptR	543
Solute carrier family 13 member 3	SLC13A3	MHS1011-7509920	BanI	pDNR-LIB	585
Tectorin beta	TECTB	EHS1031-322067	EcoRI	pT7T3D-Pac	356
Translocase of inner mitochondrial membrane 10 homolog	TIMM10	MHS1011-7509016	EcoRI/XhoI	pOTB7	688
Tolloid-like 2	TLL2	EHS1031-315512	NotI/EcoRI	pT7T3D-Pac	545
Transmembrane protease, serine 2	TMPRSS2	MHS1010-9205475	MscI	pCMV-Sport6	733
	ZNF652	EHS1001-17930	EcoRI	pBluescriptR	765

Table 3-2.		**Primers used for RT-PCR (IDT)**		
Gene	**Gene Symbol**	**Forward (5'-3')**	**Reverse (5'-3')**	**Product size (bp)**
Kelch-like 3	KLHL3	CAACTTGGCTTCGGTGGAGTA	AGTCAGAGGAGAGCGGTTCTC	251
Poly (ADP-ribose) polymerase family,member 2	PARP2	GCCAATCCTAAGGCCGAAGGA	CGCATACGGACCTGGTTGGGG	211
Phosphatidylglycerophosphate synthase 1	PGS1	GCAGCCGAGTCGCCAGGTGAA	ACCCGAGGGCTTTAGCTGAGC	403
Protein C receptor, endothelial (EPCR)	PROCR	GCACTCGGTATGAACTGCGGG	ATCAGCGTCCCATCCCAAGTC	440
Solute carrier family 13 member 3	SLC13A3	GGACACTTGCTGGTCAAAGAC	ATGGCTCATGGACTTGAGTGG	360
Tectorin beta	*TECTB	GGGCAGAGAATAGCACTTTGC	GCAGTACTTGGTTGGGTCTGC	231
Tolloid-like 2	*TLL2	TTGTAAGTTTGGCCAACAAGG	TGGGCCACACATTAGTCTCG	287
Transmembrane protease, serine 2	*TMPRSS2	CTGGCTTGGCACTCTCTGC	GTGCCACCTGGCTGTCTCC	279
ZNF652	ZNF652	GTGCCAGTGGTGTGGCAAGGA	CATAGAGGCCAGAGTGAGGAC	380

* Primers generated by the **Primer3 Output Program**

Results

Construction and validation of the hormone-inducible forms of PITX2

Two hormone-inducible constructs were built for PITX2. In one construct, PITX2-PRGC, the ligand binding domain of the progesterone human receptor was inserted 40 amino acids C-terminal to the homeobox of PITX2A (Figure 3-2). The resulting construct encodes a protein of 546 amino acids with a predicted molecular mass of 65.5kDa. In the second construct, HR-PITX2, FOXC1-PRG was used as a backbone. The inhibitory domain of FOXC1 was replaced with the progesterone binding domain (PRG), and the forkhead domain (FHD) of FOXC1 was replaced with the homeodomain (HD) of PITX2 (Figure 3-2). The resulting construct encodes a protein of 588 amino acids with a predicted molecular 70.5kDa. In order to do the hormone inducible expression systems coupled to microarray analysis, the hormone constructs of PITX2 needed to be expressed in the cells and be able to activate transcription of a synthetic PITX2 reporter in the presence of mifepristone. As shown in Figure 3-3, both constructs produced proteins of the appropriate molecular weight in transfected NPCE cells and transactivated the luciferase reporter gene 4-fold more than transfection with the empty vector, after administration of mifepristone. However, in the absence of the mifepristone, HR-PITX2 and PITX2-PRGC were unable to activate transcription of the synthetic PITX2 reporter.

Figure 3-2. Schematic representation of the two hormone-inducible constructs of PITX2. Top: FOXC1 and PITX2A wild type. FOXC1 and PITX2A contain a forkhead domain (FHD) and a homeodomain (HD), respectively, each responsible for DNA-binding. FOXC1 has a transcriptional inhibitory domain, regulated by phosphorylation. The OAR region of PITX2 mediates protein-protein interaction. **Bottom:** The progesterone-binding domain (PRG) was either inserted between the HD and the C-terminus of PITX2 (PITX2-PRGC) or replaced the inhibitory domain of FOXC1 (HR-PITX2). In the HR-PITX2, the FHD of FOXC1 was replaced with the HD of PITX2.

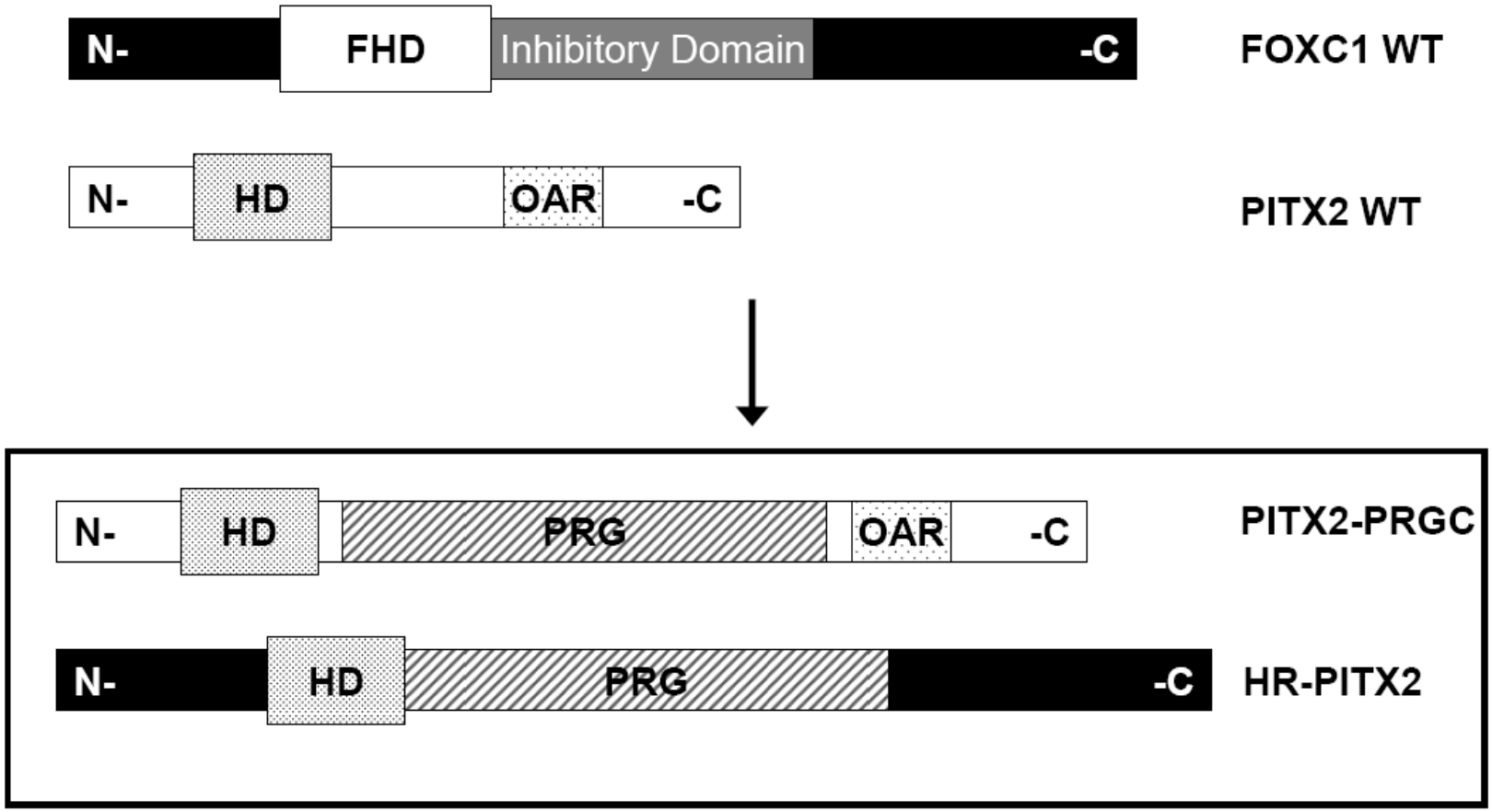
N-
FHD
Inhibitory Domain
-C
FOXC1 WT
N-
HD
OAR
-C
PITX2 WT
N-
HD
PRG
OAR
-C
PITX2-PRGC
N-
HD
PRG
-C
HR-PITX2

Figure 3-3. Top: The status of both hormone constructs of PITX2 in NPCE cells. The two hormone-responsive constructs produced proteins of the appropriate molecular weight in transfeted NPCE cells**. Bottom:** The two hormone-responsive constructs for PITX2 transactivated luciferase gene promoter after administration of mifepristone (* $p<0.05$)**.**

Protein expression in NPCE cells

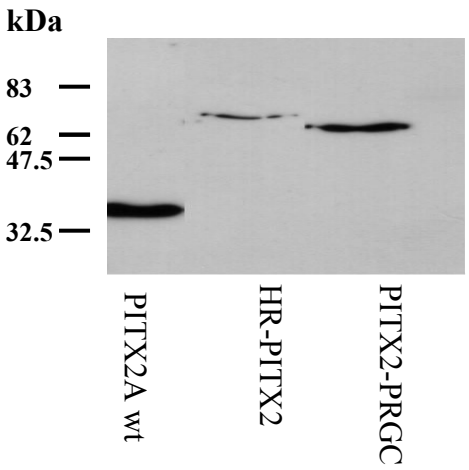

Luciferase reporter assay in NPCE cells

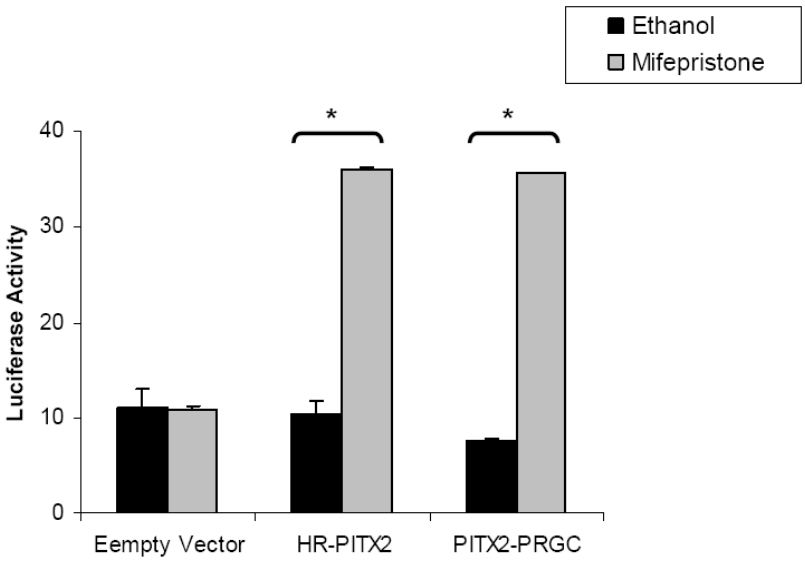

Hormone-inducible expression system and microarray results

Preliminary experiments in NPCE cells indicated that mifepristone induced HR-PITX2 and PITX2-PRGC activation. The two hormone-inducible constructs of PITX2 were then used in the hormone-inducible expression system as described in the methods. For controls, cells were transfected with an empty expression vector and treated in an identical manner with cycloheximide and mifepristone. Total RNA samples collected from three independent experiments were subjected to microarray analysis. Affymetrix U133 human chip containing representations of more than 39,000 gene transcripts (45,038 probe sets) was used in the study. The gene expression profile of NPCE cells transfected with the hormone-inducible constructs of PITX2 was directly compared to that of NPCE cells transfected with the empty vector. The genes differentially expressed at least one fold and a half with a p- value lower than 0.05 were further analyzed. Analysis of the 45,038 probe sets identified 448 genes differentially regulated in response to HR-PITX2 and 97 genes differentially regulated in response to PITX2-PRGC. Forty seven genes overlapped between the data sets for the two hormone-inducible constructs of PITX2. Dr. Fred Berry, who developed and used the hormone-inducible expression system for FOXC1, identified altered expression of 2010 genes in the presence of induced FOXC1. Ten genes displayed altered expression in the presence of all three hormone-inducible constructs: FOXC1-PRG, HR-PITX2 and PITX2-PRGC respectively (Figure 3-4).

Figure 3-4. Outline of the microarray results. Venn diagrams show the overlapping data sets of microarray results between the three hormone inducible constructs: FOXC1-PRG, HR-PITX2 and PITX2-PRGC.

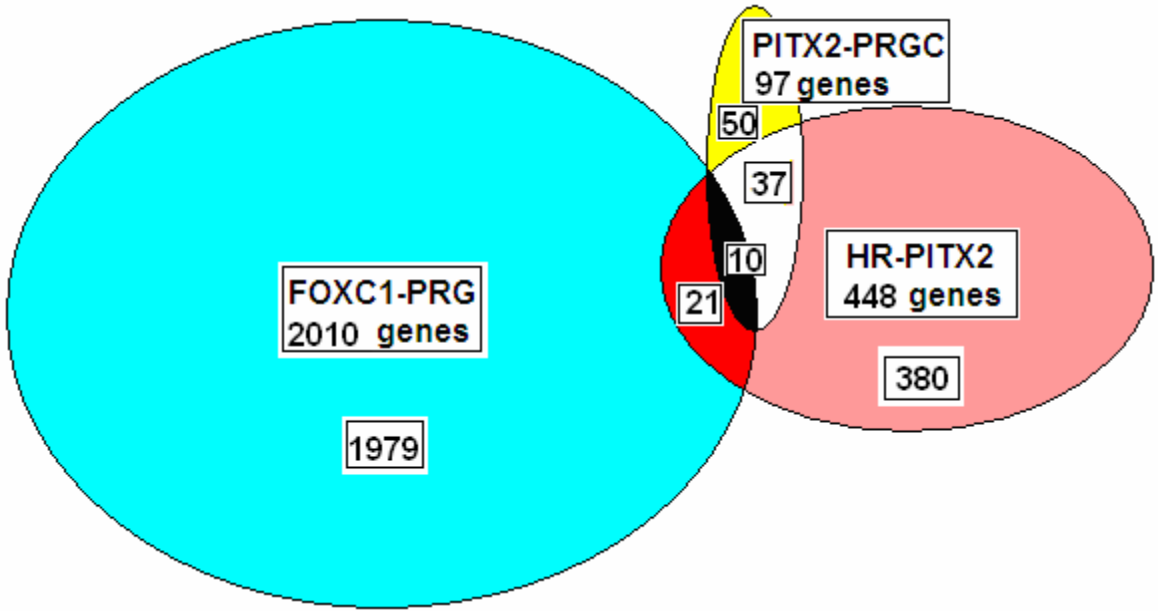
PITX2-PRGC
97 genes
50
37
10
21
HR-PITX2
448 genes
380
FOXC1-PRG
2010 genes
1979

In summary, from 448 genes differentially regulated in response to HR-PITX2, 391 genes were found to be upregulated and 57 genes were downregulated in the presence of HR-PITX2 compared to the empty vector. From 97 genes differentially regulated in response to PITX2-PRGC, 77 genes were found to be upregulated and 20 genes were downregulated in the presence of PITX2-PRGC compared to the empty vector.

Validation of the putative PITX2 target genes

In the present study, the genes with altered expression in the presence of both hormone-inducible constructs of PITX2 have been chosen for further analysis. The genes with significantly altered expression in multiple microarray experiments have been selected for validation. Six genes out of 47 were unknown and were excluded from the study. The first step in the validation process was to select genes that were expressed in eye tissues and that contain consensus PITX2 DNA binding sequences in the 5' upstream region of the gene. Forty one genes that presented an altered response to both HR-PITX2 and PITX2-PRGC were analyzed. *In silico* analysis revealed 33 genes out of 41 (80.5%) were expressed in the eye tissues and 39 genes out of 41 (95.1%) had PITX2 binding sequences in their upstream region. The ten genes that showed altered expression in the presence of the three hormone-inducible constructs, FOXC1-PRG, HR-PITX2 and PITX2-PRGC, were excluded from this study as being part of a different project in the Walter laboratory. The chromosomal locations, gene names, gene symbols, Affymetrix identification, eye expression and the presence of PITX2

DNA binding sites in the 5' upstream region of the forty seven genes are summarized in Table 3-3.

In total, 15 were selected for the next step of validation. These genes were expressed in the eye, had PITX2 DNA binding sites in the promoter region, and had known cellular function. The functions of the 15 genes selected for further analysis are presented in Table 3-4.

Among the 47 genes with altered expression in the presence of both hormone-inducible constructs of PITX2, two genes (*C20ORF133* and *PARP2*) have the chromosomal location within glaucoma loci (Table 1-1, Chapter 1). *C20ORF133* was not selected for further analysis because of unknown expression profile and unknown cellular function.

The second step of the validation was to confirm the altered expression in response to PITX2 induction by an independent method such as northern blot analysis or semi-quantitative RT-PCR.

Northern analysis and semi-quantitative RT-PCR results

Northern blots analysis of the fifteen genes (*COPG2, HDLBP, KLHL3, NUP133, PROCR, PGS1, PARP2, PDP2, RIMS4*, *SLC13A3, TECTB, TLL2, TIMM10, TMPRSS2* and *ZNF652*; Table 3-4) was performed to further confirm the results of microarray analysis. The RNA levels of six genes (*COPG2, HDLBP, NUP133, PDP2, RIMS4* and *TIMM10*) were elevated in the presence of HR-PITX2 and PITX2-PRGC compared with the empty vector (Figure 3-5). Northern blot analysis of these six genes detected RNA transcripts of the expected

size (Figure 3-5). Nine genes (*KLHL3, PARP2, PROCR, PGS1, SLC13A3, TECTB, TLL2, TMPRSS2* and *ZNF652*) either did not display altered expression or no bands were detected on the X-Ray film. Four genes (*PROCR, PGS1, SLC13A3* and *ZNF652*) (Figure 3-6) demonstrated upregulated expression in the presence of PITX2, whereas five genes (*KLHL3, PARP2, TECTB, TLL2* and *TMPRSS2*) did not show any altered expression in response to PITX2 induction RT–PCR. In total, ten genes showed altered expression (Figure 3-7) in response to PITX2 induction either by northern blot analysis or by semi-quantitative RT-PCR. Northern blotting was used as the first step in validation because northern blot analysis allows a direct comparison of the messenger RNA abundance between samples on a single membrane. However, this technique is not sensitive enough to detect low-level gene expression and not accurate enough to quantify the full range of gene expression. Semi-quantitative RT–PCR was used for the nine genes that were not validated by northern blot analysis. However, RT-PCR is not used as a first step method because of its limitations. Several variables that influence amplification, such as PCR cycling conditions, concentration of the reactives or oligonucleotide composition, might affect the quality of RT-PCR. Moreover, due to the sensitivity of RT–PCR, very small amounts of genomic DNA contamination in an RNA preparation may serve as a template for amplification and produce artefactual results.

Table 3-3. List of genes with altered expression in the presence of both hormone-inducible constructs of PITX2.

Gene name	Gene symbol	Affymetrix ID	Locus	Eye Expression	PITX2 BS
Apolipoprotein C-IV	APOC4	206738_at	19q13.32	unknown	unknown
ATP synthesis coupled proton transport	ATP6V0D2	1553153_at	8q21.1	no	yes
CDNA clone IMAGE:4794631		1554224_at	11q24.2	unknown	unknown
Chromosome 20 open reading frame 133	C20ORF133	1553564_at	20p12.1	yes	yes
Chromosome 9 open reading frame 116	C9ORF116	221946_at	9q34.3	yes	yes
Chromosome 8 open reading frame 74	C8orf74	1569245_at	8p23.1	yes	unknown
Coatomer protein complex, subunit gamma 2	COPG2	222298_at	7q37	yes	yes
Chromosome X open reading frame 33	CXORF33	222269_at	Xq21.1	yes	yes
DKFZp761B107 protein	DKFZP761B107	1553839_at	4p15.2	yes	yes
E74-like factor 2	ELF2	203822_s_at	2q32.1	yes	yes
Family with sequence similarity 13, member A1	FAM13A1	202972_s_at	4q22.1	yes	yes
Fibrillin 1 (Marfan syndrome)	FBN1	202765_s_at	15q21.1	yes	yes
Hect domain and RLD 2 pseudogene	LOC440366	16196_at	16p11.2	unknown	yes
High density lipoprotein binding protein (vigilin)	HDLBP	235624_at	2q37	yes	yes
Clone IMAGE:5170503, mRNA		1563069_at	21q23	unknown	unknown
Hyaluronoglucosaminidase 4	HYAL4	220249_at	7q31.32	no	yes
Hypothetical LOC401093	LOC401093	235173_at	3q25.1	unknown	unknown
Insulin-like growth factor 2 mRNA binding protein 2	IGF2BP2	223963_s_at	3q27.2	yes	yes
Kelch-like 3 (Drosophila)	KLHL3	1555110_a_at	5q31.2	yes	yes
KIAA1652 protein	KIAA1652	230880_at	22q11.21	yes	yes
KIAA1840	KIAA1840	232403_at	15q14	yes	yes
Leptin (obesity homolog, mouse)	LEP	207092_at	7q31.3	no	yes
Melatonin receptor 1A	MTNR1A	221369_at	4q35.2	no	yes
Mitogen-activated protein kinase kinase 5	MAP2K5	211371_at	15q23	yes	yes
Myosin binding protein C, cardiac	MYBPC3	208040_s_at	11p11.2	no	yes
Nucleoporin 133kDa	NUP133	236905_at	1q42.13	yes	yes

Table 3-3. Continued.					
Poly (ADP-ribose) polymerase family, member 2	PARP2	204752_x_at	14q11.2-q12	yes	yes
Progesterone receptor	PGR	208305_at	11q22.1	no	yes
Pyruvate dehydrogenase phosphatase isoenzyme 2	PDP2	232861_at	16q22.1	yes	yes
Phosphatidylglycerophosphate synthase 1	PGS1	227906_s_at	17q25.3	yes	yes
Protein C receptor, endothelial (EPCR)	PROCR	203650_at	20q11.22	yes	yes
3-phosphoinositide dependent protein kinase 1 pseudogene	PDPK2	244630_at	16p13.3	yes	yes
Regulating synaptic membrane exocytosis 4	RIMS4	233299_at	20q13.12	yes	yes
Sal-like 4 (Drosophila)	SALL4	229661_at	20q13.2	no	yes
Solute carrier family 13 member 3	SLC13A3	205244_s_at	20q12-q13.1	yes	yes
Similar to hypothetical protein	MGC33657	237151_s_at	2q14.2	yes	yes
Tectorin beta	TECTB	1553656_at	10q25-q26	yes	yes
Translocase of inner mitochondrial membrane 10 homolog (yeast)	TIMM10	1555764_s_at	11q12.1-q12.3	yes	yes
Tolloid-like 2	TLL2	215843_s_at	10q23-q24	yes	yes
Transmembrane protease, serine 2	TMPRSS2	226553_at	21q22.3	yes	yes
Transcribed locus		239051_at	10q11.21	unknown	unknown
Transcribed locus		241879_at	3q28	unknown	unknown
X-ray repair complementing defective repair in Chinese hamster cells 4	XRCC4	210812_at	5q14.2	yes	yes
Zinc finger protein 236	ZNF236	222227_at	7q32.3	yes	yes
Zinc finger protein 652	ZNF652	205594_at	17q21.32	yes	yes
Unknown		207915_at	Xq22.3	unknown	unknown

	Genes with altered expression in the presence of FOXC1-PRG, HR-PITX2 and PITX2-PRGC

PITXBS- PITX2 Binding Sites presented in the promoter region

Table 3-4. The fifteen genes chosen for further analysis and their function.

Gene name	Gene symbol	Function
Coatomer protein complex, subunit gamma 2	COPG2	Transport-protein, retrograde Golgi to ER
High density lipoprotein binding protein (vigilin)	HDLBP	RNA binding, nucleic acid binding, lipid transport and metabolism
Kelch-like 3	KLHL3	Protein binding
Nucleoporin 133kDa	NUP133	mRNA export from nucleus, nucleocytoplasmic transport
Poly (ADP-ribose) polymerase family, member 2	PARP2	DNA binding, DNA repair, ribosyltransferase activity
Pyruvate dehydrogenase phosphatase isoenzyme 2	PDP2	Phosphatase activity, hydrolase activity, catalytic activity, ion binding (Mg)
Phosphatidylglycerophosphate synthase 1	PGS1	Catalytic activity, metabolism
Protein C receptor, endothelial (EPCR)	PROCR	Receptor activity, inflamatory response, blood coagulation
Regulating synaptic membrane exocytosis 4	RIMS4	Exocytosis activity, neurotransmitter transporter
Solute carrier family 13 member 3	SLC13A3	Transport-protein, retrograd Golgi to ER
Tectorin beta	TECTB	Transporter activity, ion transporter
Translocase of inner mitochondrial membrane 10 homolog	TIMM10	Protein transport
Tolloid-like 2	TLL2	Proteolysis, ion binding (Ca, Zn)
Transmembrane protease, serine 2	TMPRSS2	Peptidase activity, hydrolase activity, proteolysis, receptor activity
Zinc finger protein 652	ZNF652	Nucleic acid binding, zinc ion binding

Figure 3-5. Northern blot hybridization analysis of the putative PITX2 target genes. Each lane contains approximately 25 μg of total RNA extracted from NPCE cells transfected with empty vector, HR-PITX2 and PITX2-PRGC. Transcript sizes for each gene are indicated in the figure. β-Actin was used as control probe of the same blots.

Lane 1: Empty vector, *Lane 2*: HR-PITX2 and *Lane 3*: PITX2-PRGC

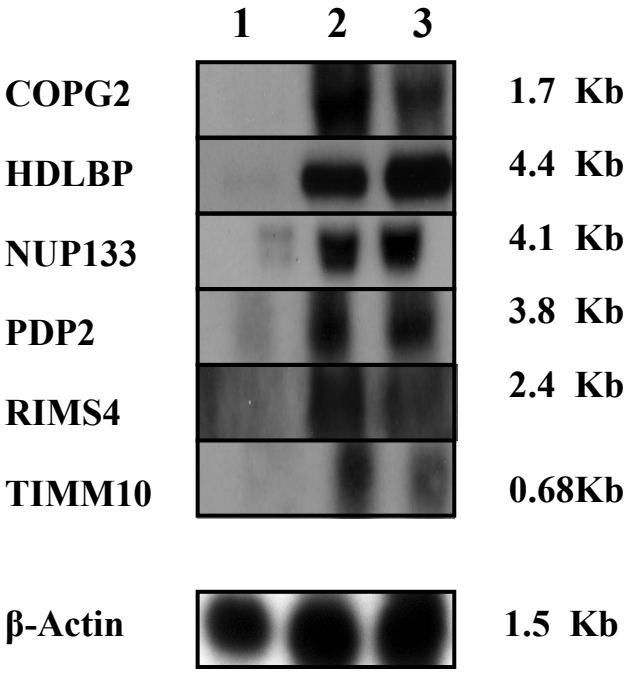

COPG2, Coatomer protein complex, subunit gamma 2

HDLBP, High density lipoprotein binding protein (vigilin)

NUP133, Nucleoporin 133kDa

PDP2, Pyruvate dehydrogenase phosphatase isoenzyme 2

RIMS4, Regulating synaptic membrane exocytosis 4

TIMM10, Translocase of inner mitochondrial membrane 10 homolog

Figure 3-6. Reverse transcription analysis of putative PITX2 target genes. PCR reactions were performed using 28 cycles and the products were separated by size on an agarose gel. Total RNA was extracted form NPCE cells transfected with empty vector, HR-PITX2 and PITX2-PRG and 2μg of total RNA was used in a standard of 20μl reverse transcription reaction.

Lane 1: H_2O control. *Lane 2*: empty vector RNA. *Lane 3*: HR-PITX2 RNA. *Lane 4*: PITX2-PRGC RNA. *Lane 5*: empty vector RT-PCR. *Lane 6*: HR-PITX2 RT-PCR. *Lane 7*: PITX2-PRGC RT-PCR.

β-Actin c-DNA primers were used in positive control reactions to verify the integrity. *Lanes 2-4* are used as negative controls

.

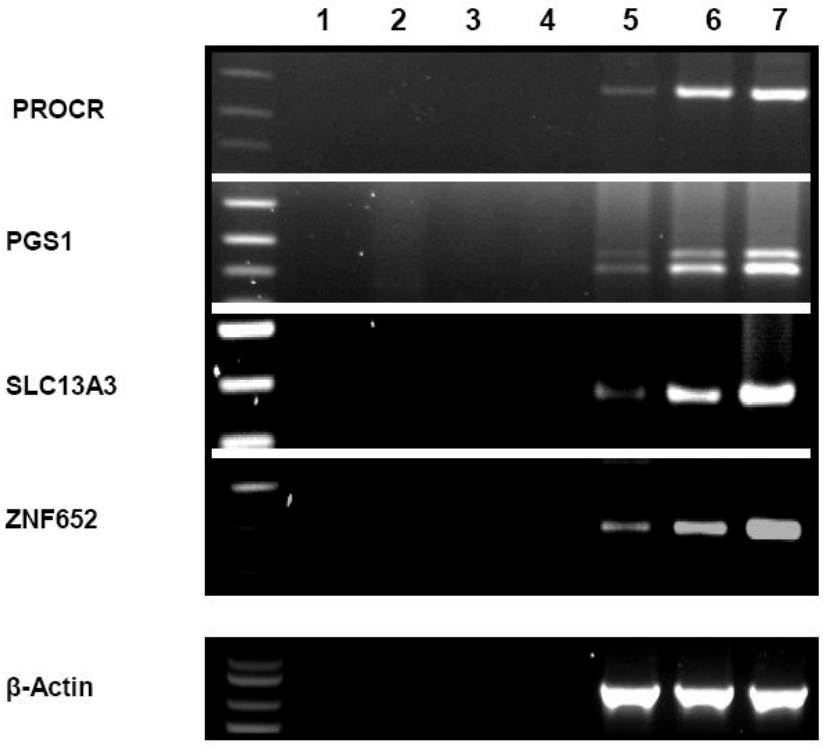

PROCR, Protein C receptor, endothelial (EPCR)

PGS1, Phosphatidylglycerophosphate synthase 1

SLC13A3, Solute carrier family 13 member 3

ZNF652, Zinc finger protein 652

Figure 3-7. Summary of the northern blot analysis and semi-quantitative RT-PCR resluts. From fifteen putative PITX2 genes chosen for validation, ten genes displayed altered expression (positive results) and five genes did not display altered expression (negative results) in response to PITX2 induction.

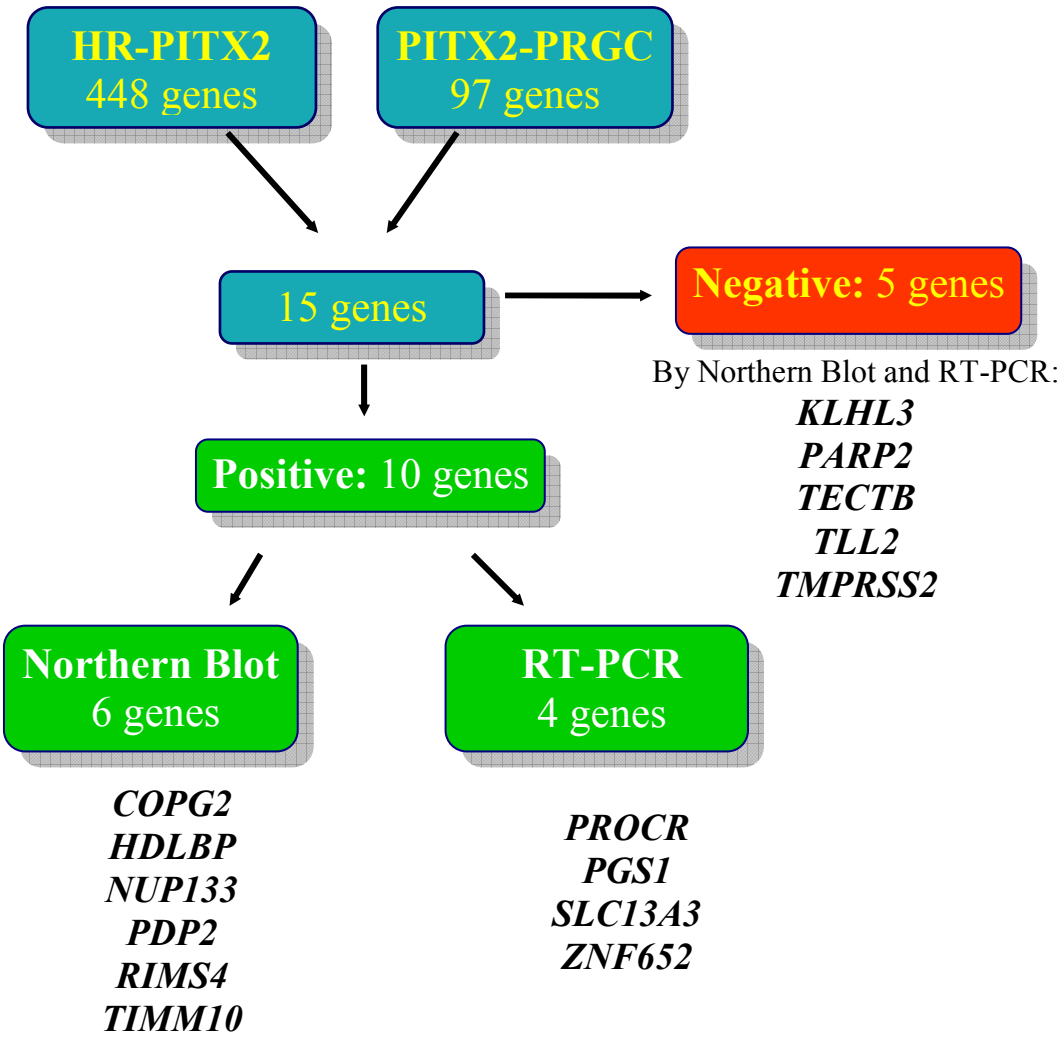
HR-PITX2
448 genes
PITX2-PRGC
97 genes
15 genes
Negative: 5 genes
By Northern Blot and RT-PCR:
KLHL3
PARP2
TECTB
TLL2
TMPRSS2
Positive: 10 genes
Northern Blot
6 genes
RT-PCR
4 genes
COPG2
HDLBP
NUP133
PDP2
RIMS4
TIMM10
PROCR
PGS1
SLC13A3
ZNF652

Discussion

Identification of the target genes using hormone inducible expression system

In the current study, I used the hormone-inducible expression system method to isolate candidate target genes of PITX2. The use of this method has several advantages, one important advantage being identification of direct PITX2 target genes through cycloheximide treatment. Using this method, secondary induction events are eliminated as cycloheximide inhibits any new proteins from being expressed. Prevention of new protein synthesis provides an enrichment of mRNA expressed directly in response to PITX2 activation. In this way, only genes directly regulated by PITX2 are identified. Another advantage is the use of the hormone chimeras. Two inducible PITX2 proteins were built where the truncated form of the progesterone receptor was inserted. The truncated form of the progesterone receptor has advantages over other steroid hormone receptors such as estrogen or glucocorticoid by no having biological effect in ocular tissues. Furthermore, this receptor binds with very high affinity to the synthetic steroid mifepristone. Mifepristone allows activation of genes through specific induction of the PITX2 hormone constructs, but prevents activation of genes through endogenous progesterone receptors. Another advantage is that gene-expression profiles are compared by microarray analysis making hormone-inducible expression system a powerful method used in identifying genes. Over the last decade, microarray technology has become one of the most powerful approaches for dissecting the regulatory mechanism and transcriptional networks that underlie biological processes.

To distinguish the changes in gene expression that occur in response to the transcription factor activation versus the changes that occur from adding the steroid hormone and cycloheximide, we compared the HR-PITX2 and PITX2-PRGC RNA with RNA extracted from cells transfected with empty vector and treated with cycloheximide and mifepristone. In this way, we know that the changes in gene expression occurred in response to PITX2 and not in response to the drug treatment.

However, like all sophisticated techniques, the hormone-inducible expression system has some limitations. One limitation is that the fusion of the protein with hormone binding domain could disrupt the function of the protein. To overcome this limitation, I used two different hormone constructs of PITX2: HR-PITX2 built on FOXC1-PRG backbone and PITX2-PRGC built on PITX2 structure. The overlapped data sets were chosen for further analysis. In total 47 genes were identified to have altered expression in response to both PITX2 constructs, the analysis of these 47 genes became the high priority of my project. The results obtained by microarray analysis also suggest that the two constructs are not entirely equivalent, and further work using validation experiments of more genes would be required to determine if they are equivalent or not. Another disadvantage of this method may be the isolations of false positives due to an overexpression of protein by adding too much of the hormone which can lead to different cascade gene activation. This limitation is mainly due to transient transfection, and therefore, the choice of an appropriate cell line and an appropriate control are necessary to overcome this difficulty. Human NPCE cells

were chosen to be used in the hormone-inducible expression system, because these cells express both FOXC1 and PITX2, which allows both general and tissue specific targets of FOXC1 and PITX2 to be identified. Moreover, NPCE cells are implicated in 80-90% of the aqueous humor production [4], as a consequence these cells may have important roles in glaucoma pathology. I used an empty vector as negative control to avoid harvesting nonspecific target genes. Cells were transfected with the empty expression vector and treated with an identical regimes of cycloheximide and mifepristone.

The hormone expression system coupled with microarray analysis was successfully used in isolating PITX2 target genes in NPCE cells. 89% of the 498 gene identified in our array turned out to be upregulated in the presence of PITX2. This outcome of this study suggests that a fairly extensive upregulation is the main gene expression change associated with PITX2.

Fifteen genes were further selected for validation on the basis of their expression in the eye, putative binding sites of PITX2 in the upstream region, and their function. Ten genes out of fifteen showed altered expression (Figure 3-7) either by northern blot or by semi-quantitative RT-PCR, suggesting that these ten genes are true target genes regulated by PITX2 in the eye. Five genes that showed altered expression in the presence of PITX2 in microarray analysis did not present any altered expression in northern blot and RT-PCR experiments. These results confirmed that microarray analysis may give false positive results and that an independent method is needed to confirm the microarray results.

The results presented in this chapter showed that the hormone-inducible expression system was successfully used to identify PITX2 and FOXC1 [104] target genes. As a result we propose that this method can be used for any other transcription factor to isolate genes.

FOXC1 and PITX2 involved in the same pathway

Overall the microarray analysis showed the expression of 2010 genes to be altered by activation of FOXC1 and that of 498 genes altered by activation of PITX2. Notably, thirty-one genes showed altered expression in the presence of both FOXC1 and PITX2. The similar expression patterns of *PITX2* and *FOXC1* during development, the similar phenotypes caused by defects in *PITX2* and *FOXC1* and the direct interaction between FOXC1 and PITX2 [64] demonstrated that both genes have same common biological roles in eye development and function. Results presented in this study provide further evidence that at least a part of the gene pathway of these two proteins is common. It will be interesting to see the effects of FOXC1-PITX2 interaction on genes that are both FOXC1 and PITX2 target genes. The analysis of the genes regulated by both proteins will improve the understanding of the link between FOXC1 and PITX2 and of how mutations of these two transcription factors cause the same disease.

Roles of genes regulated by PITX2

Gene ontology analysis [156] was performed to provide a broad view of the probable physiological functions of the genes differentially regulated in response

to PITX2. As shown in Figure 3-8 and Table 3-5, some genes look promising as their functions are relevant to the Axenfeld-Rieger Syndrome and glaucoma pathology. Oxidative stress induces apoptosis in the anterior eye structures, and also induces progressive loss of optic nerve axons and retinal ganglion cells (RGCs), resulting in characteristic optic nerve atrophy, visual field defects and elevated IOP in glaucoma patients [157, 158]. Genes regulated by PITX2 involved in response to stress and in regulation of apoptosis may have key roles in glaucoma pathology. Our hypothesis is that changes in the expression of these target genes, and therefore the activities of their proteins, are what impair the resistence to cellular stress and apoptosis by increasing the sensitivity of the cells to oxidative stress, leading to impaired anterior segment outflow in PITX2-associated glaucoma.

Genes implicated in cell adhesion, cell-cell signaling or neurogenesis may be involved in multiple developmental processes, including cell migration and axon growth. Thus, the altered expression of these genes may explain both the ocular and systemic AR phenotypes which result from disruption of migration and differentiation processes specific to the neural crest (NC) lineage [64, 91]. Genes implicated in cell proliferation may be also important into the ARS pathology. For example, in the gain of function of PITX2, these genes may promote cell proliferation, explaining for example the peripheral anterior synechiae (PAS), ocular defect frequently found in ARS patients.

Genes involved in immune response might initiate or contribute to the progression of glaucoma. The expression of inflammatory molecules in aged

tissues is believed to result from the production of reactive oxygen species (ROS) and free-radical chain reactions generated from lipid peroxidation [159]. The generation of ROS, which may initiate or contribute to the progression of glaucoma, is likely to occur in the NPCE and TM (trabecular meshwork), cells constantly exposed to an oxidative environment [160, 161]. Indeed, decreased antioxidant potential [162, 163], increased expression of oxidative stress markers [163], as well as increased oxidative DNA damage [164] and peroxized lipids [165] have been described in the TM of glaucoma patients.

Interestingly, the microarray analysis revealed that two genes, *C20ORF133* and *PARP2*, located within the glaucoma loci have altered expression in the presence of both induced hormone constructs of PITX2. These results confirmed furthermore the implication of PITX2 in glaucoma pathology. *C20ORF133* was not selected for further analysis, because of its unknown expression profile and unknown cellular function. Semi-quantitative RT-PCR or northern blotting failed to confirm *Poly (ADP-ribose) polymerase family, member 2* (PARP2) to be a true target gene of PITX2.

In summary, I have identified for the first time target genes of PITX2 in ocular tissues. This study did not reveal previously identified target genes of PITX2 in other tissues such as heart, tooth or pituitary (Table 1-2), suggesting a different role of PITX2 in the eye than other organs.

Knowledge of the identity of the PITX2-regulated genes described in this chapter is a key step in understanding the gene-regulatory pathways in the eye. Nevertheless, understanding these pathways has profound implications for

treating the glaucoma, these target genes becoming candidates for therapies based upon the processes in which they function.

Figure 3-8. GoSurfer analysis of differentiately regulated genes by both hormone constructs of PITX2. The genes with altered expression were analyzed by GoSurfer according to biological process.

Biological process functions

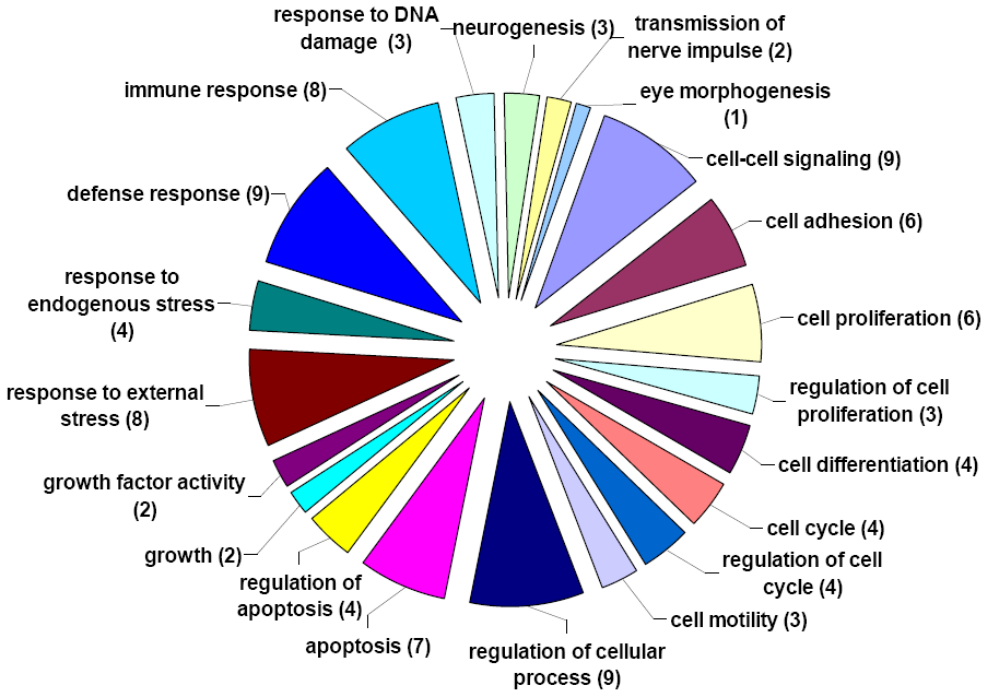

Table 3-5. Genes involved in biological process	
Function	**Gene name**
cell-cell signaling (9)	myelin protein zero-like 1
	a disintegrin and metalloproteinase domain 17
	thyrotropin-releasing hormone
	neuregulin 2
	leptin
	glycine receptor, alpha 2
	chemokine (C-C motif) ligand 17
	Indian hedgehog homolog
	BAI1-associated protein 3
cell adhesion (6)	myosin binding protein C, cardiac
	CD6 antigen
	amyloid beta (A4) precursor protein
	protein tyrosine phosphatase, receptor type, F
	claudin 1
	contactin associated protein 1
cell proliferation (6)	growth arrest-specific 7
	Mdm2, transformed 3T3 cell double minute 2
	colony stimulating factor 1 (macrophage)
	transcription factor Dp family, member 3
	CSE1 chromosome segregation 1-like
	neurofibromin 1
regulation of cell proliferation (3)	Mdm2, transformed 3T3 cell double minute 2
	colony stimulating factor 1 (macrophage)
	neurofibromin 1
cell differentiation (4)	suppressor of cytokine signaling 2
	colony stimulating factor 1
	pre-B-cell leukemia transcription factor interacting protein 1
	core promoter element binding protein

Table 3-5. Continued	
cell cycle/ regulation of cell cycle (4)	growth arrest-specific 7
	Mdm2, transformed 3T3 cell double minute 2
	transcription factor Dp family, member 3
	neurofibromin 1
cell motility (3)	autocrine motility factor receptor
	troponin I, skeletal, slow
	myosin binding protein C, cardiac
regulation of cellular process (9)	huntingtin
	suppressor of cytokine signaling 2
	CD27-binding (Siva) protein
	Mdm2, transformed 3T3 cell double minute 2
	neuregulin 2
	colony stimulating factor 1 (macrophage)
	core promoter element binding protein
	neurofibromin 1
	caspase 8, apoptosis-related cysteine protease
apoptosis (7)	huntingtin
	TNF receptor-associated factor 4
	CD27-binding (Siva) protein
	neuregulin 2
	CSE1 chromosome segregation 1-like
	caspase 8, apoptosis-related cysteine protease
	amyloid beta (A4) precursor protein
regulation of apoptosis (4)	huntingtin (Huntington disease)
	CD27-binding (Siva) protein
	neuregulin 2
	caspase 8, apoptosis-related cysteine protease
growth (2)	suppressor of cytokine signaling 2
	core promoter element binding protein

Table 3-5. Continued	
growth factor activity (2)	neuregulin 2
	colony stimulating factor 1 (macrophage)
response to external stress (8)	protein C receptor, endothelial (EPCR)
	ribosomal protein S6 kinase, 90kDa, polypeptide 5
	basic leucine zipper transcription factor, ATF-like
	chemokine (C-C motif) ligand 17
	serine (or cysteine) proteinase inhibitor, clade A
	stannin
	keratocan
	myosin IC
response to endogenous stress (4)	thyrotropin-releasing hormone
	X-ray repair complementing defective repair
	hypothetical protein FLJ21415
	general transcription factor IIH, polypeptide 3, 34kDa
defense response (9)	CD27-binding (Siva) protein
	protein C receptor, endothelial (EPCR)
	G-protein signalling modulator 3 (AGS3-like, C. elegans)
	basic leucine zipper transcription factor, ATF-like
	chemokine (C-C motif) ligand 17
	CD6 antigen
	core promoter element binding protein
	serine (or cysteine) proteinase inhibitor, clade A
	immunoglobulin lambda constant 2 (Kern-Oz- marker)
immune response (8)	protein C receptor, endothelial (EPCR)
	G-protein signalling modulator 3 (AGS3-like, C. elegans)
	basic leucine zipper transcription factor, ATF-like
	chemokine (C-C motif) ligand 17
	CD6 antigen
	core promoter element binding protein

Table 3-5. Continued	
	serine (or cysteine) proteinase inhibitor, clade A
	immunoglobulin lambda constant 2 (Kern-Oz- marker)
response to DNA damage (3)	X-ray repair complementing defective repair
	hypothetical protein FLJ21415
	general transcription factor IIH, polypeptide 3, 34kDa
neurogenesis (3)	growth arrest-specific 7
	neurotrophic tyrosine kinase, receptor, type 3
	distal-less homeo box 2
transmission of nerve impulse (2)	glycine receptor, alpha 2
	BAI1-associated protein 3
eye morphogenesis (1)	keratocan

Chapter four:

SLC13A3 as a candidate gene of PITX2 regulation

Introduction

A new hormone-inducible expression system was adapted to find PITX2 target genes. As presented in chapter three, this method was successfully used to identify PITX2 target genes. Ten genes were validated as PITX2 target genes by two independent assays, microarray analysis and northern blot or semi-quantitative RT-PCR. One of the ten genes is *Solute carrier family 13 (sodium-dependent dicarboxylate transporter), member 3* (*SLC13A3*). *SLC13A3* has been selected for further analysis and its potential involvement in glaucoma pathology is described below.

SLC13A3 is located on chromosome 20q12-13 and consists of 13 exons and 12 introns. It encodes a 602 amino acids transmembrane protein that acts as a Na^+/dicarboxylate cotransporter (NaDC3). It is predicted that NaDC3 has 11 transmembrane domains with the amino-terminus in the cell and the carboxyl-terminus outside of the cell. NaDC3 transports with high affinity succinate, dimethlsuccinate, α-ketoglutarate, oxaloacetate, malate and fumarate, all of them being Krebs cycle intermediates [166, 167]. The transporter is Na^+- dependent with three sodium ions for each substrate molecule and is electrogenic with inward currents of transferring one positive charge across the membrane [168, 169].

NaDC3 is expressed in the liver, kidney [170], brain [171], eye and optic nerve [172, 173]. The location of NaDC3 in hepatocytes is at the sinusoidal membrane. The role of NaDC3 in the liver is to provide the cells with α-ketoglutarate for glutamine synthesis. Glutamine synthesis is important for

scavenging the ammonia from blood [170]. In the kidney, NaDC3 is located at the basolateral cell membrane [174] in proximal tubules. One of its roles in the kidney is to provide substrates for energy metabolism and gluconeogenesis. The α-ketoglutarate outward gradient provided by NaDC3 has also a role in secretion of toxins and drugs in the urine [175]. A postulated role of NaDC3 in the kidney cells is to transport glutathione (GSH), a well-known antioxidant with the role of preventing cellular damage under stress conditions [176].

In the brain, NaDC3 is only expressed in astrocytes and not in neurons of rat cerebral cortex [177]. In situ hybridization of adult mouse eye showed that NaDC3 mRNA is present in anterior and posterior segment of the eye. In anterior part of the eye, NaDC3 mRNA is expressed in iris, ciliary body and lens [172]. In the posterior segment of the eye, NaDC3 mRNA is expressed in different layers of retina such as ganglion cell layer, cells of the inner nuclear layer, the inner segments of the photoreceptors cells and retinal pigment epithelial cells; it is also expressed in the optic nerve [172]. It was shown that NaDC3 transports N-acetyl-L-aspartate (NAA) in rat cerebrocortical astrocytes [171, 172]. N-acetyl-L-aspartate is one of the most abundant amino acids in the nervous system, including the retina [178]. It is synthesized by neurons with the help of L-aspartate-*N*-acetyl transferase, released into the extracellular space and uptaken by glia cells through NaDC3 [172, 179]. In glia cells, NAA is hydrolyzed by aspartoacylase II releasing acetyl groups [180]. Further, the acetyl groups are used in the synthesis of lipids necessary for myelination. NAA has important functions in neuronal survival. NAA is involved in myelination, cell-signaling during

development, synthesis of neuromodulators such as N-acetyl-L-aspartlyglutamate and in osmotic regulation being protective against osmotic stress [181-183]. Deficiency of aspartoacylase II causes Canavan disease, an autosomal recessive disorder associated with optic neuropathy, mental retardation and brain degeneration [184]. George et *al* [172] hypothesized that mutations in *SLC13A3* may produce similar effects as aspartoaclase II deficiency since NAA is required to be transported by NaDC3 in glia cells in order to be hydrolyzed by aspartoaclase II.

I selected *SLC13A3* for further analysis for several reasons. First, *SLC13A3* mRNA is expressed in the ciliary body, the site of aqueous humor production; therefore the protein encoded by *SLC13A3* might have important functions in the production of aqueous humor. Furthermore, the retinal expression of *SLC13A3* and its potential involvement in Canavan disease pathology, characterized by optic neuropathy, provide us more evidence that *SLC13A3* might be important in glaucoma pathology. Second, there is indirect evidence that NaDC3 is involved in cellular stress pathway. Cellular stresses such as oxidative damage or mechanical strain have been implicated in the pathology of glaucoma [185]. Glaucoma incidence increases with age which might be explained by the prolonged exposure to cellular stresses on the eye. Oxidative stress can compromise the function of the anterior segment tissues implicated in the production and the drainage of the aqueous humor leading to imbalance of aqueous humor dynamics and ultimately to elevated intraocular pressure (IOP) [185]. Retinal ganglion cells (RGC) are degenerated in glaucoma which could also be a consequence of the apoptosis

induced by the oxidative damage. The involvement of *SLC13A3* in the cellular stress pathways makes this gene a good candidate for involvement in glaucoma.

This chapter describes functional dissection of the *SLC13A3* upstream region, direct binding of PITX2 to the upstream region of *SLC13A3* and the involvement of *SLC13A3* in cellular stress pathway. This analysis may have important implications, not only for the regulation of *SLC13A3*, but also for the role of PITX2 in oxidative stress ocular regulation pathways.

Methods

Where not explicitly stated, the composition of all reagents used in the following procedures is found in Appendix A.

Computer based *in silico* analyses

The *in silico* tissue expression profile of *SLC13A3* was determined via an electronic search on Source Stanford University database (http://genome-www5.stanford.edu/cgi-bin/source/sourceSearch). The PITX2 DNA binding motif search on the upstream region of *SLC13A3* was performed using Possum (http://zlab.bu.edu/~mfrith/possum/) and EMBL - EBI -Sanger Institute (http://www.ensembl.org/index.html) websites. The conserved PITX2 DNA binding motifs among species, the *SLC13A3* nucleotide sequence alignment and *SLC13A3* upstream region sequence alignment were performed by on the European Bioinformatics Institute website (http://www.ebi.ac.uk/clustalw/). The human sequences were submitted to RepeatMasker (http://www.repeatmasker.org) to exclude the sequence placed into the repeat regions.

Percent identity plot (PIP)

The 20kb of genomic sequence from hChr20 and 13kb of genomic sequence from mChr2 were extracted from the EMBL - EBI -Sanger Institute (http://www.ensembl.org/index.html) website (hChr20: GRCh37:20:45172668:45192728:1 and mChr2: NCBIM37:2: 165222505:

165235868: 1). The human sequence was first submitted to RepeatMasker (http://www.repeatmasker.org) to generate the annotation file needed for the PIPMaker submission (http://pipmaker.bx.psu.edu/pipmaker). NCBI website was used (http://www.ncbi.nlm.nih.gov/sites/entrez) to find the gene structures of *SLC13A3* and *C20orf123*.

Plasmids

N-terminal flagged hemagglutinin epitope (HA) PITX2 C wt was expressed in pCI-HA and was courtesy provided by Tim Footz**.** pcDNA4-His-Max PITX2 A mutant constructs, T30P, V45L and R52C and pCI-FGF19-V5 were also provided by Tim Footz and have been previously described and published [116]. pcDNA4-His-Max PITX2 C wt was produced by subcloning the insert from pCI-HA-PITX2 C wt into the XbaI and EcoRI sites of pcDNA4-His-Max. pcDNA4-His-Max PITX2 C mutants, T30P, V45L and R52C, were produced by subcloning the insert from pcDNA4-His-Max PITX2 A mutants into the XhoI and NarI sites of pcDNA4-His-Max PITX2 C wt. C-terminally flagged V5 epitope SLC13A3 wt was expressed in pCI by first PCR amplifying from cDNA clone (Open Biosystems MHS1011-7509920) using Platinum Pfx DNA poly kit (Invitrogen) according to the manufacturer's protocol. The primers were designed using the Primer3 Input website (http://frodo.wi.mit.edu/primer3/) and are F: 5'-GCTAGCATGGCGGCGCTGGCAGCAGC-3' and R: 5'-GGTAACCGAGGGTCCGAAATGTGTCAT. An 1865bp fragment was subcloned first into pGEM-T vector (Promega), according to the manufacturer's

protocol, and then subcloned into KpnI and NheI sites of pCI-FGF19-V5. To build *SLC13A3* promoter plasmids, different lengths of the 5'-UTR flanking region of the human *SLC13A3* promoter were PCR -amplified from genomic DNA. The primer pairs used for amplification are shown in Table 4-1. PCR primers were designed using the Primer3 Input website. These promoter constructs were designated p2BS-SLC13A3, p1BS-SLC13A3 and p0BS-SLC13A3, respectively. The *SLC13A3* promoter fragments were subcloned first into pGEM-T vector (Promega), and then subcloned into pGL3 vector (Promega). The final constructs were sequenced to ensure their integrity. For pCI-SLC13A3-V5 sequencing, another two internal primers were used to check its integrity (F-5' GTGTGACGTGGTGAATTTCG-3' and R-5'-CTGTTCGGCAAACTTGATGG).

Cell culture and transfection

HTM (human trabecular meshwork) cells were cultured in Dulbecco's modified Eagle's medium containing 10% fetal bovine serum. Cells were transfected using Fugene6 transfection reagent (Roche) according to the manufacturer's protocol. HTM cells were transfected in 24-well plates using 160ng of empty vector (pcDNAHisMax4) or PITX2 wt ((pcDNAHisMax4), 60ng of the different pGL3-SLC13A3 promoter constructs, 20ng of the pCMV beta-galactosidase transfection controls and 3µl of Fugene6 transfection reagent.

Transactivation assays

HTM cells were cultured in 24-well plates at a density of 4x 10^4 cells/plate twenty four hours prior to transfection. Cells were transfected, harvested after forty eight hours of incubation and luciferase activities were monitored following the manufacturers' protocols (Promega). Transfections were performed in triplicate and repeated three times.

Immunoprecipitation

NPCE cells were transfected with pcDNA-PITX2 C wt. The cells were harvested 48 hours after transfection and lysed in the RIPA lysis buffer (9.1mM Na2HPO4, 1.7mM NaH2PO4, 150mM NaCl, 0.1% wt/vol SDS, 1% vol/vol IGEPAL CA-630, 0.5% wt/vol Deoxycholic acid sodium salt, 0.1M PMSF and Sigma Protease Inhibitor Cocktail). After determining protein concentrations via the Bradford Assay, 300µg of protein extract was aliquoted to a microcentrifuge tube and brought to 1mL with RIPA-PI buffer. The blocked beads were prepared by transferring 1ml of homogeneously resuspended protein G beads to a 1.5ml tube and centrifuged at 4°C, at 3000rpm, for 5 min. The protein G beads were washed with PBS three times and blocked with 1% BSA by incubating them at 4°C for one hour on a rotator. 75µl of blocked beads (25µl-worth of beads) were added to the diluted lysates and incubated, on rotator, at 4°C, for one hour. The blocked beads were resuspended in 1mL RIPA-PI to create a 33% solution. The precleared cell lysates were centrifuged at 4°C, at 13000rpm, for 5 minutes and the supernatant was carefully transferred to new pre-chilled 1.5ml tubes. The

precleared cell lysates were incubated with 0.5-3µg anti-PITX2 antibody (Abnova Mab) or 2µg anti-Xpress (Invitrogen) on rotator, at 4°C, overnight. Next day, the blocked beads were centrifuged at 4°C, at 3000rpm, for 5 min and resuspended in RIPA-PI buffer. 75µL of blocked beads (25µL-worth of beads) were again added to the immunoprecipitated (IP) samples and incubated, on rotator, at 4°C, for one hour and a half. The IP samples were centrifuge at 4°C, at 13000rpm, for 5 minutes and washed three times with 1ml RIPA with PMSF and PIC, rotating at 4°C for 10 min. The IP samples were washed two more times with 1ml RIPA with PMSF (only), rotating at 4°C for 10 min. After the final wash and spin, the complexed beads were resuspended with 20µl 2x SDS-PAGE loading buffer and denatured at 95°C sand bath for 5 min. Samples were then analyzed by immunblot with anti-Xpress antibody (Invitrogen) 1:5000 and goat anti mouse as secondary antibody 1:5000.

Immunofluorescence

NPCE cells were plated ($1X10^5$ cells) onto sterile coverslips in 6 well plates and transfected with pcDNA-PITX2C wt. After 48h post transfection, the cells were washed twice with PBS and fixed with 2% paraformaldehyde (buffered in PBS pH 7.4), for 20 min at room temperature. The cells were then washed twice for 5 min each with PBS-X and blocked with 5% BSA in PBS-X, for 15 min to reduce nonspecific protein binding of antibodies. The cells were incubated in primary antibody, anti-PITX2 monoclonal antibody (ABNOVA) or anti-Xpress antibody (diluted 1:500 in 100µl of PBS-X containing 5% BSA), at room

temperature. After one hour, cells were washed twice for 5 min each with PBS-X and incubated with secondary antibody Cys 2 Donkey anti mouse (diluted 1:500 in 100µl of PBS-X containing 5% BSA), at room temperature. From this step, the plates were covered with aluminum foil. After one hour, cells were washed twice for 5 min each with PBS-X and incubated with DAPI (diluted 1:500 in 100µl of PBS), for 5 min, at room temperature. Diamidino-2-phenylindole (DAPI) is a DNA-specific dye that can pass through intact, living cell membranes. After two-5 minutes final washes with PBS, the coverslips were mounted onto glass slides with mounting medium (90% Glycerol, 10% PBS containing 1µg/ml p-phenylenediamine) and sealed with nail polish. Slides were stored at -20°C in dark or subjected to image analysis. The images were collected using Leica DMR immunofluorescence microscopy.

Chromatin immunoprecipitation

Chromatin Immunoprecipitation (ChIP) was performed using Active Motif ChIP-IT^{TM} Express kit (catalog no: 53008) according to the protocol. Non-pigmented ciliary epithelial cells (NPCE) were grown to 70-80% confluency, (~$6x10^7$ cells). After 48 hours of growing, NPCE cells were crossed-linked with fixation solution (1% formaldehyde final concentration added to the cell culture medium) for 10 minutes at room temperature with gentle rocking. Formaldehyde treatment is used to cross-link proteins to their target DNA by formation of bonds between lysine -amino groups. The crosslink reaction was stopped by adding glycine stop-fix solution (10X Glycine Buffer, 10XPBS and dH_2O) to each plate,

swirling to cover and then rocking at room temperature for 5 minutes. The glycine stop-fix solution was poured off the plates and cells were washed twice with PBS. Cell scraping solution (10XPBS, dH_2O and 100mM PMSF) was added to each plate; cells were scraped and pooled into 50ml tube. The pooled cells were pelleted by centrifugation for 10 minutes at 2500rpm (720rcf) at 4°C. The pellet was resuspended in 1ml ice-cold Lysis Buffer (supplemented with 5µl PIC and 5µl PMSF) and incubated on ice for 30 min. The cell lysates were subject to homogenizing by 10 stokes of Dounce homogenizer and centrifuged at 5000rpm (2400 RCF) for 10 min at 4°C to pellet the nuclei. The pellet was resuspended in 1ml Shearing Buffer (supplemented with 5µl PIC) and aliquoted in three tubes. The lysate from each tube was sheared by sonication, six times- 15 seconds bursts at setting 7 on a Sonic dismembrator 60 (Fisher Scientific). The sheared DNA samples were centrifuged at 10000rpm in a 4°C microcentrifuge for 12 min. The supernatants were transferred to fresh tubes, and 25µl was removed for checking the DNA shearing efficiency and DNA concentration. The remaining lysate was aliquoted into four tubes (220µL) and each tube used for four ChIP reactions. Ten µl of lysate was transfected to a tube for "Input" DNA to use as controls in PCR analysis. Twenty five microliter of dH2O was added to the 25µl of supernatant to check DNA concentration. Distilled H2O, 5M NaCl and RNase A were added to DNA sample to reverse cross-link reaction, and then the solution was incubated at 65°C, overnight. The next day, 24:1 chloroform: isoamyl alcohol was added to the DNA sample and centrifuged for 5 min, 13000rpm. The supernatant was transferred to a fresh tube, then 3M NaOAc pH 5.2 and 95% cold ethanol were

added and left it at -20°C for one hour. The DNA sample was centrifuged at 13000rpm, for 10 min, at 4°C. The supernatant was carefully removed and discarded. 70% cold ethanol was added to the pellet and spin at 13000rpm, for 5 min, at 4°C. The pellet was allowed to air-dry for 5 min, resuspended in dH2O and the DNA concentration was determined at 260nm (1.0A260=50µg/ml). The ChIP reactions were set up by adding 25µl of Protein G Magnetic beads, 10µl of ChIP buffer 1, 6.3µg of sheared chromatin, 1µl of PIC, 2µg of antibody (anti-PITX2 Abnova Mab, Normal Rabbit IgG –Caltag laboratories and anti- acetylated lysine 9 of Histone 3- Cell Signaling Technologies) and dH20 to 100µl reaction. One ChIP reaction did not contain any antibody. The ChIP reactions were incubated on a rolling shaker overnight, at 4°C. The next day, the tubes containing the ChIP reactions were briefly centrifuged to collect the liquid from inside of the cap and placed on a magnetic stand to pellet beads on the tube side. The supernatant was carefully removed and discarded, while the beats were washed once with ChIP Buffer 1 and twice with ChIP Buffer 2. After the final wash, the beads were resuspended with 50µl Elution Buffer AM2 and incubated for 15 min at room temperature on a rotator. Fifty µl of Reverse Cross Link Buffer was added to elute the chromatin, and the tubes were immediately placed in magnetic stand, allowing the beads to pellet to the sides of tubes. The supernatant containing chromatin was quickly transferred to a fresh tube. To "Input DNA", 88µl ChIP Buffer 2 and 2µl 5M NaCl were added and all sample reactions were incubated at 95ºC for 15 min. The sample reactions were returned to room temperature; 2µl Proteinase K was added and incubated at 37ºC for 1

hour. The sample reactions were returned to room temperature, 2µl Proteinase K Stop Solution was added and 5µl of DNA was used for PCR reactions. A 166bp fragment in the *SLC13A3* promoter containing PITX2 binding site B was amplified with following primer set: 5'- TCCACTTTCAGGCTCAGAGG-3' and 5'- GCAGCTGGCTTATCCTCTCC-3'. A 243bp fragment in the *SLC13A3* promoter containing PITX2 binding site A was amplified with following primer set: 5'- AGTGCCTAACTTTCTCCAACG -3' and 5'- CGCTCCACACCTTCTTGG -3'

siRNA transfection

Transfection efficiency of siRNA in NPCE cells was determined by immunocytochemistry and Block-IT Fluorescent Oligo (Invitrogen, cat no: 2013). Cells were transfected with 10nM, 50nM, 100nM, 150nM and 200nM Block-IT Fluorescent Oligo using Lipofectamine 2000 (Invitrogen, cat no: 11668-027) according to the protocol. Lipofectamine 2000 has the highest transfection efficiency, not interfering with siRNA. Human PITX2 specific siRNA was purchased from Ambion (Target: 5'-GUACGAGUGGCAAGAGGUGtt-3', Sense: 5'-CAGCCUGAAAUAACUUGAACtt-3' and Antisense: 5'-GUUCAAGUUAUUCAGGCUGtt-3'), human SLC13A3 specific siRNA was purchased from ThermoScientific (Target: 5'-NNGGAGGAAGAAUAAAUCUGA-3', Sense: 5'-GGAGGAAGAAUAAAUCUGAUU-3' and Antisense: 5'-UCAGAUUUAUUCUUCCUCCUU-3') and non-targeting control siRNA was

purchased from Ambion (AM4611). NPCE or HTM cells were cultured on six well plate ($5x10^5$ cells/ well) or 100mm plate ($1x10^6$ cells), 24 hours prior to transfection. 100nM of PITX2 specific siRNA, SLC13A3 specific siRNA or non-targeting siRNA was diluted in 250µl of Opti-MEM I Reduced Serum Medium (Invitrogen), incubated for 5 min at room temperature in a 15ml tube for transfection of six well plate. In the same time, 5µl of Lipofectamine 2000 was diluted in 250µl of Opti-MEM I Reduced Serum Medium incubated for 5 min at room temperature in another tube. 100nM of PITX2 specific siRNA, SLC13A3 specific siRNA or non-targeting siRNA was diluted in 1.5ml of Opti-MEM I Reduced Serum Medium (Invitrogen), incubated for 5 min at room temperature in a 15ml tube for transfection of 100mm plate. At the same time, 30µl of Lipofectamine 2000 was diluted in 1.5ml of Opti-MEM I Reduced Serum Medium incubated for 5 min at room temperature in another tube. After 5 minutes incubation, both tubes were mixed and incubated for 20 min at room temperature to allow the siRNA: Lipofectamine 2000 complexes to form. After 20 min, the siRNA: Lipofectamine 2000 mixture was added directly to the cells. NPCE cells were transfected with pCI-HA-PITX2C wt or pCI-SLC13A3wt-V5 and Fugene6 transfection reagent (Roche, 1:3 DNA to Fugene6), 24 hours post transfection with siRNA when the specificity of siRNA for *PITX2* or *SLC13A3* was checked**.** Cell lysate, membrane lysate or RNA was extracted 48 hours after the last transfection and western blot or RT-PCR was performed.

Whole cell protein extraction and expression

Whole cell protein extraction was performed forty eight hours after transfection of NPCE cells with different concentrations of PITX2 specific siRNA or non-targeting control siRNA and pCI-HA-PITX2C wt. Western blot analysis was performed using a mouse monoclonal anti-PITX2 antibody (Abnova, 1:1000) to detect exogenous PITX2C wt. HRP-conjugated goat anti-mouse (1:5000) was used as secondary antibody. Anti phosphor-ERK 1/2 antibody (Phospho p44/ 42 Map Kinase, Cell Signaling, 1:1000), was used as a control with goat anti-rabbit (1:5000) HRP-conjugated as secondary antibody. Protein extraction was performed forty-eight hours after transfection of HTM cells with 100nM of PITX2- specific siRNA or 100nM of non-targeting control siRNA. Western blot analysis was performed using a mouse monoclonal anti-PITX2 antibody (Abnova, 1:1000) to detect endogenous PITX2C wt. HRP-conjugated secondary antibody, goat anti-mouse (1:5000), was used. Labeling of Anti alpha- tubulin antibody, (1:1000) was used as control with goat anti-rabbit (Abcam, 1:5000) HRP-conjugated goat anti-mouse was used as secondary antibody. The protein extraction protocol is described in Chapter 3.

Membrane protein extraction and expression

HTM cells cultured in 100mm plates ($1x10^6$ cells) were transfected with 100nM of SLC13A3 specific siRNA or 100nM of non-targeting control siRNA and 4μg of pCI-SLC13A3wt-V5. Protein extraction was performed forty eight hours after the recombinant protein transfection. The cells were washed twice

with phosphate buffered saline (PBS) at room temperature. After removing the last rinse, 5ml ice-cold homogenization buffer with protease inhibitor (0.32M sucrose, 1mM EGTA, 0.1mM EDTA, 10mM HEPES, pH 7.5, 10µl 0.1M PMSF and 5µl PIC per mL) was added on each plate. The cells were harvested and homogenized by 12 strokes of a Dounce homogenizer. A cell pellet was obtained by centrifugation at 3000rpm (1440g) for 5 minutes. The supernatant was collected and centrifuged at 30,000 rpm (66,700g) for 1h at 4°C (ultracentrifuge). The pellet was resuspended in 80µl of nuclear lysis buffer for whole cell protein extraction, following the whole lysis extraction protocol as described in Chapter 3. After one hour of ultracentrifugation, the supernatant was removed and the pellet was resuspended in PBS with protease inhibitor (140mM NaCl, 3mM KCl, 6.5mM Na_2HPO_4, 1.5mM KH_2PO_4, pH 7.5, add 10µl 0.1M PMSF and 5µl PIC per mL PBS). The lysates were assayed for total protein concentration using the Bradford assay. Western blot analysis was performed using a rabbit anti-V5 antibody (Sigma-Aldrich, 1:5000) against the pCI vector encoded C-terminal V5-tag. HRP-conjugated secondary antibody, goat anti-rabbit (1:5000), was used. Alpha-transferin antibody was used as a control for membrane proteins (CD71, Santa Cruiz, 1:5000) with goat anti-mouse HRP-conjugated (1:5000) as secondary antibody.

RNA extraction

HTM cells were transfected with 100nM of PITX2 specific siRNA, 100nM of SLC13A3 specific siRNA, 100nM of non-targeting control siRNA or

pcDNAHisMaxC4-PITX2C wt. RNA extraction was performed 48 hours post-transfection, as described in Chapter 3.

Semi-quantitative RT-PCR

RNA samples were extracted from HTM cells as described above. Total RNA was used as a substrate for semi-quantitative reverse transcription–polymerase chain reaction (RT-PCR). A standard 20µl reverse transcription recipe contained the following components: 2µg total RNA, 500ng oligo d(T), 0.5mM dNTPs, 1x First Strand Buffer, 0.01M DTT, 40U RNaseOUT, 200U reverse transcriptase (Invitrogen). A 20µl reverse transcription reaction without reverse transcriptase corresponding to each type of transfection (100nM of PITX2 specific siRNA, 100nM of SLC13A3 specific siRNA, 100nM of non-targeting control siRNA or pcDNA4-PITX2C wt) was used as negative control. Specific PCR primers to check SLC13A3 expression are described in Chapter 3 and are shown in Table 3-2. Reactions were cycled in a thermocycler for 28 cycles. PCR products were separated using agarose gel electrophoresis and visualized with ethidium bromide. Beta-actin was used as "input" control. β-actin forward primer was 5'-ATCATGTTTGAGACCTTCAACAC-3 and β-actin reverse primer was 5'-TCTGCGCAAGTTAGGTTTTGTC-3'.

Cell viability assay

This protocol is adapted from Alice L. Yu et al, 2008, IOVS [186]. HTM cells were cultured on 6-well culture plates with coverslips ($4x10^5$ cells/ well). After 48

hours of growing, the DMEM medium was replaced by fresh serum medium and the cells are exposed to 200, 400, 600 or 800 μM hydrogen peroxide (H_2O_2) for one hour in order to determine the cytotoxic concentrations of hydrogen peroxide. After exposure to H_2O_2, the cells were placed in serum medium H_2O_2 free for 24 hours. In control cultures, the medium was changed at the same time points, but no H_2O_2 was added. After 24 hours of H_2O_2 treatment, the cells were washed twice with 2ml of PBS two times, gentle dispensing it along the sides of the walls. After the second wash, the cells were incubated with 2.0 μg/ml propidium iodide (Sigma Aldrich P4170) diluted in PBS (1:500, 0.2μl in 100μl PBS) and DAPI (1:500 in 100μl PBS) for 15 minutes at 37°C. Propidium iodide was used to stain DNA in dying cells. Propidium iodide is membrane impermeant being excluded from viable cells. The cells were washed three times, for 5 min each. After the last wash, the coverslips were mounted onto glass slides with 25μl of mounting media. The slides were examined with florescence microscope immediately after the last wash.

Table 4-1.	**Primers used for *SLC13A3* Promoter construction**		
Construct	**Forward**	**Reverse**	**Product size (bp)**
p2BS-SLC13A3	GCTAGCTCCACTTTCAGGCTCAGAGG	CTCGAGGGAGGAGGCGTTACCTTGG	500
p1BS-SLC13A3	GCTAGCAGGGAGAGGGCGGGTTCC	CTCGAGGGAGGAGGCGTTACCTTGG	244
p0BS-SLC13A3	GCTAGCAGCGGCCAAGAAGGTGTGG	CTCGAGGGAGGAGGCGTTACCTTGG	108

BS= PITX2 Binding Site

Results

In silico analysis identified PITX2 binding sites on *SLC13A3* promoter

In silico analysis of *SLC13A3* showed *SLC13A3* is highly expressed in the eye and brain. In order to determine whether the first 3kbp upstream of the untranslated region of exon 1 of the human *SLC13A3* gene contains PITX2 binding sites, the promoter sequence was first uploaded on RepeatMasker to exclude the sequence placed into the repeat elements and then uploaded on the Possum website. This *in silico* analysis revealed 12 putative PITX2 DNA binding motifs. One of these binding motifs, which I named putative PITX2 binding site **A**, is highly conserved in Pan troglodytes (chimpanzee), Macaca mulatta (monkey) and Canis (dog) promoter region (Figure 4-1, Table 4-2). Another binding motif, called putative PITX2 binding site **B**, is highly conserved in Pan troglodytes (chimpanzees) and Macaca mulatta (monkeys) promoter region (Figure 4-1).

The human sequence between *SLC13A3* and the nearest upstream neighboring gene, *C20orf123,* was compared with the homologue mouse sequence and a percent identity plot (PIP) was produced. Comparison of 20kbp of human genomic sequence located on chromosome 20 to 13kb of the homologous region in mouse on chromosome 2 showed no homologous sequence regions between *SLC13A3* and *C20orf123* (Figure 4-2).

By comparing the human nucleotide sequence of *SLC13A3* promoter and *SLC13A3* gene to the corresponding sequences of the Pan troglodytes and Macaca mulatta, the *in silico* search showed 82-98% identity of the 3000bp of *SLC13A3*

Figure 4-1. Putative PITX2 binding sites in the first 3kbp upstream region of human *SLC13A3* and other species. The PITX2 binding sites are represented by red vertical lines. The length of each line represents log-likelihood ratio score, the higher the score is, the longer the line is. The log-likelihood ratio score is calculated by comparing every sequence fragment to the PITX2 binding motif. The black circle (A) represents putative PITX2 binding site A and the blue circle (B) represents putative PITX2 binding site B. The up (+) and down (-) lines represent the strand of DNA.

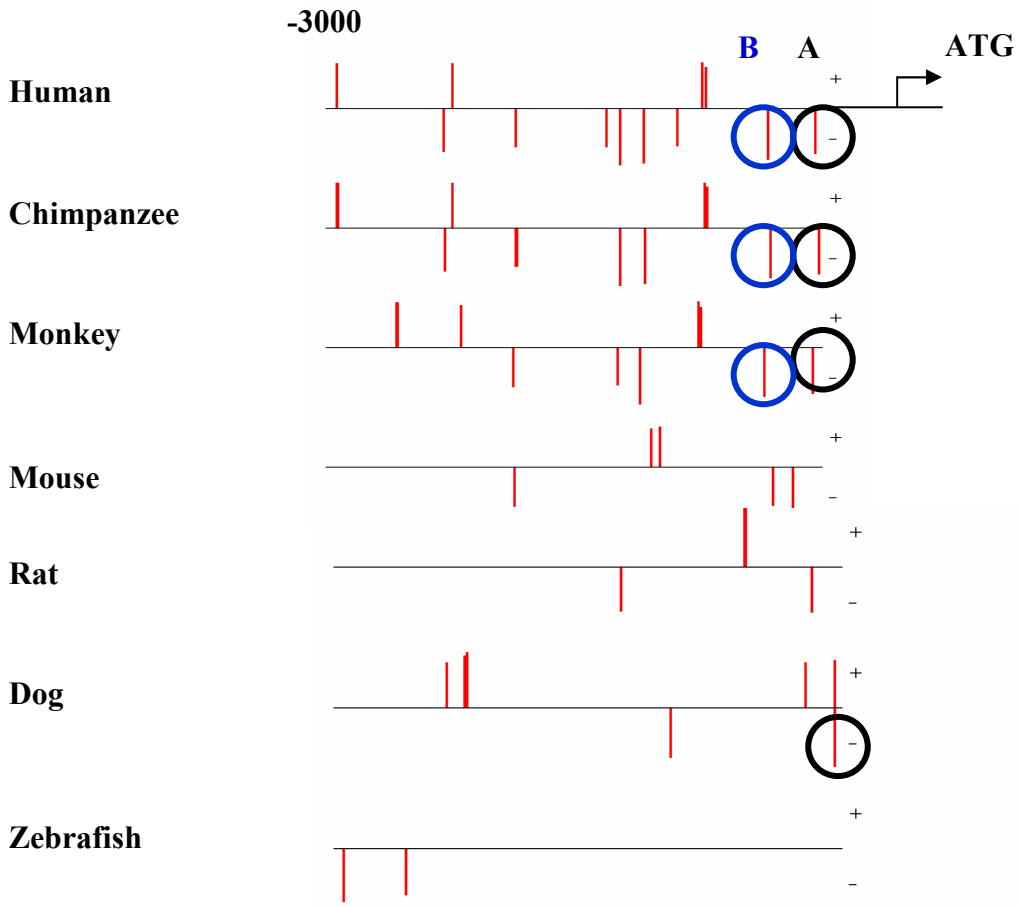
-3000
B
A
ATG
Human
Chimpanzee
Monkey
Mouse
Rat
Dog
Zebrafish
+
-

Table 4-2. PITX2 Bindings sites in different species upstream of *SLC13A3*

Species	position	strand	sequence
Human	65 - 72	+	tggattat
	710 - 717	-	ctaatcac
	759 - 766	+	cagattaa
	1142 - 1149	-	ttaacccg
	1692 - 1699	-	ataatcag
	1771 - 1778	-	gtaatccc
	1920 - 1927	-	gtaatccc
	2121 - 2128	-	ctaatcac
	2270 - 2277	+	cagattat
	2289 - 2296	+	ggtattaa
	2669 - 2676	-	ttaatcct
	2954 - 2961	-	ttaagccg
	2954 - 2961	-	ttaagccg
Chimpanzee	68 - 75	+	tggattat
	716 - 723	-	ctaatcac
	765 - 772	+	cagattaa
	1148 - 1155	-	ttaacccg
	1776 - 1783	-	gtaatccc
	1926 - 1933	-	gtaatccc
	2281 - 2288	+	cagattat
	2300 - 2307	+	ggtattaa
	2680 - 2687	-	ttaatcct
	2973 - 2980	-	ttaagccg
Monkey	428 - 435	+	cagattaa
	811 - 818	+	tggattac
	1127 - 1134	-	ttaacccg
	1758 - 1765	-	gtgatccc
	1894 - 1901	-	gtaatccc
	2245 - 2252	+	cagattat
	2264 - 2271	+	ggtattaa
	2642 - 2649	-	ttaatcct
	2935 - 2942	-	ttaagccg
Mouse	1139 - 1146	-	ctaatgcc
	1961 - 1968	+	gggatcaa
	2014 - 2021	+	tagattat

Table 4-2. Continued

Species	position	strand	sequence
	2700 - 2707	-	ttaaaccc
	2817 - 2824	-	ttagtccc
Rat	1695 - 1702	-	ttgatccc
	2423 - 2430	+	tggattat
	2815 - 2822	-	caaatccc
Dog	662 - 669	+	ggggttaa
	770 - 777	+	cagattat
	782 - 789	+	cagattaa
	1984 - 1991	-	ttactctc
	2781 - 2788	+	gtgactaa
	2950 - 2957	+	ggctttaa
	2954 - 2961	-	ttaagccg
Zebrafish	60 - 67	-	ttaatcag
	422 - 429	-	ttactccc

Figure 4-2: Comparison of 20kbp of human genomic sequence (hChr 20) to 13kb of the homologous region in mouse (mChr2). The homology between the two sequences is present only in exons. No homology is present in the upstream region of *SLC13A3*. The small horizontal lines or dots represent the matching regions of homology between the two sequences. The position of lines or dots represents the percentage of nucleotide identity.

Gene
Exon
UTR
RNA
Simple
MIR
Other SINE
LINE1
LINE2
LTR
Other repeat
CpG/GpC≥0.60
CpG/GpC≥0.75
100%
75%
50%
19781
SLC13A3
C20orf123
0k
2k
4k
6k
8k
10k
12k
14k
16k
18k

gene promoter, whereas the identity of the *SLC13A3* gene was 92-98% among the three species.

PITX2 activates transcription from the *SLC13A3* promoter region

To determine the possible role of PITX2 in the transcription regulation of *SLC13A3*, the transcriptional regulatory element of *SLC13A3* was investigated using the luciferase reporter assay. By cloning different sizes of *SLC13A3* promoter into luciferase reporter vector, the activation of the *SLC13A3* reporter by PITX2 was monitored and thus the efficiency of different promoter regions could be assessed. The longest construct of 566bp in length (-411/+155), p2BS-SLC13A3, included the two PITX2 DNA binding motifs, A and B. The second construct, p1BS-SLC13A3, contained one PITX2 DNA binding motive, PITX2BS A, and was 326bp in length (-171/+155). The shortest construct of 106bp (+106), p0BS-SLC13A3, presented no PITX2 DNA binding motif (Figure 4-3). I monitored luciferase activity, after co-transfecting HTM cells with pcDNA4-PITX2C wt and pGL3-SLC13A3 upstream region expression vectors. Xpress-tagged PITX2 activated the expression from the p2BS-SLC13A3 luciferase reporter (Figure 4-3). However, deletion of putative PITX2 binding site B produced an enhanced in activation (Figure 4-3). The removal of the two sites, A and B, completely abolished PITX2 activation of this reporter. Activation of the p2BS-SLC13A3 and p1BS-SLC13A3 luciferase reporter is diminished when disease-causing R52C, V45L and T30P PITX2 alleles are transfected into cells. It was previously showed that R52C and T30P PITX2 did not bind the DNA and

produced a decreased activation [116, 130]; V45L presented a decreased binding and an increased in activity on the synthetic target promoter suggesting that it is a gain-of-function mutation in PITX2 [127]. The luciferase assays were performed in triplicate, and each experiment was repeated three times with similar results.

PITX2 binds to *SLC13A3* promoter through chromatin immunoprecipitation (ChIP) assays

ChIP was performed to determine whether PITX2 is able to bind the promoter region of *SLC13A3 in vivo*. The specificity of the antibodies used for the immunoprecipitation of PITX2 in ChIP experiments was tested before performing ChIP, as these antibodies were not previously used for ChIP. Human corneal endothelium (HCEC), HTM and NPCE cells were transfected with pCI-HA-PITX2C wt and cell lysates were then analyzed by immunblotting with Abnova PITX2 antibody to determine whether this antibody recognizes exogenous PITX2. As shown in Figure 4-4 A, Abnova PITX2 antibody detected a band at the correct molecular weight between 32.5 and 47.5 kDa. Cell lysates from HCEC, HTM and NPCE cells were analyzed by immunbloting with the Abnova PITX2 antibody to determine whether this antibody recognizes endogenous PITX2. As shown in Figure 4-4 A, Abnova PITX2 antibody detected two bands between 32.5 and 47.5 kDa. NPCE cells were also transfected with pcDNA-PITX2C wt and immunoprecipitation and immunofluorescence were performed. As shown in Figure 4-4 B and C, Abnova PITX2 antibody is able to recognize and immunoprecipitate exogenous PITX2.

Figure 4-3. Effects of PITX2 on *SLC13A3* upstream elements in HTM cells. Luciferase reporter plasmid containing different deletion constructs of *SLC13A3* promoter were co-transfected in HTM cells with empty vector, wild type PITX2 or three different ARS missense mutations (T30P, V45L, R52C- numbering according to position within the homeodomain). Luciferase activity was normalized relative to the activity of pGL3-basic.

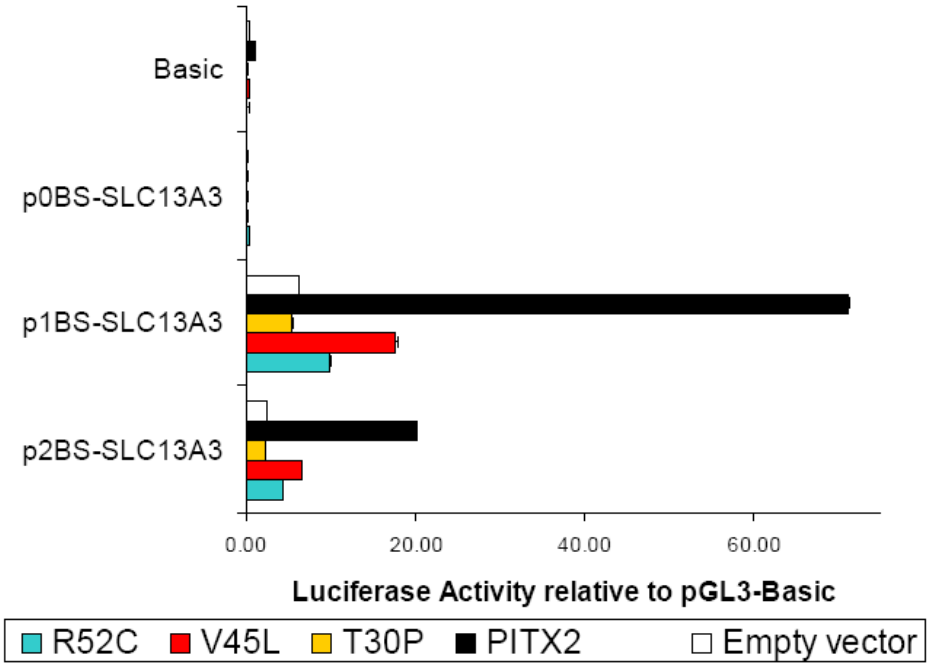
Basic
p0BS-SLC13A3
p1BS-SLC13A3
p2BS-SLC13A3
0.00
20.00
40.00
60.00
Luciferase Activity relative to pGL3-Basic
R52C
V45L
T30P
PITX2
Empty vector

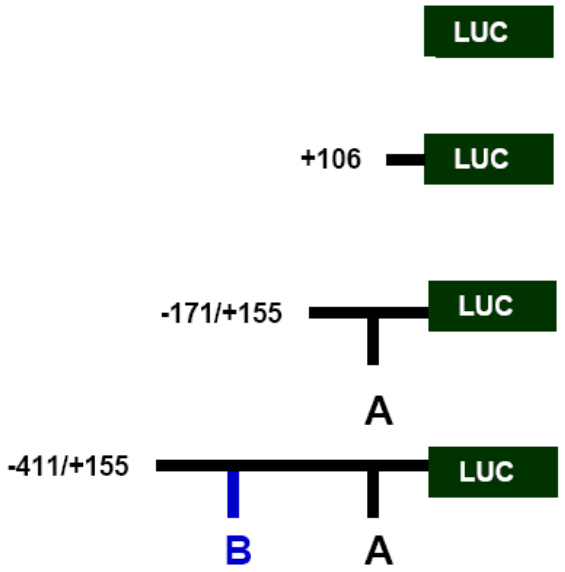
LUC
+106
LUC
-171/+155
LUC
A
-411/+155
LUC
B
A

Figure 4-4: Mouse monoclonal PITX2 antibodies (Abnova Mab) are specific to PITX2.

A. PITX2 antibodies recognize exogenous and endogenous PITX2 by Western Blot. *Left panel*: Recognition of exogenous PITX2. HCEC, HTM and NPCE cells were transfected with pCI-HA-PITX2C wt and PITX2C wt was recognized by the Abnova PITX2 antibody. *Right panel*: Recognition of endogenous PITX2. PITX2 in HCEC, HTM and NPCE cell lysates was recognized by the Abnova PITX2 antibody.

B. PITX2 antibodies recognize exogenous PITX2 by immunoprecipitation. NPCE cells were transfected with pcDNA-PITX2C wt and cell lysates were immunoprecipitated with anti-Xress antibody or different concentrations of Abnova PITX2 antibody. Samples were then analyzed by anti-Xpress antibody (Invitrogen). The arrow indicates PITX2 band.

C. PITX2 antibodies recognize exogenous PITX2 by immunofluorescence. NPCE cells were transfected with pcDNA-PITX2C wt and stained with Xpress antibody and Abnova PITX2 antibody, respectively. The blue staining represents DAPI corresponding to the nucleus and the red staining corresponds to Xpress-PITX2.

HCEC- Human Corneal Endothelium Cells, HTM - Human Trabecular Meshwork Cells, NPCE- Non-Pigmented Ciliary Epithelium Cells

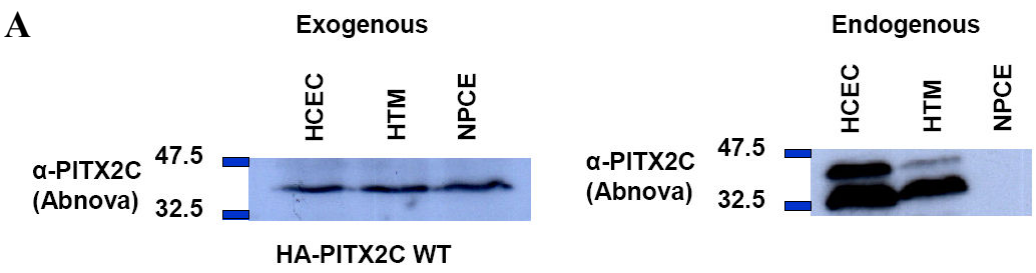
A
Exogenous
HCEC
HTM
NPCE
α-PITX2C
(Abnova)
47.5
32.5
HA-PITX2C WT
Endogenous
HCEC
HTM
NPCE
α-PITX2C
(Abnova)
47.5
32.5

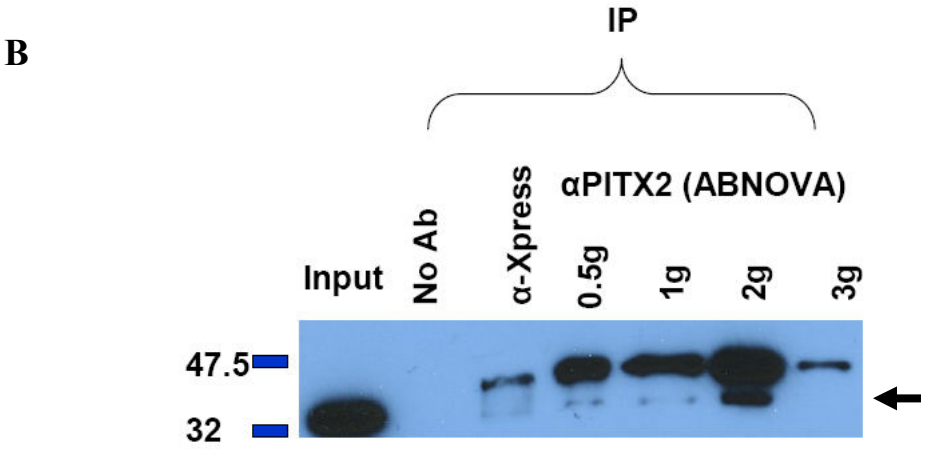
B
IP
αPITX2 (ABNOVA)
Input
No Ab
α-Xpress
0.5g
1g
2g
3g
47.5
32

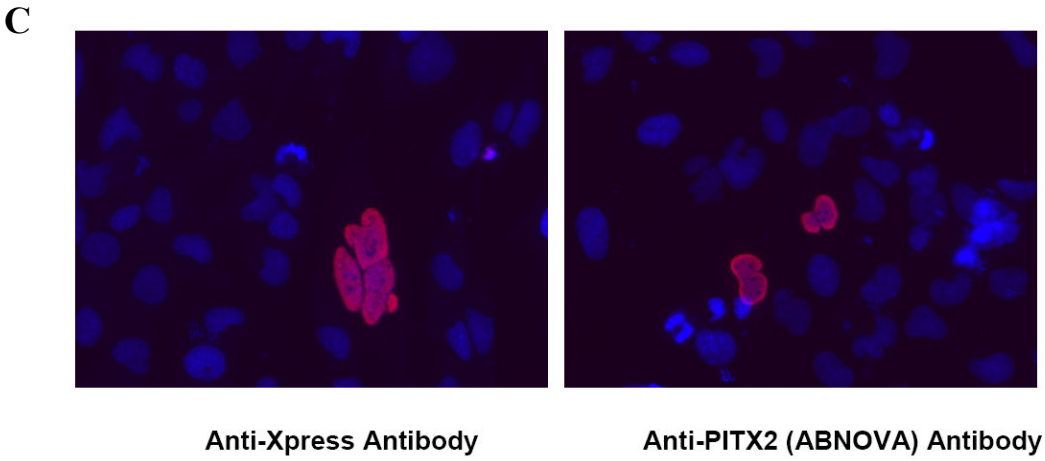
C
Anti-Xpress Antibody
Anti-PITX2 (ABNOVA) Antibody

Figure 4-5: PITX2 binds to the *SLC13A3* upstream elements *in vivo*. Chromatin immunoprecipitation (ChIP) revealed that chromatin was immunoprecipitated by antibodies against PITX2 and H3-AcK9 (positive controls). Experiments conducted without antibody added or with IgG antibody did not immunoprecipitate chromatin (negative controls). PCR was performed to amplify the immunoprecipitated DNA using primers designed to span **(A)** PITX2 binding site A and **(B)** PITX2 binding site B. Endogenous PITX2 binds to regions containing either the 'A' or 'B' binding sites. gDNA is genomic DNA.

A

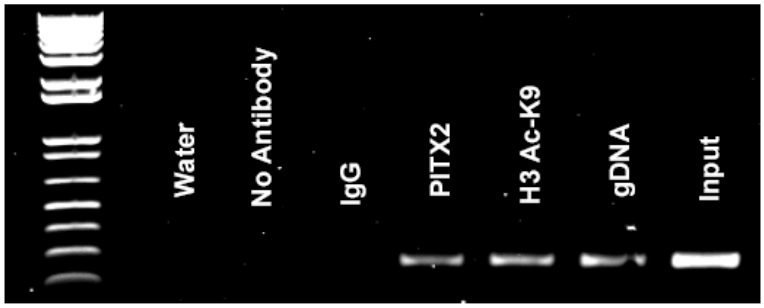
Water
No Antibody
IgG
PITX2
H3 Ac-K9
gDNA
Input

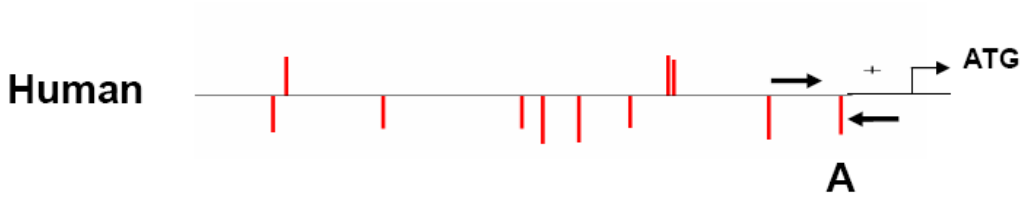
Human
+
ATG
A

B

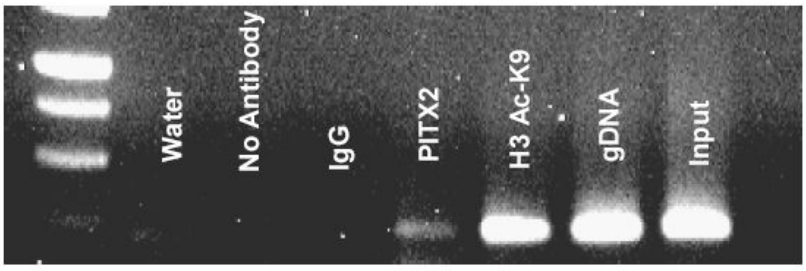
Water
No Antibody
IgG
PITX2
H3 Ac-K9
gDNA
Input


Human
+
ATG
–
B

After checking the PITX2 antibody for specificity, ChIP analysis was performed and showed upstream DNA sequences of *SLC13A3* containing PITX2 binding site A and PITX2 binding site B being recovered with PITX2 and H3-AcK9 antibodies (Figure 4-5). These data indicate that PITX2 occupies the promoter regions of *SLC13A3* on both PITX2 binding sites, *in vivo*.

SLC13A3 expression is affected by variation in PITX2 expression

siRNA suppression of PITX2 translation followed by semi-quantitative RT-PCR was performed to determine whether reducing *PITX2* expression affects *SLC13A3* expression. The specificity of the siRNA used for suppressing PITX2 was tested by western blot before looking at *SLC13A3* expression through RT-PCR, as this siRNA was not previously used. As illustrated in Figure 4-6, human PITX2 specific siRNA suppressed both exogenous and endogenous PITX2. HTM cells were transfected with 100nM of PITX2 specific siRNA and 100nM of non-targeting control siRNA. RNA extraction and RT-PCR were performed 48 hours post-transfection. The RNA levels of *SLC13A3* were reduced when PITX2 expression is reduced (Figure 4-7).

HTM cells were transfected with PITX2 followed by semi-quantitative RT-PCR was performed to determine whether overexpressing *PITX2* affects *SLC13A3* expression. The RNA levels of *SLC13A3* were increased when PITX2 is overexpressed (Figure 4-7).

Figure 4-6: Human PITX2 specific siRNA suppressed expression both exogenous and endogenous PITX2.

A. siRNA suppressed expression of exogenous PITX2. Non-pigmented ciliary epithelium (NPCE) cells were transfected with non-targeting siRNA (control) and different concentrations of PITX2 specific siRNA. PITX2 was detected with HA antibody (1:5000) and HRP-conjugated secondary antibody, goat anti-mouse (1:5000). Labeling with anti phosphor ERK 1/ 2 antibody was used as loading control.

B. siRNA suppressed expression of endogenous PITX2. Trabecular meshwork (TM) cells were transfected with non-targeting siRNA and 100nM PITX2 specific siRNA. PITX2 was detected with Abnova PITX2 antibody (1:1000). HRP-conjugated goat anti-mouse (1:5000) was used as secondary antibody. Labeling with alpha-tubulin antibody was used as loading control.

A

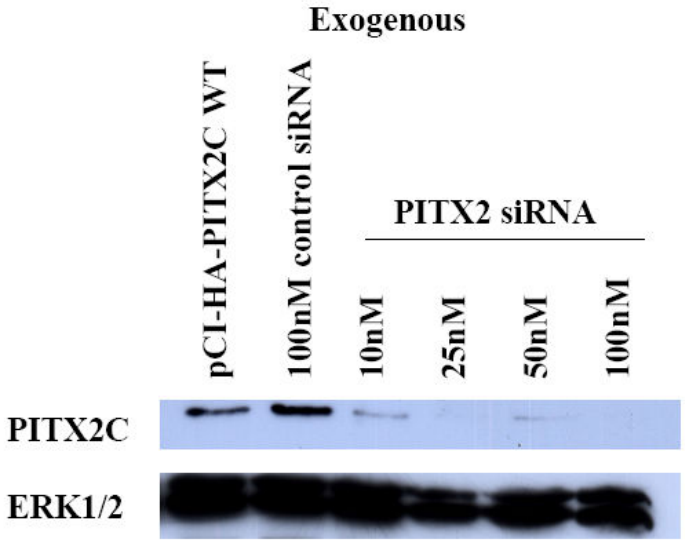

NPCE cells transfected with HA-PITX2Cwt

B

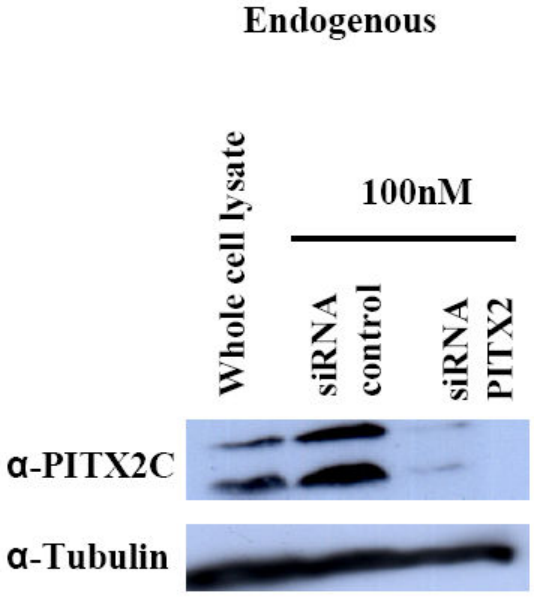

HTM cells

Figure 4-7: *SLC13A3* expression is regulated by PITX2. TM cells were transfected with 100nM of PITX2 specific siRNA, 100nM of non-targeting control siRNA (ctr) or wild-type PITX2. RNA extraction and RT-PCR were performed 48 hours post-transfection. PCR reactions were performed using 28 cycles and the products were separated by size on an agarose gel.

Lane 1: H_2O control. *Lane 2*: RNA extracted from HTM cells. *Lane 3*: RNA extracted from HTM cells transfected with pcDNA4-PITX2C wt. *Lane 4*: RNA extracted from HTM cells transfected 100nM of non-targeting control siRNA. *Lane 5*: RNA extracted from HTM cells transfected with 100nM of PITX2-specific siRNA. *Lane 6*: HTM cells RT-PCR. *Lane 7*: RNA extracted from HTM cells transfected with pcDNA4-PITX2C wt RT-PCR. *Lane 8:* HTM cells transfected with 100nM of non-targeting control siRNA RT-PCR. *Lane 9*: HTM cells transfected with 100nM of PITX2- specific siRNA RT-PCR. β-Actin c-DNA primers were used in positive control reactions to verify the integrity. *Lanes 2-4* are used as negative controls. The quantification of the bands in the experiment reactions was performed using Image J program and compared to the corresponding β-Actin control reactions bands.

*Overexpression of PITX2 increased *SLC13A3* expression

**Silencing PITX2 expression decreased *SLC13A3* expression

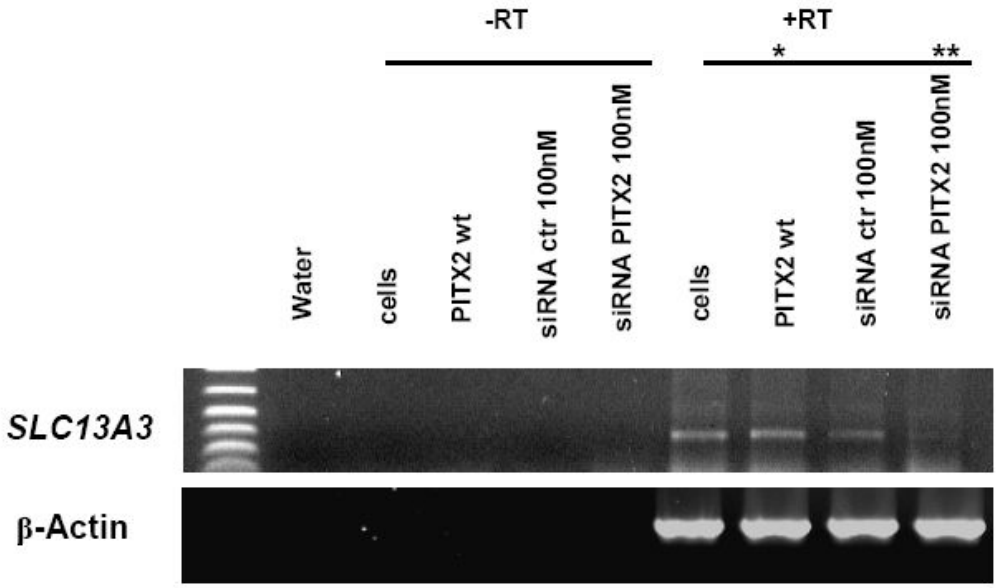
-RT
+RT
*
**
Water
cells
PITX2 wt
siRNA ctr 100nM
siRNA PITX2 100nM
cells
PITX2 wt
siRNA ctr 100nM
siRNA PITX2 100nM
SLC13A3
β-Actin

PITX2 and *SLC13A3* are involved in stress response pathway

Cell viability assay was performed to examine whether *PITX2* and *SLC13A3* are involved in stress response pathways and whether oxidative stress is able to cause a stronger effect on cell viability when the expression of *PITX2* or *SLC13A3* is reduced. The cytotoxic concentrations of hydrogen peroxide were first tested on HTM cells before testing the viability of cells when expression of *PITX2* or *SLC13A3* is reduced. HTM cells were treated with different H_2O_2 concentrations 200, 400, 600, and 800 μM H_2O_2 for 1 hour. Nonviable cells were detected by propidium iodide staining 24 hours after stress exposure. In this assay, untreated control cells demonstrated almost no dead cells stained red by propidium iodide. The number of nonviable cells when the HTM cells were treated with 200 μM H_2O_2 was not statistically different than the number of dead cells without treatment. In contrast, exposure to 400, 600 and 800 μM H_2O_2 significantly increased the proportion of nonviable TM cells (Figure 4-8). In order to observe a significant effect of H_2O_2 on the cell viability, the next experiments were conducted with 600μM H_2O_2. HTM cells were transfected with 100nM of PITX2 specific siRNA or 100nM of non-targeting control siRNA 48 hours before 600μM H_2O_2 exposure and cell viability assay was performed to determine whether HTM cells are more susceptible to cell death when PITX2 expression is reduced. As shown in Figure 4-9, the number of dead HTM cells is significantly increased by at least four times when cells with reduced PITX2 expression are exposed to H_2O_2. We tested the efficiency of 100nM of *SLC13A3* specific siRNA to suppress *SLC13A3* expression by western blot and semi-quantitative RT-PCR

before determining whether HTM cells are more susceptible to cell death when *SLC13A3* expression is reduced. HTM cells were transfected with 100nM of SLC13A3 specific siRNA or 100nM of non-targeting control siRNA and pCI-SLC13A3wt-V5. Protein extraction was performed forty eight hours after the recombinant protein transfection. HTM cells were transfected with 100nM of SLC13A3 specific siRNA or 100nM of non-targeting control siRNA and 48 hours post-transfection, RNA extraction and semi-quantitative RT-PCR were performed to determine whether 100nM of SLC13A3 specific siRNA reduces SLC13A3 endogenously. As illustrated in Figure 4-10, the protein expressed by *SLC13A3* was successfully reduced by 84% (Figure 4-10 A) and the *SLC13A3* RNA levels were reduced by 72% (Figure 4-10 B). HTM cells were transfected with 100nM of SLC13A3 specific siRNA or 100nM of non-targeting control siRNA 48 hours before 600μM H_2O_2 exposure and cell viability assay was performed to determine whether HTM cells are more susceptible to cell death when *SLC13A3* expression is reduced. As shown in Figure 4-9 and Figure 4-10, the number of dead HTM cells was significantly increased by at least 2-fold when cells with reduced SLC13A3 expression were exposed to H_2O_2.

Figure 4-8: The effect of 200, 400, 600, and 800 μM H_2O_2 treatments on HTM cell viability. HTM cells were treated with different H_2O_2 concentrations (200, 400, 600, and 800 μM H_2O_2) for one hour. Nonviable cells were detected by propidium iodide staining 24 hours after stress exposure. Nonviable cells were quantified by counting cells from at least six representative fields. Data presented as a mean ± SD of three sets of experiments (*$P < 0.05$).

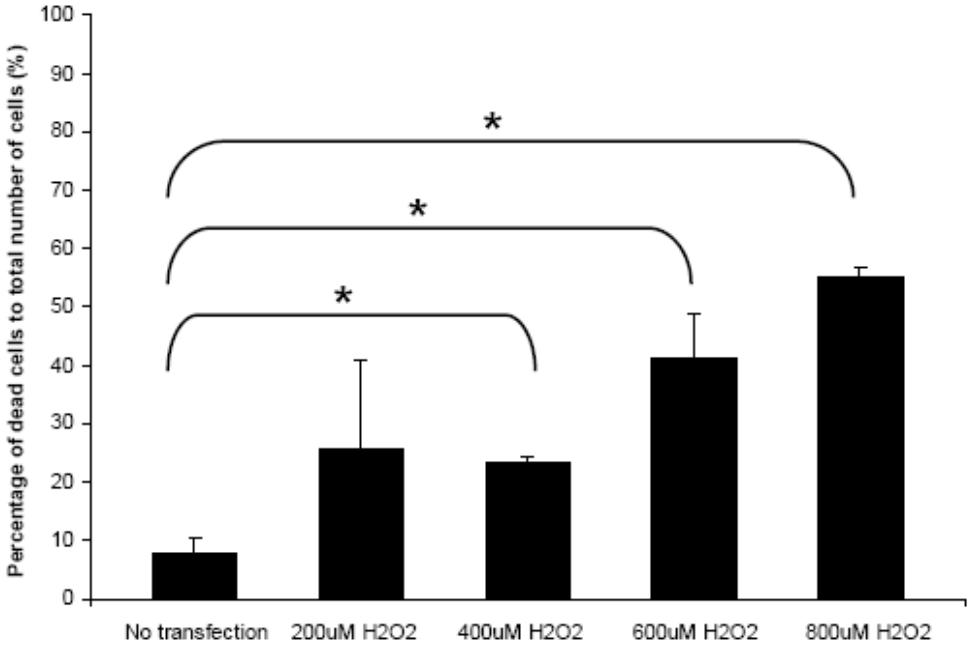
Percentage of dead cells to total number of cells (%)
100
90
80
70
60
50
40
30
20
10
0
*
*
*
No transfection
200uM H2O2
400uM H2O2
600uM H2O2
800uM H2O2

Figure 4-9: *PITX2* and *SLC13A3* are involved in stress response in HTM cells. HTM cells were transfected with 100nM of PITX2 specific siRNA, 100nM of SLC13A3 specific siRNA or 100nM of non-targeting control siRNA 48 hours before 600 μM H_2O_2 exposure and cell viability assay was performed. Nonviable cells were detected by propidium iodide staining 24 hours after stress exposure. **A.** Representative fluorescence photomicrographs of HTM cells stained with propidium iodide. **B**. Quantification of nonviable cells by counting cells from at least six representative fields. Data presented as a mean ± SD of three experiments (*$P < 0.05$).

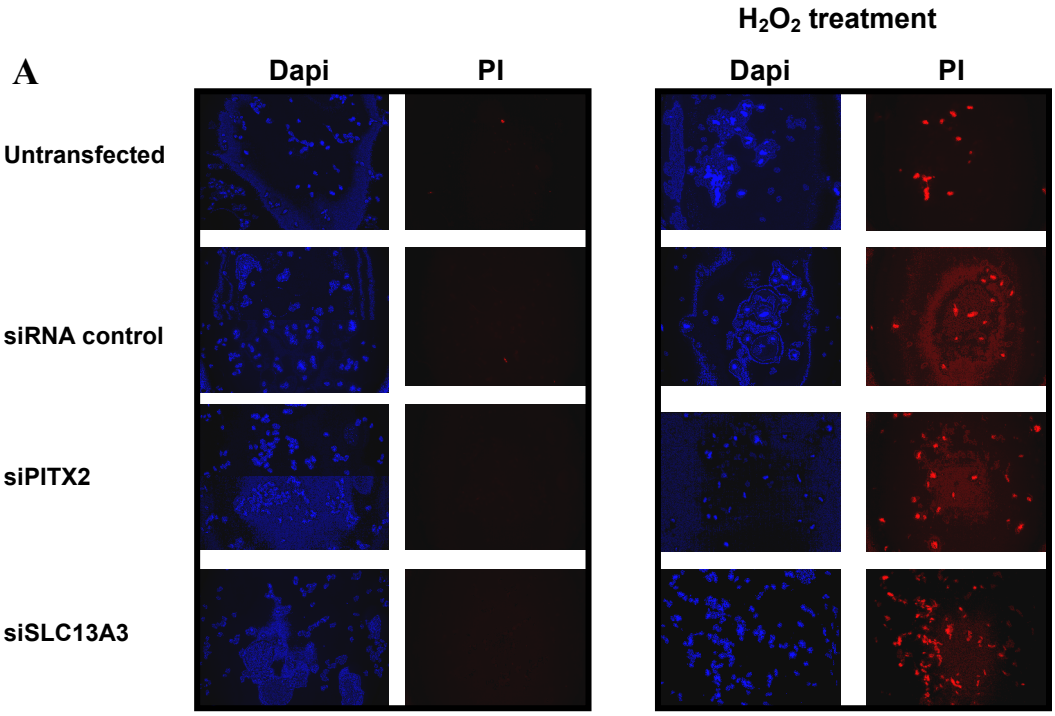
A
Dapi
PI
H_2O_2 treatment
Dapi
PI
Untransfected
siRNA control
siPITX2
siSLC13A3

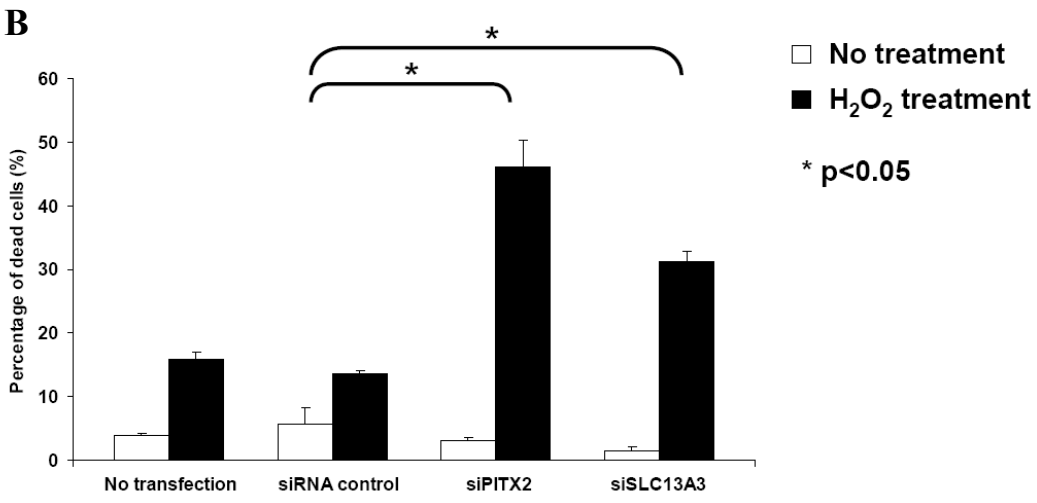
B
Percentage of dead cells (%)
60
50
40
30
20
10
0
No transfection
siRNA control
siPITX2
siSLC13A3
*
*
No treatment
H_2O_2 treatment
* p<0.05

Figure 4-10: The efficiency of human SLC13A3 specific siRNA.

A. siRNA suppressed the protein expressed by *SLC13A3* by western blot. HTM cells were transfected with non-targeting siRNA and SLC13A3 specific siRNA. HTM cells were then transfected with pCI-SLC13A3-V5, 24 hours post transfection with siRNA**.** SLC13A3 was detected using anti-V5 antibody. Alpha-transferin antibody was used as a loading control.

B. siRNA suppressed SLC13A3 RNA. HTM cells were transfected with non-targeting siRNA and SLC13A3 specific siRNA. RNA was extracted 48 hours after the transfection and RT-PCR was performed.

Lane 1: H_2O control. *Lane 2*: RNA extracted from HTM cells. *Lane 3*: RNA extracted from HTM cells transfected with 100nM of non-targeting control siRNA. *Lane 4*: RNA extracted from HTM cells transfected with 100nM of SLC13A3 specific siRNA. *Lane 5*: HTM cells RT-PCR. *Lane 6*: HTM cells transfected with 100nM of non-targeting control siRNA RT-PCR. *Lane 7*: HTM cells transfected with 100nM of SLC13A3 specific siRNA RT-PCR. β-Actin primers were used in positive control reactions to verify the integrity of the cDNA samples. *Lanes 2-4* are used as negative controls. The bands were quantified using Image J program and compared to the corresponding Alpha-transferin in western blot or β-Actin control in RT-PCR.

A

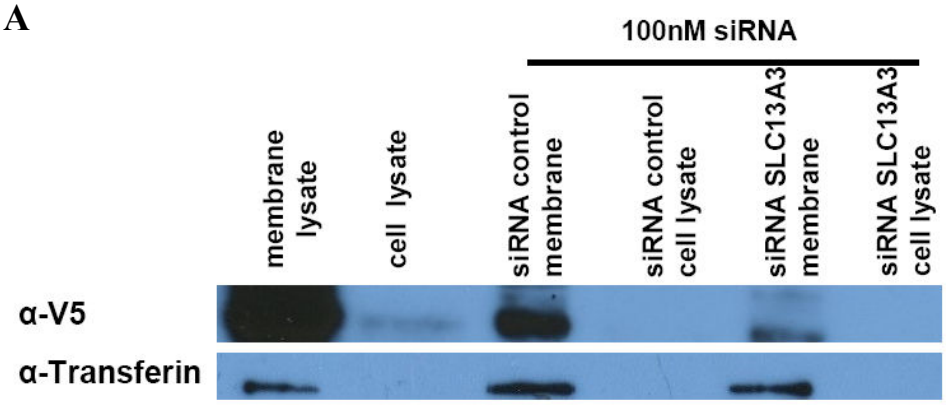

HTM cells transfected with pCI-SLC13A2wt-V5

B

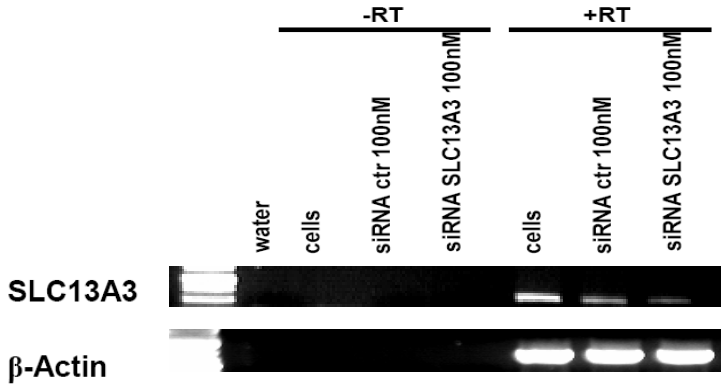

Discussion

SLC13A3 as a direct target gene of PITX2

The data presented in the Chapter 3 and Chapter 4 indicate that *SLC13A3* gene is a bona fide direct target gene of PITX2. *SLC13A3* was identified as a potential PITX2 target gene by microarray analysis and was upregulated as determined by RT-PCR. The *in silico* analysis revealed that *SLC13A3* gene is highly conserved among species and is expressed in the eye and brain. The proximal *SLC13A3* promoter is only conserved in primates such as chimpanzee or monkey, however the promoter sequence is not well known for many species. The proximal human *SLC13A3* promoter contains several PITX2 putative binding sites. The luciferase reporter assay showed that PITX2 specifically activated transcription from the *SLC13A3* promoter. Two of the PITX2 DNA binding sites found upstream of *SLC13A3* are conserved among chimpanzee and monkey, suggesting that these DNA binding motifs might be functionally important. To test this hypothesis, I made different deletion constructs of the *SLC13A3* promoter containing different numbers of PITX2 binding sites. The upstream region of *SLC13A3* promoter containing the first two PITX2 binding sites, A and B, showed a 20-fold greater activity than the pGL3- basic activity. Deletion of the putative PITX2 binding motif B increased the activity of *SLC13A3* promoter by three-fold compared to the fragment containing both PITX2 binding sites, while deletion of both PITX2 binding motifs, A and B, decreased the activity of *SLC13A3* promoter by almost 100%, to the level of pGL3- basic activity. These results suggested that PITX2 binding site A might be important in the activation of the *SLC13A3* gene and the

region surrounding PITX2 binding site B might contain negative regulatory elements. Three missense mutations of PITX2 found in ARS patients, T30P, V45L and R52C, resulted in significantly reduced expression from *SLC13A3* promoter. ChIP analysis revealed that PITX2 did indeed bind to both PITX2 binding sites, A and B, *in vivo*. I observed a reduced expression of *SLC13A3* when PITX2 expression was reduced and an increased expression of *SLC13A3* when PITX2 expression was increased. The data presented here provide compelling evidence that expression of *SLC13A3* is directly regulated by PITX2 *in vitro* and *in vivo*.

The role of *PITX2* and *SLC13A3* in cellular stress pathway

The most important clinical consequence of ARS is glaucoma. ARS-glaucoma typically develops in childhood or early adulthood, however, patients with ARS may develop glaucoma at birth or after middle age. Patients with ARS remain at risk of developing glaucoma throughout their lives. Generation of reactive oxygen species (ROS) is increasingly recognized as an important cellular process involved in numerous physiological and pathophysiological processes, including glaucoma [185]. Reactive oxygen species (ROS) are partially reduced and highly reactive metabolites of oxygen (O2) and include superoxide anion ($O^{-}_{2}\cdot$), hydrogen peroxide (H_2O_2) and hydroxyl radical ($OH\cdot$) [187, 188]. ROS can be formed intracellularly through products of normal aerobic metabolism and as second messengers in various signal transduction pathways [185]. ROS can be also derived by being taken directly by cells from the extracellular environment.

During the past years, many experimental studies performed *in vitro* and *in vivo*, either in animals or humans showed that local oxidative stress is a determining factor in pathology of glaucoma. *In vitro* studies showed that HTM cells' morphology is altered when they are exposed to hydrogen peroxide, cell adhesion and integrity being compromised [189]. *In vivo,* aqueous humor drainage from the anterior chamber of the calf eye is affected when HTM cells are perfused with hydrogen peroxide [190]. Moreover, it has been shown in humans that HTM cells from glaucoma patients presented more oxidative DNA damage than in unaffected controls and this damage is significantly correlated with elevation of IOP and visual field damage [164, 191]. I proposed that in patients with ARS and PITX2 mutations, the defending mechanisms against the cellular stress may be altered resulting in glaucoma. In the present chapter, this hypothesis was tested and a reduction in PITX2 protein levels produced an increase in HTM cell death when the cells were exposed to hydrogen peroxide. Moreover, a reduction in *SLC13A3* also produced an increase in HTM cell death when the cells were exposed to hydrogen peroxide, however the cell viability was less affected comparing with HTM cells with reduced PITX2. These results indicate for the first time that PITX2 through SLC13A3 and other genes is involved in cellular stress pathway.

A proposed glaucoma mechanism in ARS patients and PITX2 mutations involving *SLC13A3*

The defense mechanisms against oxidative stress in the eye involve ascorbic acid and reduced glutathione (GSH). Ascorbic acid is present in high concentrations in aqueous humor [192, 193], vitreous humor [194] and cornea [195] and it is seen as one of the main substrate in ocular protection. One of the main defense mechanisms of the human body, including the eye, against free radicals is reduced glutathione (GSH). GSH is formed by three amino-acids (L-cysteine, glycine and glutamic acid) and it is present in high concentrations in aqueous humor [193] and HTM cells [190]. Furthermore, aqueous humor of glaucoma patients presented with reduced of total antioxidant potential [163] and a decreased of plasmatic GSH levels [162]. A postulated role of the protein encoded by *SLC13A3,* NaDC3, in the kidney cells is to transport gluthione (GSH). This hypothesis is sustained by many evidences. Most of the cells have the capacity to synthesize *de novo* GSH and this production is sufficient in a normal redox state. However, when the cells are exposed to oxidative stress, the cells have to transport GSH from the extracellular environment into the cells in order to maintain an adequate concentration of GSH. The main source of GSH is the liver, where GSH is produced and eliminated into the plasma [196]. GSH circulates through the body and it is extracted by the kidney [197]. The site where GSH is extracted is the renal proximal tubular cells being transported across the basolateral plasma membrane (BLM) [198]. It was shown that the GSH transport at the BLM requires at least two Na^+ ions with a net negative charge of -1 at

physiological pH. The GSH transport is inhibited by dimethylsuccinate, γ-glutamyl amino acids and ophthalmic acid [176]. The exact carrier of GSH across the renal BLM is still unidentified. There are two sodium-dicarboxylate transporters in the kidneys: NaDC1 encoded by *SLC13A1* and NaDC3 encoded by *SLC13A3;* however NaDC1 is present only in the brush border membranes [199], not in the BLM. Therefore, NaDC3 has the correct subcellular localization and functional properties to transport GSH. Ophthalmic acid is a GSH endogenous derivative and represents an oxidative stress biomarker [200]. Ophthalmic acid is glutamate-2-aminobutyrate-glycine, a tripeptide produced by the same enzymes as GSH [201]. It was recently shown that ophthalmic acid concentration is increased when GSH pool is depleted [200]. It is not known whether ophthalmic acid is also transported from the extracellular environment into the cells or whether ophthalmic acid is found in aqueous humor.

I suggest the following pathway as a part of a network serving important functions in protection against the cytotoxic effects of ROS (Figure 4-12). PITX2 activates *SLC13A3* which encodes the membrane NaDC3 protein. NaDC3 transports GSH or ophthalmic acid from the aqueous humor into the HTM cells. GSH protects the cells against the accumulation of ROS being a cofactor in reduction of hydrogen peroxide to water. When the GSH pool is depleted, the ophthalmic acid concentration is increased by production or possible transportation. The protection of GSH and ophthalmic acid against ROS will maintain a normal HTM cells function with normal drainage of aqueous humor and normal IOP.

In ARS patients with PITX2 defects, mutation of PITX2 will reduce *SLC13A3* expression and the transportation of GSH and possible ophthalmic acid into the HTM cells will be affected. Low concentrations of GSH and ophthalmic acid will decrease the defense against ROS accumulation. When ROS generation exceeds the cell's antioxidant capacity to prevent oxidative injury, they create a constant threat to cells with cell dysfunction and cell death. Our data presented here showed that reduction of PITX2 expression increased TM cells death. The cell death will be increased over time resulting in the compromise aqueous humor drainage, elevated IOP and glaucoma.

The study presented here shows a new function of PITX2 as a factor involved in cellular stress pathway. It provides evidence that *SLC13A3* is a direct target gene of PITX2 being also involved in cellular stress pathway.

Figure 4-11. Schematic representation of the proposed mechanism.

A. In unaffected individuals. *SLC13A3* gene expression is induced by PITX2 activation. *SLC13A3* gene encodes the membrane NaDC3 protein which transports GSH from the aqueous humor into the HTM cells. Glutathione peroxidase reduces hydrogen peroxide to water using reduced glutathione as cofactor. Reduced glutathione is transformed to oxidized glutathione (GSSH). GSH protects the cells against the accumulation of ROS.

B. In ARS patients with PITX2 defects. Mutation of PITX2 will reduce *SLC13A3* expression and the transportation of GSH into the HTM cells will be affected with hydrogen peroxide accumulation.

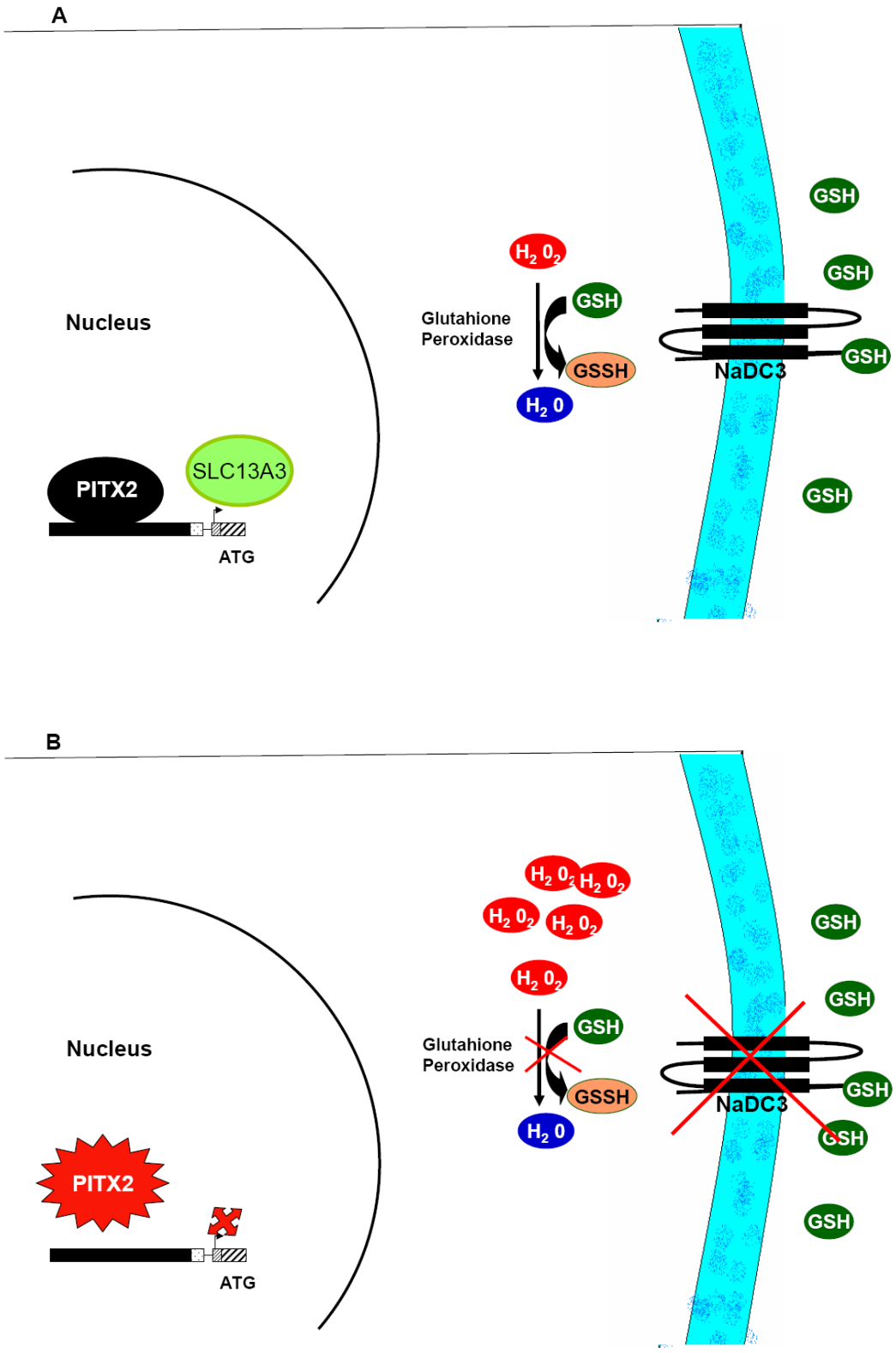
A
Nucleus
PITX2
SLC13A3
ATG
Glutahione
Peroxidase
GSH
GSSH
H_2O_2
H_2O
NaDC3
B
Nucleus
PITX2
ATG
Glutahione
Peroxidase
GSH
GSSH
H_2O_2
H_2O
NaDC3

Chapter five:

PDP2 as a candidate gene of PITX2 regulation

Introduction

PDP2 (*Pyruvate dehydrogenase phosphatase*) was identified as a potential target gene of PITX2 by microarray analysis and northern blot. I have selected *PDP2* (*Pyruvate dehydrogenase phosphatase*) for further analysis for several reasons. First, *PDP2* is located on chromosome 16q22.1, near a previously mapped ARS locus, and therefore is a good candidate for a gene causing disease. Distal 16q is already a chromosomal region of interest to those working on ARS. The first authors to make this link, Ferguson and Hicks, described in 1987 a patient with a partial trisomy of 16q associated with Rieger's syndrome [202]. Later, a deletion of 16q23.1–16q24.2 was found in a patient with bilateral coloboma of the iris, short stature, moderate developmental delay, and minor craniofacial anomalies [51]. Linkage analysis has also mapped a family with inherited foveal hypoplasia and anterior segment dysgenesis to a locus on 16q23.2–24.2 [203].

Second, PDP2 activity is affected by chemical stresses such as starvation and diabetes which decrease PDP2 activity. As discussed in Chapter four, cellular stresses such as oxidative damage or mechanical strain have been implicated in the pathology of glaucoma [185]. Glaucoma incidence increases with age which reflects the effect of prolonged exposure of cellular stresses on the eye. Oxidative stress can compromise the function of the anterior segment tissues implicated in the production and the drainage of the aqueous humor leading to imbalance of aqueous humor dynamics and ultimately to elevation of intraocular pressure (IOP) [185]. Retinal ganglion cells (RGC) are degenerated in glaucoma which could

also be a consequence of the apoptosis induced by the oxidative damage. The involvement of *PDP2* in the cellular stress pathways makes this gene a good candidate for involvement in glaucoma.

Last, both PDP2 and PITX2 are known to be involved in embryonic development and organogenesis pathways. PITX2 is expressed in the developing eye and continues to be expressed in the adult eye. It is already known that PITX2 acts downstream in the TGF-β /Activin/Nodal pathway, being involved in development of left-right (L-R) asymmetry [78]. Recently, Hong et *al*. [204] showed in their paper published in 2006 that PDP proteins are involved in dephosphorylation of SMAD proteins in the BMP/DPP pathway. Phosphorylation of the SSXS motif of SMADs is critical in activating transforming growth factor β (TGF-β) and bone morphogenetic protein (BMP) pathways. The authors of the above paper identified PDP as being required for dephosphorylation of Mothers against Decapentaplegic (MAD), a *Drosophila* SMAD, which inhibits signal transduction via Decapentaplegic (DPP). It was also shown that the mammalian PDPs are important in dephosphorylation of BMP-activated SMAD1 but not TGF-β-activated SMAD2 or SMAD3 [204]. Thus, PDPs specifically inactivate SMADs in the BMP/DPP pathway.

This chapter describes functional analysis of the *PDP2* as a direct target gene of PITX2. This analysis may have important implications, not only for the regulation of *PDP2*, but also for the role of PITX2 in ocular regulation pathways.

Methods

Computer based *in silico* analyses

The *in silico* tissue expression profile of *PDP2* was determined via an electronic search on Source Stanford University database as described in Chapter four. The PITX2 DNA binding motif (TAATCC, GGATTA, GGCTTAG or CTAAGCC) search on the upstream region of *PDP2* was performed on Source Stanford University database and EMBL - EBI -Sanger Institute websites as described in Chapter four. The conserved PITX2 DNA binding motifs among species, the *PDP2* nucleotide sequence alignment and *PDP2* upstream region sequence alignment were performed by on the European Bioinformatics Institute website as described in Chapter four. The human sequences were submitted to RepeatMasker to exclude the sequence placed into the repeat regions as described in Chapter four.

Percent identity plot (PIP)

The 34kb of genomic sequence from hChr16 and 46kb of genomic sequence from mChr8 were extracted from the EMBL - EBI -Sanger Institute website (hChr16: GRCh37:16:66885789:66920140:1 and mChr8: NCBIM37:8:107072569:107118924:1) as described in Chapter four. To find the gene structures of *PDP2* and *CA7* (Carbonic anhydrase 7), NCBI website was used as described in Chapter four.

Plasmids

N-terminally flagged hemagglutinin epitope (HA) PITX2 C wt, pcDNA4-His-Max PITX2 C wt and pcDNA4-His-Max PITX2C mutant constructs, T30P, V45L and R52C, were described in Chapter four. Different lengths of the 5'-UTR flanking region of the human *PDP2* promoter were PCR -amplified from genomic DNA. The primer pairs used for amplification are shown in Table 5-1. These promoter constructs were designated p2BS-PDP2 (-2571/+151), p1BS-PDP2 (-2159/+151) and p0BS-PDP2 (-1662/ +151), respectively. *Xho*I and *Bgl*II sites were used for of all promoter fragments. The *PDP2* promoter fragments were subcloned first into pGEM-T vector (Promega), according to the manufacturer's protocol, and then subcloned into *Xho*I/ *Bgl*II sites of pGL3 vector (Promega). The longest *PDP2* promoter fragment (p2BS-PDP2) was generated by combining two shorter fragments. One shorter fragment contains the first 1662bp (fragment b) upstream of the *PDP2* transcription site, and the other one contains the sequence between 1443bp and 2571bp (fragment a) upstream of *PDP2* transcription site. The two shorter fragments were PCR-amplified from genomic DNA, and then subcloned into separate pGEM-T vectors. The two fragments were ligated together at the *Hind*III site and then subcloned into *Xho*I/ *Bgl*II sites of pGL3 vector. The final constructs were sequenced to ensure their integrity.

Cell culture and transfection

Cell culture and transfection were done as described in Chapter four. HTM cells were transfected in 24-well plates using 160ng of empty vector or PITX2 wt,

60ng of the different pGL3-PDP2 promoter constructs, 20ng of the pCMV beta-galactosidase transfection controls and 3µl of Fugene6 transfection reagent.

Transactivation assays

HTM cells were cultured in 24-well plates at a density of 4x 10^4 cells/plate twenty four hours prior to transfection. Cells were transfected, harvested after forty eight hours of incubation and luciferase activities were monitored following the manufacturers' protocols (Promega). Transfections were performed in triplicates and repeated three times.

Protein expression

Whole cell protein extraction was performed forty eight hours after transfection of HTM cells with 100nM PITX2 specific siRNA or 100nM non-targeting control siRNA to check siRNA efficiency. Western blot analysis was performed using a mouse monoclonal anti-PITX2 antibody (Abnova, 1:1000) to detect endogenous PITX2C wt. HRP-conjugated goat anti-mouse (1:5000) was used as secondary antibody. Anti alpha-tubulin antibody (1:1000) was used as loading control with goat anti-rabbit (Abcam, 1:5000) HRP-conjugated goat anti-mouse as secondary antibody. The protein extraction protocol is described in Chapter three.

Chromatin immunoprecipitation

Chromatin Immunoprecipitation (ChIP) was performed using Active Motif ChIP-IT^{TM} Express kit (catalog no: 53008) according to the protocol and as described in Chapter four. The primer pairs used for amplification spanning the PITX2 binding sites are shown in Table 5-2. The primers were designed using the Primer3 Input website (http://frodo.wi.mit.edu/primer3/).

siRNA transfection

HTM cells were cultured on six well plate ($5x10^5$ cells/ well) or 100mm plate ($1x10^6$ cells), 24 hours prior to transfection and transfection protocol of siRNA was described in Chapter four. Cell lysate or RNA was extracted 48 hours after the last transfection and western blot or RT-PCR was performed.

RNA extraction

HTM cells were transfected with 100nM of PITX2 specific siRNA or 100nM of non-targeting control siRNA. RNA extraction was performed 48 hours post-transfection and it is described in Chapter four.

Semi-quantitative RT-PCR

RNA samples were extracted from HTM cells as described above. Total RNA was used as a substrate for semi-quantitative reverse transcription–polymerase chain reaction (RT-PCR) and RT-PCR protocol is as described in Chapter four. A 20µl reverse transcription reaction without reverse transcriptase corresponding to

each type of transfection (100nM of PITX2 specific siRNA or 100nM of non-targeting control siRNA) was used as negative control. Specific PCR primers to check PDP2 expression are F: 5'-GCGGTTTGAGAGCAACC-3' and R: 5'-CCATAGCTCCCTCCATGTGC-3'. Reactions were cycled in a thermocycler for 28 cycles. PCR products were separated using agarose gel electrophoresis and visualized with ethidium bromide. Beta-actin was used as "input" control. β-actin forward primer is 5'-ATCATGTTTGAGACCTTCAACAC-3 and β-actin reverse primer is. 5'-TCTGCGCAAGTTAGGTTTTGTC-3'.

Table 5-1.	**Primers used for *PDP2* Promoter construction**		
Construct	**Forward**	**Reverse**	**Product size (bp)**
p2BS-PDP2 a	CTCGAGGAGCTATGCTTTCCCTTTCT	AGATCTGTTTCACCGTTTTAGCCGGG	1129
p2BS-PDP2 b	CTCGAGTCAACCTACCAGCCGCCAGC	AGATCTCGCTCGTTACCTTCCCTACC	1812
P1BS-PDP2	CTCGAGTATATGACCTGTCTGCTGGG	AGATCTCGCTCGTTACCTTCCCTACC	2310
p0BSPDP2	CTCGAGTCAACCTACCAGCCGCCAGC	AGATCTCGCTCGTTACCTTCCCTACC	1813

BS= PITX2 Binding Site

Table 5-2.	**Primers used for ChIP**		
Construct	**Forward**	**Reverse**	**Product size (bp)**
PITX2 binding site A	CCAATCGAGCTATGCTTTCC	CCCTGGAGGATTTTATGTGC	194
PITX2 binding site B	CTCCAAGTGGCTTTTTCTGG	GGTTGAGAGAGACAGCGAACC	194
PITX2 binding site C	CCGAACTGACAAGTAACTACAGG	AGCACTTTGAGAGGCCAAGC	463
PITX2 binding site D	AGGCATGAGAAGCTTGAACC	GTGCAAGGAACCTCAACTGC	390

Results

In silico analysis identified PITX2 binding sites on *PDP2* promoter

In silico analysis of *PDP2* indicated that *PDP2* is highly expressed in the eye and brain. I did a manual search looking for putative PITX2 binding sites (TAATCC/ GGATTA) in the first 3000bp upstream of the untranslated region of exon 1 of the human *PDP*. The promoter sequence was first uploaded on RepeatMasker to exclude the sequences placed into the repeat elements. The manual search revealed two putative PITX2 DNA binding motifs, which I named putative PITX2 binding site A and B. The manual search revealed that putative PITX2 binding site A is conserved in Macaca mulatta (monkeys), while putative PITX2 binding site B is conserved in Pan troglodytes (chimpanzee) and Macaca mulatta (monkey) promoter region (Figure 5-1A). I did an electronic search looking for putative PITX2 binding sites in the first 3000bp upstream of the human *PDP2* when Possum website and PITX2 binding sites matrix were available. The electronic search revealed only putative PITX2 DNA binding site A. The electronic search revealed that putative PITX2 binding site A is conserved in Pan troglodytes (chimpanzee) and Macaca mulatta (monkey) promoter region (Figure 5-1B). The PITX2 binding sites sequences are presented in Table 5-3.

The human sequence between *PDP2* and the nearest upstream neighboring gene, *CA7* (Carbonic anhydrase 7), was compared with the homologue mouse sequence and a percent identity plot (PIP) was generated. Comparison of 26kbp of human genomic sequence located on chromosome 16 to 41kb of the homologous region in mouse on chromosome 8 showed seven regions of homologous

sequence between *SLC13A3* and *CA7* (Figure 5-2). The sequence between *PDP2* and *CA7* was first uploaded on RepeatMasker and then uploaded on the Possum website to determine whether this sequence contains PITX2 DNA binding motifs that are outside of repeat elements and are conserved in mouse. This *in silico* analysis revealed two putative PITX2 DNA binding motifs conserved in mouse, called putative PITX2 binding site C at 11kb upstream of *PDP2* and D at 13kb upstream of *PDP2* (Figure 5-3 and Table 5-4).

PITX2 activates transcription from the *PDP2* promoter region

The transcriptional regulatory element of *PDP2* was investigated using the luciferase reporter assay to determine the possible role of PITX2 in the transcription regulation of *PDP2*. The activation of the *PDP2* reporter by PITX2 was monitored by cloning different sizes of *PDP2* promoter into luciferase reporter vector. The longest construct of 2772bp in length (-2571/+151), p2BS-PDP2, included the PITX2 DNA binding sites A and B. The second construct, p1BS-PDP2, contained PITX2 DNA binding site A is 2310bp in length (-2159/+151). The shortest construct of 1813bp in length (-1662/ +151), p0BSPDP2, presented no PITX2 DNA binding motif (Figure 5-4). We monitored luciferase activity, after co-transfecting HTM cells with pcDNA4-PITX2C wt and pGL3-PDP2 upstream region expression vectors. Xpress-tagged PITX2 activated the expression from the p2BS-PDP2 luciferase reporter (Figure 5-4). Deletion of putative PITX2 binding site B produced less activation compared with PITX2 expression from the p2BS-PDP2 (Figure 5-4). The removal of the two sites, A and

B, completely abolished PITX2 activation of this reporter. Activation of the p2BS-PDP2 and p1BS-PDP2 luciferase reporter was diminished when disease-causing R52C, V45L and T30P PITX2 alleles were transfected into cells.

PITX2 binds to *PDP2* promoter through chromatin immunoprecipitation (ChIP) assays

ChIP was performed to determine whether PITX2 is able to bind the promoter region of *PDP2 in vivo*. ChIP analysis showed upstream DNA sequence of *PDP2* containing PITX2 binding site C being recovered with PITX2 and H3-AcK9 antibodies (Figure 5-5). However, no binding was found at the PITX2 binding sites A, B or D. These data indicate that PITX2 occupies *in vivo* the promoter regions of *PDP2* on conserved PITX2 binding site C.

***PDP2* expression is affected by variation in PITX2 expression**

siRNA suppression of PITX2 followed by semi-quantitative RT-PCR was performed to determine whether reducing *PITX2* expression by silencing PITX2 affects *PDP2* expression. Before looking at *PDP2* expression through RT-PCR, the efficiency of the PITX2 suppression by siRNA was tested by western blot. As illustrated in Figure 5-6 A, human PITX2 specific siRNA suppressed endogenous PITX2. HTM cells were transfected with 100nM of PITX2 specific siRNA and 100nM of non-targeting control siRNA. RNA extraction and RT-PCR were performed 48 hours post-transfection. The RNA levels of *PDP2* were reduced when PITX2 expression is reduced (Figure 5-6 B). In order to determine whether

overexpressing *PITX2* affects *PDP2* expression, HTM cells were transfected with of PITX2 and RT-PCR was performed. The RNA levels of *PDP2* were increased when PITX2 was overexpressed (Figure 5-6C).

Figure 5-1. *In silico* analysis showed many putative PITX2 binding sites.

A. Putative PITX2 binding sites in the first 3kbp upstream region of human *PDP2* and other species identified by a manual search.

B. Putative PITX2 binding sites in the first 3kbp upstream region of human *PDP2* and other species identified by an electronic search.

The PITX2 binding sites are represented by red vertical lines. The black circle represents putative PITX2 binding site A and the blue circle represents putative PITX2 binding site B. For electronic search: The length of each line represents log-likelihood ratio score, the higher the score is, the longer the line is. The log-likelihood ratio score is calculated by comparing every sequence fragment to the PITX2 binding motif.

A

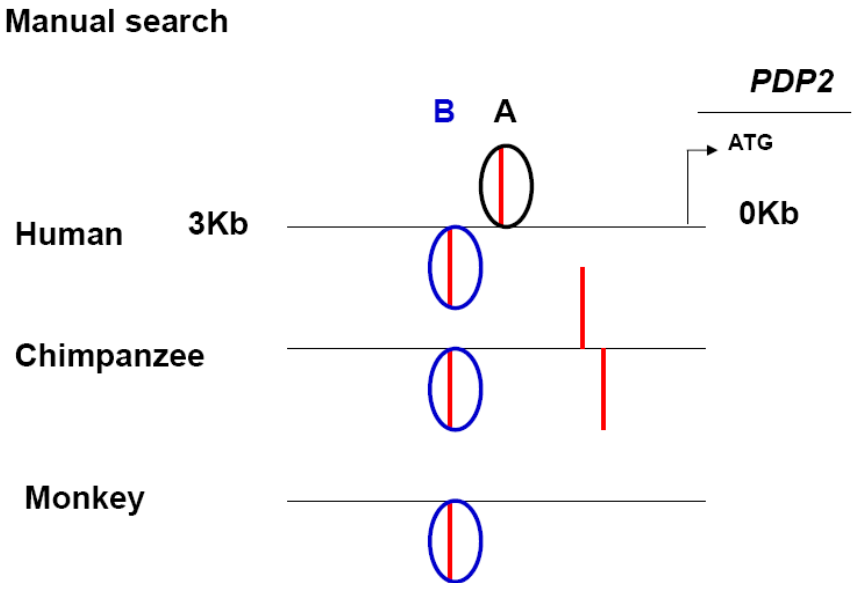
Manual search
PDP2
B
A
ATG
0Kb
Human
3Kb
Chimpanzee
Monkey

B

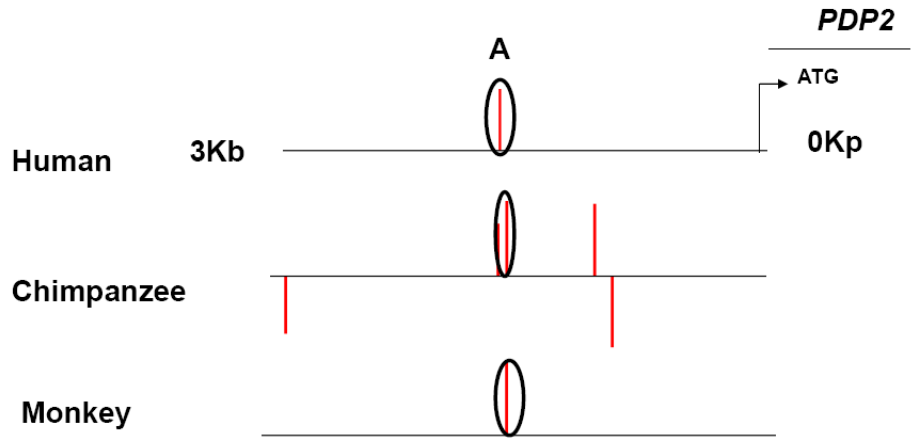
Possum search
PDP2
A
ATG
0Kp
Human
3Kb
Chimpanzee
Monkey

Table 5-3. PITX2 Bindings sites upstream of *PDP2* in different species by manual search

Species	position	strand	sequence
Human	1687 - 1695	+	gggattat
	2529 - 2535	-	taatcc
Chimpanzee	777-783	-	taatcc
	862 - 868	+	ggatta
	1305-1311	+	ggatta
Monkey	2191-2197	+	taatcc

Table 5-4. PITX2 Bindings sites upstream of *PDP2* in different species by Possum search

Species	position	strand	sequence
Human	1306 - 1313	+	gggattat
Chimpanzee	517 - 524	-	ttagtccc
	1586 - 1593	+	gtgattac
	1629 - 1636	+	gggattat
	2072 - 2079	+	gggattac
	2157 - 2164	-	gtaatccc
Monkey	1648 - 1655	+	gggattat

Figure 5-2: Comparison of 34kbp of human genomic sequence (hChr 16) to 46kb of the homologous region in mouse (mChr8). There are seven homology sequence regions between the two sequences indicated by arrows. The small horizontal lines or dots represent the matching regions of homology between the two sequences. The position of lines or dots represents the percentage of nucleotide identity.

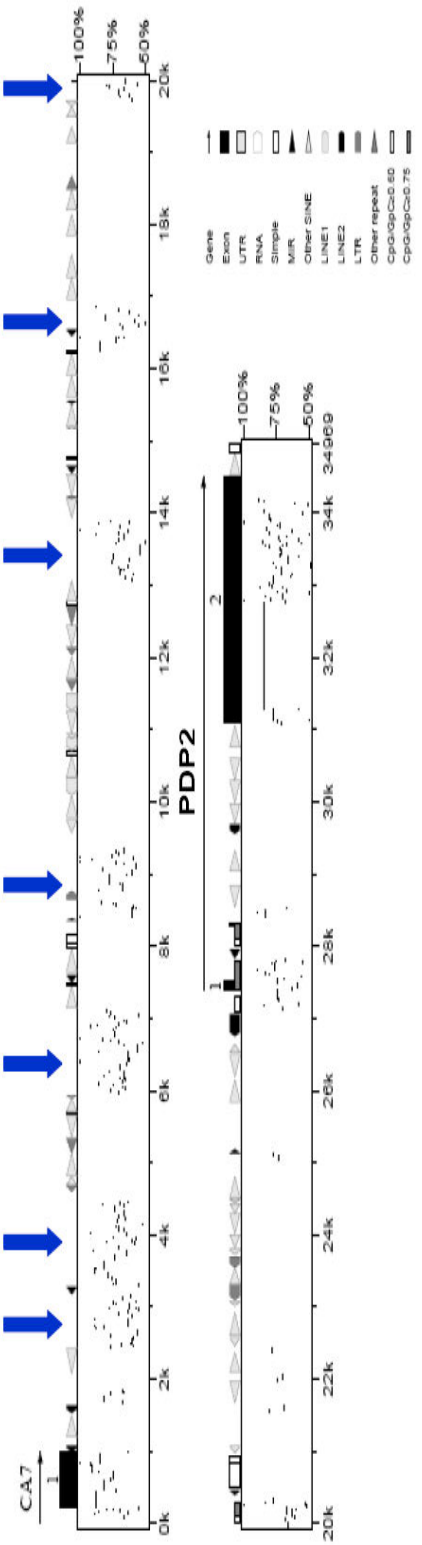
PDP2
CA7
100%
75%
50%
0k
2k
4k
6k
8k
10k
12k
14k
16k
18k
20k
22k
24k
26k
28k
30k
32k
34k
34969
Gene
Exon
UTR
RNA
Simple
MIR
Other SINE
LINE1
LINE2
LTR
Other repeat
CpG/GpC≥0.60
CpG/GpC≥0.75

Figure 5-3. Putative PITX2 binding sites in the 26kbp upstream region of human *PDP2*, between *PDP2* and the neighboring gene, *CA7* and comparison with mouse homologue region. Red circle indicates putative PITX2 binding site C and green circle indicates putative PITX2 binding site D. Putative PITX2 binding sites C and D are conserved in mouse and are outside of repeat elements. The length of each line represents log-likelihood ratio score, the higher the score is, the longer the line is. The log-likelihood ratio score is calculated by comparing every sequence fragment to the PITX2 binding motif.

Possum search

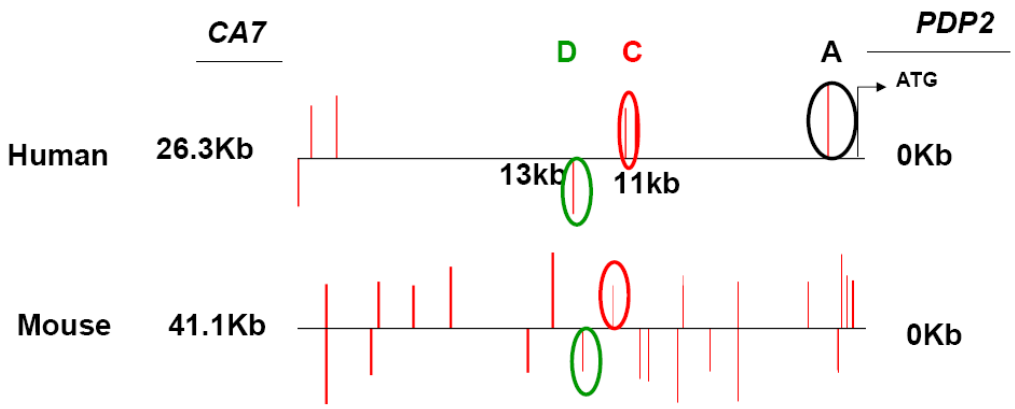

Table 5-5. PITX2 Bindings sites upstream of *PDP2* in human and mouse by Possum search

Species	position	strand	sequence
Human	21 - 28	-	ttaagcac
	636 - 643	+	gggcttat
	1780 - 1787	+	tagattaa
	12834 - 12841	-	ttaatcag
	15230 - 15237	+	ctgattac
	2157 - 2164	-	gtaatccc
Mouse	1162 - 1169	+	gtgattac
	1201 - 1208	-	ctaatccc
	2982 - 2989	-	ttactccg
	3359 - 3366	+	gggatgac
	4816 - 4823	+	gggaatag
	6318 - 6325	+	gagattaa
	9510 - 9517	-	taaatccc
	10489 - 10496	+	gggattaa
	10539 - 10546	+	gggattaa
	12111 - 12118	-	ttaattcc
	15182 - 15189	+	ctgattac
	17910 - 17917	-	ttaatctg
	18820 - 18827	-	ttaatcca
	21854 - 21861	-	ttaatccc
	22390 - 22397	+	gggatttc
	22496 - 22503	+	gggatcaa
	25168 - 25175	-	ttaattcc
	27971 - 27978	+	gggattca
	27996 - 28003	-	ttactccc
	28041 - 28048	-	ttaatccc
	35173 - 35180	+	gggactaa
	38151 - 38158	-	ttaatcga
	38409 - 38416	-	ctaatcct
	38664 - 38671	+	gggattaa
	39211 - 39218	+	cagattat
	39881 - 39888	+	gggattta
	41039 - 41046	-	gtaatctc

Figure 5-4. Effects of PITX2 wild type on different deletion constructs of *PDP2* promoter in HTM cells. Luciferase reporter plasmid containing different deletion constructs of *PDP2* promoter (p2BS-PDP2, p1BS-PDP2 and p0BS-PDP2) were co-transfected in HTM cells with empty vector (pcDNAHisMaxA), PITX2C wild type, R52C, V45L or T30P PITX2 alleles. Luciferase activity was normalized relative to the activity of pGL3-basic.

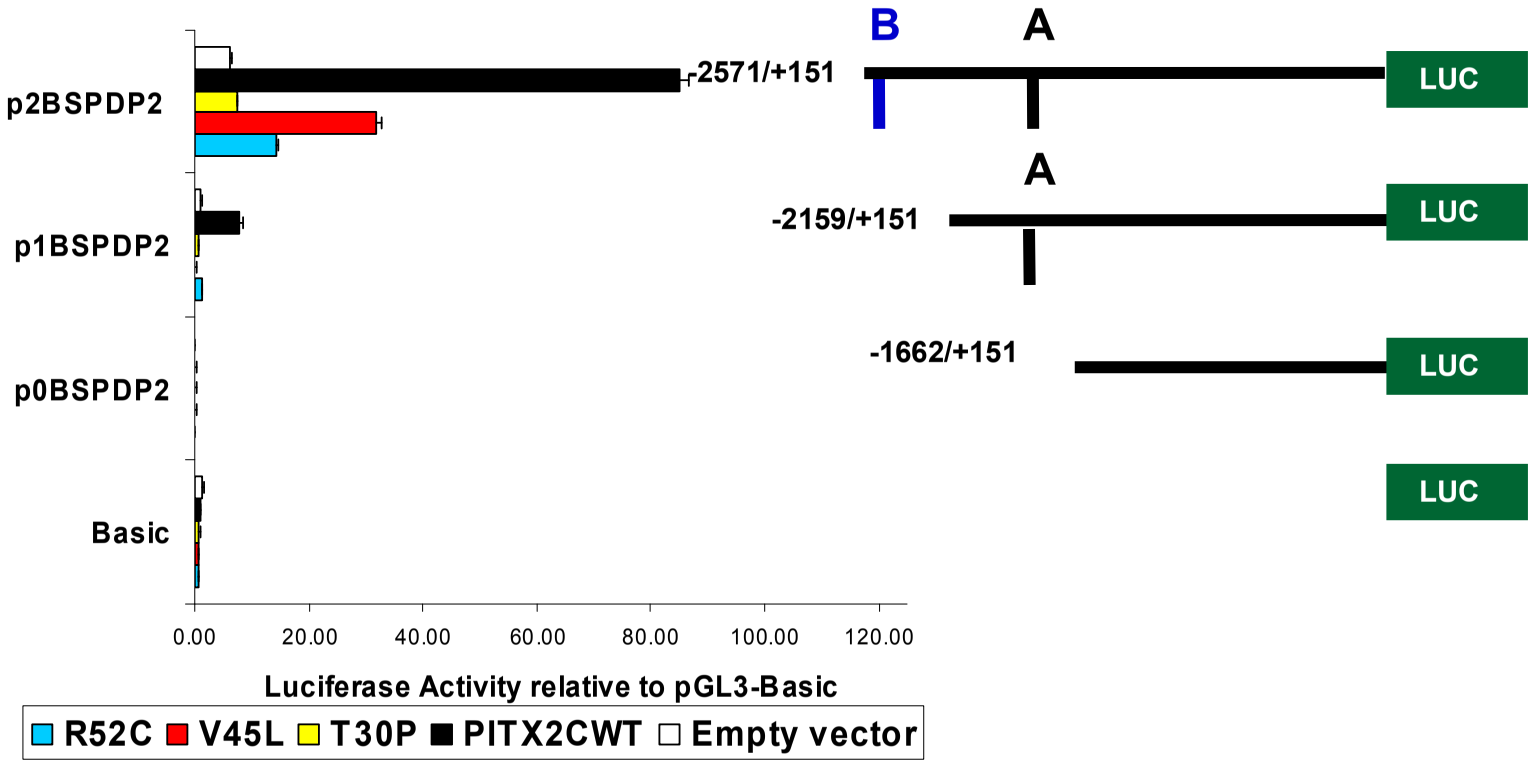
p2BSPDP2
p1BSPDP2
p0BSPDP2
Basic
0.00
20.00
40.00
60.00
80.00
100.00
120.00
Luciferase Activity relative to pGL3-Basic
R52C
V45L
T30P
PITX2CWT
Empty vector
B
A
-2571/+151
LUC
A
-2159/+151
LUC
-1662/+151
LUC
LUC

Figure 5-5: PITX2 binds to the *PDP2* promoter *in vivo* through PITX2 binding site C. Top: Schematic representation of the putative PITX2 binding sites positions. **Bottom:** Chromatin immunoprecipitation was performed and PCR was used to amplify the immunoprecipitated DNA using designed primers to span **(A)** PITX2 binding site A, **(B)** PITX2 binding site B, **(C)** PITX2 binding site C, **(D)** PITX2 binding site D. **A, B** and **D** showed chromatin was not immunoprecipitated by antibodies against PITX2 and H3-AcK9, as well as no antibody added or IgG antibody did not immunoprecipitate chromatin. **C** showed chromatin was immunoprecipitated by antibodies against PITX2 and H3-AcK9. No antibody added or IgG antibody did not immunoprecipitate chromatin.

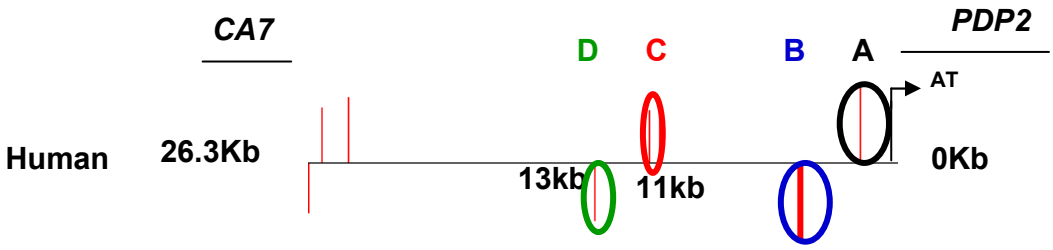
CA7
PDP2
D
C
B
A
AT
Human
26.3Kb
13kb
11kb
0Kb

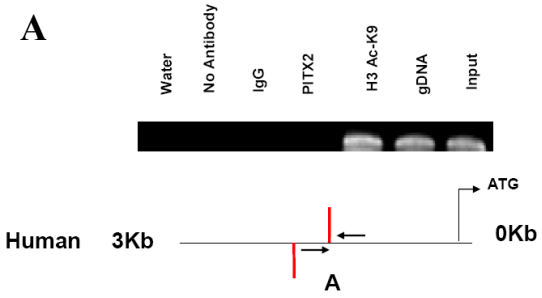
A
Water
No Antibody
IgG
PITX2
H3 Ac-K9
gDNA
Input
ATG
Human
3Kb
0Kb
A

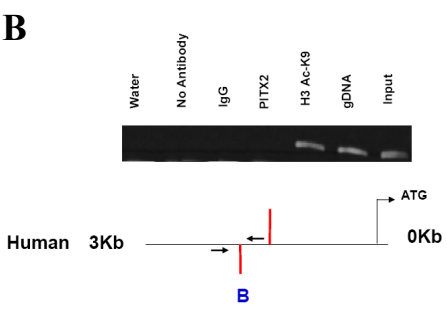
B
Water
No Antibody
IgG
PITX2
H3 Ac-K9
gDNA
Input
ATG
Human
3Kb
0Kb
B

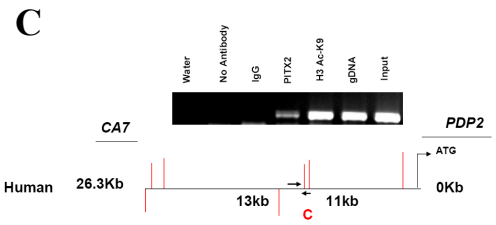
C
Water
No Antibody
IgG
PITX2
H3 Ac-K9
gDNA
Input
CA7
PDP2
ATG
Human
26.3Kb
0Kb
13kb
11kb
C

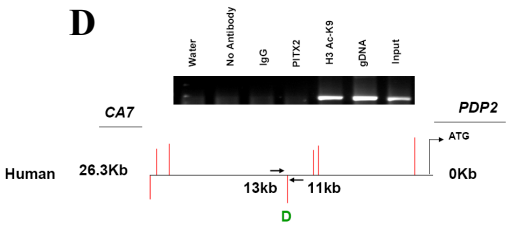
D
Water
No Antibody
IgG
PITX2
H3 Ac-K9
gDNA
Input
CA7
PDP2
ATG
Human
26.3Kb
0Kb
13kb
11kb
D

Figure 5-6: *PDP2* expression is regulated by PITX2.

A. PITX2 specific siRNA efficiently suppressed PITX2. Western blot was performed 48 hours post-transfection with 100nM of PITX2 specific siRNA or 100nM of non-targeting control siRNA to check the efficiency of siRNA. PITX2 was recognized by a mouse monoclonal anti-PITX2 antibody. Anti alpha-tubulin antibody as a loading control.

B. Reduced PITX2 expression affects *PDP2* expression. RNA extraction and RT-PCR were performed 48 hours post-transfection with 100nM of PITX2 specific siRNA or 100nM of non-targeting control siRNA. *Lane 1*: H_2O control. *Lane 2*: RNA extracted from HTM cells. *Lane 3*: RNA extracted from HTM cells transfected 100nM of non-targeting control siRNA. *Lane 4*: RNA extracted from HTM cells transfected with 100nM of PITX2 specific siRNA. *Lane 5*: HTM cells RT-PCR. *Lane 6*: HTM cells transfected with 100nM of non-targeting control siRNA RT-PCR. *Lane 7*: HTM cells transfected with 100nM of PITX2 specific siRNA RT-PCR.

C. PITX2 overexpression affects *PDP2* expression. RNA extraction and RT-PCR were performed 48 hours post-transfection with pcDNA-PITX2C wt. *Lane 1*: H_2O control. *Lane 2*: RNA extracted from HTM cells. *Lane 3*: RNA extracted from HTM cells transfected with pcDNA-PITX2C wt. *Lane 4*: HTM cells RT-PCR. *Lane 5*: HTM cells transfected with pcDNA-PITX2C wt RT-PCR.

β-Actin primers were used in positive control reactions to verify the integrity of the cDNA samples.

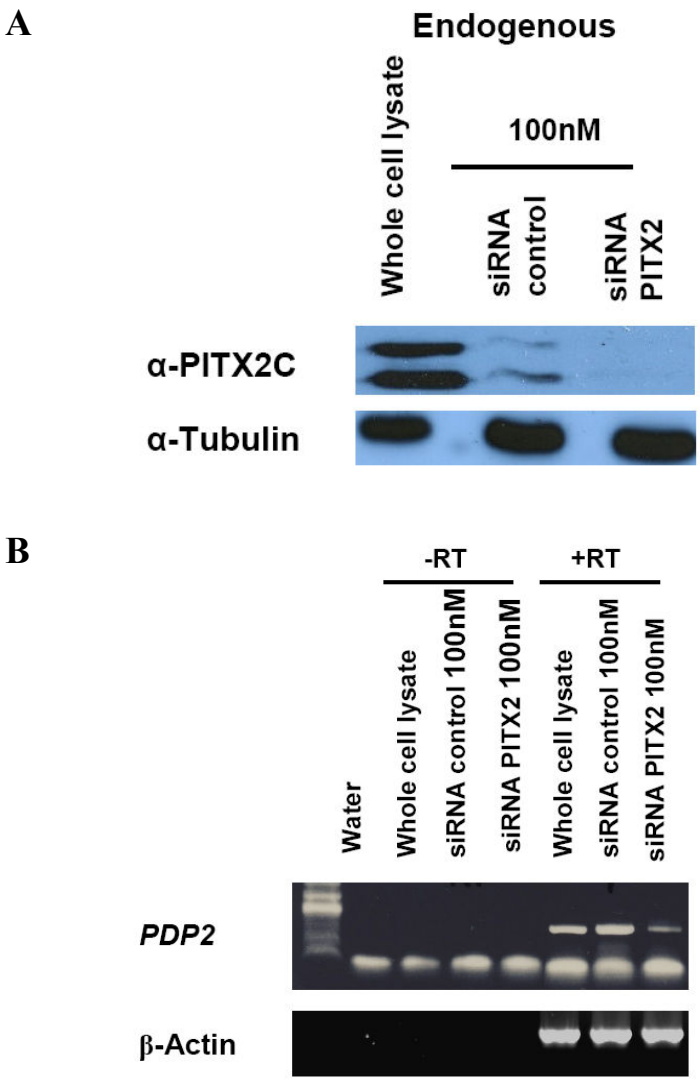
A
Endogenous
Whole cell lysate
100nM
siRNA control
siRNA PITX2
α-PITX2C
α-Tubulin
B
-RT
+RT
Water
Whole cell lysate
siRNA control 100nM
siRNA PITX2 100nM
Whole cell lysate
siRNA control 100nM
siRNA PITX2 100nM
PDP2
β-Actin
C
-RT
+RT
Water
Whole cell lysate
PITX2 wt
Whole cell lysate
PITX2 wt
PDP2
β-Actin

Discussion

PDP2 as a target gene of PITX2

The data presented in Chapter 3 and Chapter 5 indicate that *PDP2* gene is a bona fide target gene of PITX2. *PDP2* was identified as a potential PITX2 target gene by microarray analysis and also upregulated expression by northern blot analysis. The *in silico* analysis revealed that *PDP2* gene is highly conserved among species and it is expressed in the eye and brain. The first 3000bp upstream of *PDP2* is only conserved in the mammalian organisms such as chimpanzee or monkey. However, the percent identity plot (PIP) which compared the 26kbp of human genomic sequence to the 41kb of the homologous region in the mouse between the *PDP2* and the neighboring gene, CA7, showed seven homology sequence regions between the two sequences. The *in silico* analysis results suggests that the regions conserved between human and mice may have important functions. The upstream region of human *PDP2* contains putative binding sites for several transcription factors, including PITX2. The luciferase reporter assay showed that PITX2 activated expression from the *PDP2* promoter, which indicates that PITX2 binds to *PDP2* promoter. Three missense mutations of PITX2 found in ARS patients, T30P, V45L and R52C, resulted in significantly reduced expression from *PDP2* promoter. Two of PITX2 DNA binding sites found in the first 3000bp upstream of *PDP2* are conserved among chimpanzee and monkey, suggesting that these DNA binding motifs may have important functions. To test this hypothesis, I made different deletion constructs of *PDP2* promoter containing different number of PITX2 binding sites. The longest

fragment of *PDP2* promoter containing PITX2 binding sites A and B showed an increased in luciferase activity over the pGL3- basic activity. Deletion of the PITX2 binding motif B decreased the activity of *PDP2* promoter almost to the level of the pGL3- basic activity, while deletion of the PITX2 binding motives A and B abolished the PITX2 activity. These results suggested that the PITX2 binding site B might be functionally important in the activation of *PDP2* gene. However, ChIP analysis showed no binding of PITX2 at the PITX2 binding sites, A and B. An explanation of the luciferase and ChIP results might be the indirect effect of PITX2 on *PDP2* in the first 3000bp upstream of *PDP2*. PITX2 might form a molecular complex with other transcription factors and synergistically activate *PDP2* gene. *In silico* analysis of the 3000bp upstream of *PDP2* showed many cis-elements such as TATA, LSF, GATA, AP-1, WF-1 or TEF binding motifs. Another explanation of no binding of PITX2 at the PITX2 binding sites A or B is the sensitivity of ChIP to identify an interaction between PITX2 and *PDP2* promoter. ChIP is a powerful method for studying interactions between transcriptional factors and DNA in living cells. ChIP can determine whether a transcription factor interacts with a candidate target gene. However negative results do not necessarily mean that a given factor is not associated with the site. The resolution of the ChIP procedure could be affected by the size of the fragments that are created and the selective enrichment of a chromatin fraction containing a specific protein. Looking at the 26kbp upstream sequence of *PDP2*, *in silico* analysis showed two PITX2 binding sites, C at 11kbp and D at 13kbp, being conserved between human and mice. *In silico* analysis results indicated that

these two PITX2 binding sites, C and D, might be functionally important. ChIP analysis revealed binding of PITX2 at the PITX2 binding sites C. Further work on the PITX2 binding sites C and D might include luciferase assay analysis.

Semi-quantitative RT-PCR was performed to determine whether variation in PITX2 expression affects *PDP2* expression. I observed a reduction in *PDP2* expression when PITX2 expression was reduced and an increased expression of *PDP2* when PITX2 expression was increased. The data presented here provide compelling evidence that expression of *PDP2* is directly regulated by PITX2 *in vitro* and *in vivo*.

A proposed transcriptional network of PITX2 involving *PDP2*

Pyruvate dehydrogenase phosphatase (PDP) is one of the mammalian phosphatases localized within the mitochondrial matrix space. Mammalian tissues contain two genetically and biochemically different forms of PDP: PDP1 and PDP2 [205]. Both are Mg^{2+}-dependent enzyme; and PDP1 is Ca^{2+}-sensitive, wheras PDP2 is insensitive to stimulation by Ca^{2+}[205]. PDP1 has long been recognized as an important regulator of the activity state of the pyruvate dehydrogenase complex (PDC) [206, 207], however PDP2 was more recently identified [205]. PDP1 is predominantly expressed in mitochondria from skeletal muscle, whereas PDP2 is much more abundant in the liver mitochondria [205]. Both isoenzymes are expressed in mitochondria from adipocytes, but the level of expression of PDP2 is considerably higher. The identity between PDP1 and PDP2 is approximately 55% within the sequences of the mature polypeptides. In several

regions that are presumably functionally important, the identity reaches up to 90%. PDP2 is 530 amino acids long with the molecular mass of 59.6kDa [205]. In contrast with PDP1, which has been extensively characterized [206, 207], the exact structure of PDP2 protein is not currently known. PDPs function is to regulate the pyruvate dehydrogenase complex (PDC).

The mitochondrial pyruvate dehydrogenase complex (PDC) catalyzes the irreversible oxidative decarboxylation of pyruvate to acetyl-CoA and CO_2, coupled with the reduction of NAD^+ to $NADH^+$. This reaction links the utilization of glycogen, glucose, and lactate with the citric acid cycle to meet the energy needs of cells. PDC regulation is based on reversible phosphorylation, in which two enzymes are implicated: PDPs and pyruvate dehydrogenase kinase (PDK) [205, 208]. PDKs phosphorylate PDC which completely inhibits the enzymatic activity of PDC [209, 210]. The complex can be reactivated by dephosphorylation catalyzed by PDPs [211]. PDC is inactivated in many tissues during starvation and diabetes to conserve three-carbon compounds for gluconeogenesis [212-215]. This is achieved by an increase in PDC phosphorylation caused in part by increased PDK activity and expression and in part by decreased activity and expression of PDP [216]. Therefore, opposite changes in expression of specific PDK and PDP isoenzymes contribute to hyperphosphorylation and inactivation of the PDC during starvation and diabetes. Refeeding and insulin treatment effectively reversed these effects of starvation and diabetes, respectively [216]. The effects of different hormonal, nutritional and phARSacological conditions on PDP2 protein and mRNA expressions implicate PDP2 in oxidative stress pathways.

As discussed in Chapters three and four, generation of reactive oxygen species (ROS) is recognized as an important cellular process involved in glaucoma [185]. Reactive oxygen species (ROS) can be formed intracellular through products of normal aerobic metabolism and as second messengers in various signal transduction pathways [185]. ROS can also be taken directly by cells from the extracellular environment. Mitochondria constitute the greatest source of ROS, since mitochondrial electron transport consumes approximately 85% of the O2 [185]. Aerobic energy metabolism is dependent on oxidative phosphorylation, a process by which the oxidoreduction energy of mitochondrial electron transport is converted to ATP [185]. Complex I (NADH:ubiquinone oxidoreductase) is considered as one of the major sources of ROS within mitochondria [217]. ROS are produced at low levels during normal physiological conditions, and controlled production of ROS is essential.

I suggest the following model as a part of pathways serving important functions in regulation of the production of ROS (Figure 5-7). PITX2 activates *PDP2* which encodes the mitochondrial PDP2 protein. PDP2 activates PDC by dephosphorylation, and activated PDC reduces NAD^+ to NADH. Three potential effects of mitochondrial NADH (reduced nicotinamide adenine dinucleotide) could reduce superoxide and ROS accumulation [218]. First, the increase in NADH might shift (semi)-oxidized FMN (flavin mononucleotide) to $FMNH_2$ and thus suppress superoxide formation at the FMN group in complex I. This mechanism of reduction accumulation of ROS has been reported previously in neurons [219, 220]. Second, the NADH-induced activation of complexes I, III,

and IV will increase electron transport through the electron transfer chain and favor oxygen transition to water instead of superoxide formation. Third, the generated NAD(P)H equivalents can serve as cofactors for enzymes involved in ROS scavenging, such as glutathione-disulfide reductase and thioredoxin-disulfide reductase.

Defects of PITX2 will generate impairment of the PDP2 activity, and thus PDC will not be properly activated. The inhibition of the PDC activity will inhibit the electron transfer chain at complex I and will generate the accumulation of electrons. Once generated, ROS will accumulate and may further impair the mitochondrial electron transport chain, resulting in a shutdown of mitochondrial energy production. In addition to effects on the mitochondria, ROS can cause severe damage to cellular proteins, lipids, and nucleic acids. When ROS generation exceeds the cell's antioxidant capacity to prevent oxidative injury, they create a constant threat to cells which finally leads to human disease such as glaucoma.

Figure 5-7. Schematic representation of the ROS-suppressive action of PDP2 in mitochondria. *PDP2* gene expression is induced by PITX2 activation. Mitochondrial PDP2 protein activates PDC by dephosphorilation. PDC reduces NAD^+ to NADH. Generation of NADH and NADPH increases potential of the cell to eliminate ROS. Mitochondrial NADH and FADH2 re-oxidation increases electron transport through ETC complexes I–IV and favor oxygen transition to water (complex IV) instead of superoxide. NADH shifts complex I FMN from an oxidized to the reduced state FMNH2, which lower the potential of the cell for univalent oxygen reduction to superoxide.

Abbreviations:

PDP2- Pyruvate Dehydrogenase Phosphatase

PDC- Pyruvate Dehydrogenase Complex

PDK- Pyruvate Dehydrogenase Kinase

ETC- Electron Transport Chain

NAD^+- Nicotinamide Adenine Dinucleotide , NADH- the reduced form of NAD^+, NADPH- phosphate form of NADH

FMN, FMNH2- Flavin Mononucleotide and its reduced form

FAD, FADH2- Flavin Adenine Dinucleotide and its reduced form

TCA- Tricarboxylic Acid Cycle

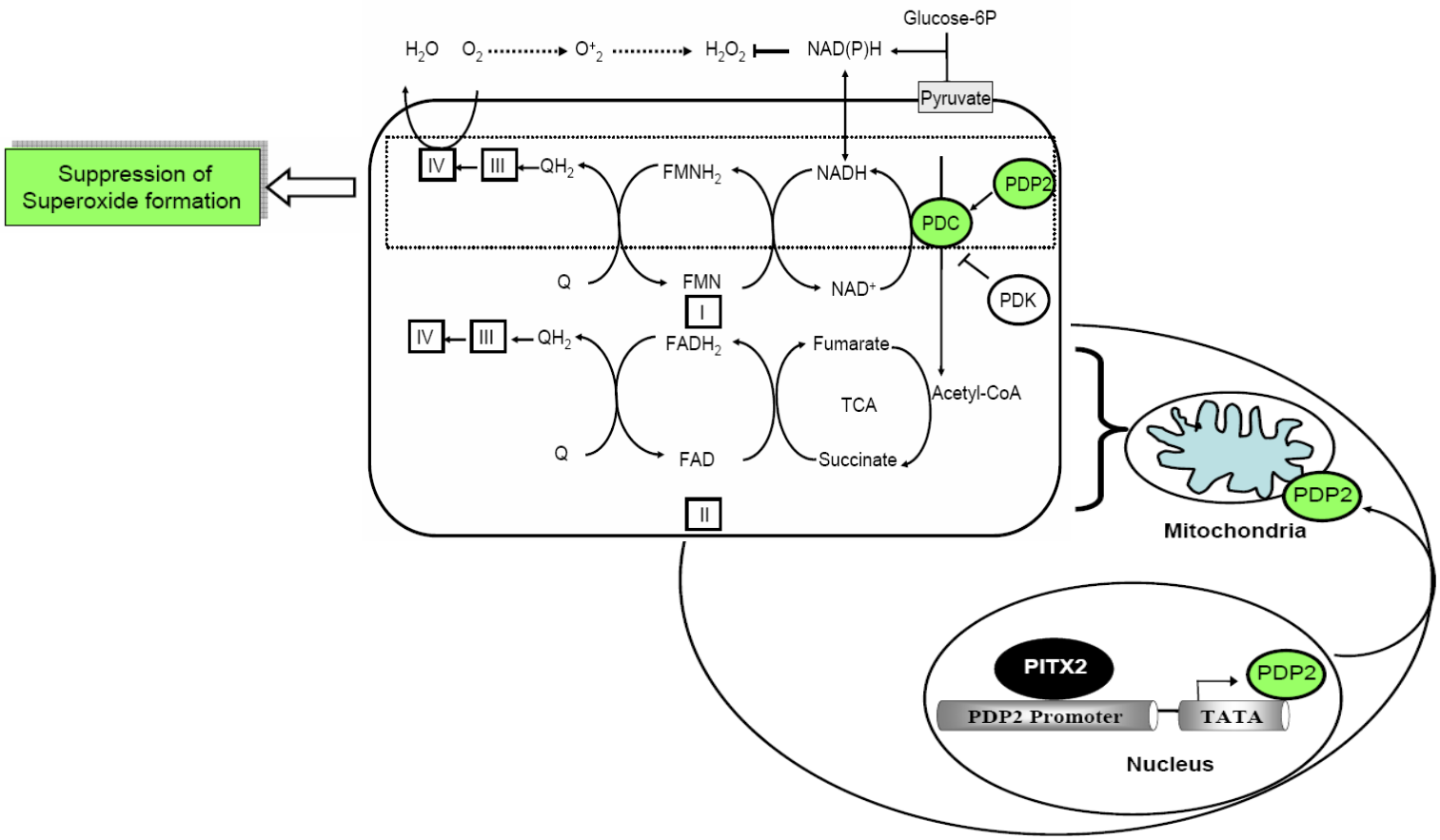
Suppression of Superoxide formation
H_2O
O_2
O^+_2
H_2O_2
NAD(P)H
Glucose-6P
Pyruvate
IV
III
QH_2
$FMNH_2$
NADH
PDP2
PDC
Q
FMN
NAD^+
PDK
I
IV
III
QH_2
$FADH_2$
Fumarate
TCA
Acetyl-CoA
Q
FAD
Succinate
II
Mitochondria
PDP2
PITX2
PDP2
PDP2 Promoter
TATA
Nucleus

Chapter six:

Conclusions and Future Directions

In this thesis, I have presented my own work over the past five years. The overall goal of my PhD project was to gain a better understanding of Axenfeld-Rieger Malformation from both the clinical and genetic points of view. Toward this goal, I have coordinated a clinical study in which I analyzed the glaucoma-related clinical presentation of Axenfeld-Rieger patients to determine there are any useful phenotype- genotype correlations and to see how different treatments improve the state of the patients [1]. By comparing the treatments and outcomes, I tried to determine the best glaucoma treatment for Axenfeld-Rieger patients. I also identified potential target genes for PITX2. Knowledge of the identity of PITX2-regulated genes is a key step in understanding how mutations of PITX2 lead to human disease. Changes in the expression of target genes, and of the activities of their proteins, may contribute to the impairment of aqueous humor outflow in PITX2-associated glaucoma. The following discussion is intended to show how the new findings make contributions to an evolving understanding of the clinical and molecular basis of ARS.

Genotype-Phenotype correlations

The retrospective study [1] presented here shows that ARS is a bilateral anterior segment dysgenesis disease, without any gender predisposition. The ocular manifestation of ARS is more severe in patients with *PITX2* defects than in patients with *FOXC1* defects. Taking into consideration the recent finding that *PITX2* inhibits *FOXC1* activity [64], our model predicts that *PITX2* defects might result in both, an inability to activate *PITX2* targets and a gain of function

activation of *FOXC1* targets. Therefore, the severity of the ocular phenotype in patients with *PITX2* defects might be the simultaneous consequence of *PITX2* haploinsuficiency and a gain of function of *FOXC1*. Patients with non-ocular findings are more likely to have *PITX2* defects rather than *FOXC1* defects. Only two patients with *FOXC1* duplication presented with systemic malformations, suggesting that the eye is particularly more sensitive to duplication of *FOXC1* than other organs. The incidence of glaucoma in this study was 75%, the highest incidence has been reported for this disease so far. This study also showed that patients with *FOXC1* mutations have the mildest prognosis in glaucoma development, while patients with *PITX2* defects and patients with *FOXC1* duplication have a more severe prognosis in glaucoma development than patients with *FOXC1* mutations. In my study, I found that current medical therapies do not successfully lower intraocular pressure or prevent progression of glaucoma in ARS patients with *FOXC1* or *PITX2* alterations. Only 18% of patients who participated in this study responded to medical or surgical (used solely or in combination) treatment. This clinical study also provides useful diagnostic criteria to identify the gene responsible for ARS. Patients presenting with polycoria and systemic malformations are more likely to have *PITX2* defects; patients with iridogoniodysenesis (IGD) without systemic malformations are more likely to have *FOXC1* duplication, and patients with peripheral anterior synechiae (PAS), posterior embryotoxon (PE) and systemic malformations are more likely to have *FOXC1* mutations. On the basis of these findings, I suggested that patients with *PITX2* defects may benefit from more frequent periodic ophthalmologic

examinations, closer monitoring of the disease and more aggressive treatment, both medical and surgical, when glaucoma appears.

Investigation of PITX2 role in ocular disease

The goal of gaining a better understanding of clinical presentation of Axenfeld- Rieger Malformation has been achieved by the retrospective study presented in Chapter 2. However, how defects of genes such as *PITX2* disrupt the developing and mature eye leading to human disease still remains a mystery and needs to be elucidated in order to develop a good treatment for ARS –glaucoma patients which so far is lacking. ARS is a human autosomal- dominantly inherited maldevelopment of the eye associated with glaucoma. PITX2 is expressed in the developing eye where it plays key roles, but also continues to be expressed in adult eye. This raises the question: what is the role of PITX2 in adult eye? In the present thesis, I aimed to answer this question and toward this goal, I identified some of the PITX2 target genes. Knowing the PITX2 target genes allows us to make predictions of the direct consequences of defects of PITX2. As presented in Chapter three, four and five, some of PITX2 target genes are involved in the resistance to cellular stress. Disruption of the PITX2 and dysregulation of its target genes would increase the eye sensitivity to the cellular stress. Increasing evidence supports the involvement of oxidative stress as a common component of glaucomatous tissues such as retinal ganglion cells (RGC) or trabecular meshwork [185]. In ARS patients with *PITX2* defects, the continuous disruption of PITX2

target genes implicated in the resistance to cellular stress would generate in time accumulation of ROS.

ROS can produce a wide range of cellular responses such as proliferation, growth arrest, senescence, and cell death [185]. A determining factor in cellular susceptibility to oxidative stress is the intrinsic antioxidant defense mechanism. The levels of superoxide and catalase decline in aging eyes changing the balance between the pro-oxidant and antioxidant factors [221]. The defense mechanisms against free radicals in the eye involve ascorbic acid [222] and reduced glutathione (GSH) [223], both of them being found in high concentrations in aqueous humor. In normal redox conditions, the antioxidant system is sufficient to reduce hydrogen peroxide and prevent the ROS accumulation and the ROS-induced cellular damage. However, over time this balance is altered resulting in accumulation of ROS and damage of TM cells. Defective genes involved in the detoxification of oxidants may cause a predispotion for ROS accumulation and tissue damage by shifting the pro-oxidant/antioxidant balance. This may explain why patients with ARS and with PITX2 defects often develop glaucoma until their early 20's. As shown in Chapter four, PITX2 is involved in ocular cellular stress pathway and might be involved through *SLC13A3* in GSH- related defense mechanism.

The balance between the intracellular signaling pathways linked to cell survival and the intracellular signaling pathways linked to cell death that are activated by ROS is important in determing the magnitude of cellular damage [224]. Cellular death may be induced by caspase activation or activation of the

mitochondrial cell death pathway. Many studies showed that mitochondria are involved in cellular death induced by different stimuli. For example, a study in a rat glaucoma model showed that neuronal apoptosis was produced by mitochondrial dysfunction [225, 226]. Another study revealed that RGC death was associated with the loss of mitochondrial membrane potential and the release of mitochondrial cell death mediators, including cytochrome c and apoptosis-inducing factor [185]. As shown in Chapter five, PITX2 might be involved through *PDP2* in mitochondrial cell death pathway related to cellular oxidative stress.

ROS can induce the expression of diferent transcriptional factors, besides causing a direct cytotoxic effect [185, 227]. ROS can also produce changes to different proteins such as site-specific amino acid modifications, fragmentation of the peptide chain, aggregation, altered electrical charge, increased susceptibility to proteolysis, and function loss. The oxidative modifications of the proteins will cause a reduction of the cell ability to cope with cellular stress and an impairament of cellular homeostasis. Recognition and degradation of the modified proteins could be possible, but oxidative stress may also inhibit proteasome function preventing the removal of such proteins [185]. Inhibition of the proteasome function and the aggregated proteins will cause a vicious cycle of increased accumulation of oxidative proteins [228, 229]. Accumulation of the protein aggregates leads to a loss in specific protein function, depletion of the cellular redox balance, and ultimately cell death [230, 231].

Perturbation of the cellular antioxidant defense mechanisms, caused by genetic defects such as mutations found in ARS patients can lead to increased accumulation of ROS with increased oxidative damage and decreased in the number of cells such as trabecular meshwork cells. Decreased number of trabecular meshwork cells has been associated with age and with primary open-angle glaucoma [191, 227]. Moreover, the accumulation of oxidative damage in the cellular component of the trabecular meshwork could directly affect the regulation of the extracellular matrix structure and associated intraocular pressure, leading to clinical onset of glaucoma. It is known that the trabecular meshwork region is the main checkpoint controlling aqueous humor outflow and intraocular pressure, alterations that are involved in the pathogenesis of glaucoma [227].

Once glaucoma has developed, elevated IOP and tissue hypoxia presented in glaucomatous tissues can stimulate production of ROS. Experimental elevation of IOP induces oxidative stress in the retina [232]. Acute IOP elevation [232], as well as moderate and chronic elevation of IOP generate ROS. Another well known stimulus leading to oxidative stress is hypoxia, cells responding to graded hypoxia by increasing the generation of ROS. Many studies have shown that hypoxia, ROS generation, and immune system are involved in persisitance of stress conditions in the glaucomatous eyes even if the elevated IOP is effectively lowered [185]. Nitric oxide is another well-known stress that could play an important role in glaucomatous optic nerve damage. It has been reported the presence of inducible nitric oxide synthase in the iris-ciliary body, retina and in the glaucomatous optic nerve head of experimental rat models [233]. The

continuing nature of the glaucomatous tissue stress appears to be important in determining cell fate. The proposed mechanism of defects of PITX2 leading to glaucoma is shown in Figure 6-1. This mechanism will require further validation in the future.

Future prospective

Genotype-Phenotype correlations

The findings of the retrospective study are novel and provided new insights into the clinical presentation and treatment of ARS-glaucoma. However as for any retrospective study, this study had limitations. One important limitation of the retrospective study was the absence of sufficient information regarding ophthalmologic tests that can have an impact on the previous findings, especially central corneal thickness (CCT). Another limitation of the retrospective study was the large number of patients coming from a small number of families, which could have influenced some of the results. To overcome these limitations and to determine the insights obtained from the retrospective study might be used to improve glaucoma treatment and management in ARS patients, a prospective study of ARS-glaucoma patients was initiated in collaboration with Dr. Ordan Lehmann. This large, multi-centered study involves patients all over the world, including patients who already participated in the retrospective study and new patients diagnosed with ARS (Table 6-1 and 6-2). Patient recruitment is done in the USA, UK, Germany, Belgium, Ireland, Italy, Netherlands and New Zealand. The patients recruited in this new prospective study will be followed clinically by

their own ophthalmologist using standardized protocols every six months over two years. In addition to clinical measures of CCT, intraocular pressure, etc., patients' glaucoma progression will be measured and compared to glaucoma treatments. At the end of the follow-up period, information will be gathered from all clinical coordinators and the clinical data will be tabulated and compared through statistical analyses. The comparisons of the underlying genetic defects with glaucoma treatment outcomes in this clinical study will result in improved glaucoma treatment for ARS patients. To date, patients from Edmonton are seen regularly by Dr. Lehmann.

Investigation of PITX2 role in ocular disease

Hormone expression system coupled with microarray analysis

The hormone expression system coupled with microarray analysis was successfully used in isolating PITX2 target genes. The results presented in this thesis showed that the hormone inducible expression system developed for FOXC1 and PITX2 can be successfully used for any other transcription factor to isolate genes. Furthermore, FOXC1-PRG backbone could be used for any other transcription factor if the transactivation domain is known. The transactivation domain of that particular transcription factor could be inserted in the FOXC1-PRG backbone, followed by hormone inducible expression system coupled with microarray analysis. In this way, the direct target genes of the transcription factor in interest could be identified.

SLC13A3 and PDP2

A detailed analysis of the PDP2 promoter region containing the two PITX2 binding sites C and D could be performed by luciferase assay. Since cellular stresses have been implicated in the pathology of glaucoma, analyses of the involvement of the PITX2-> PDP2 regulatory pathway in the ocular cellular stress response could be tested by cell viability assay. The GSH transportation by NaDC3 could be assessed in human trabecular meshwork cells expressing wild-type PITX2 or when PITX2 is suppressed to determine PITX2 involvement into antioxidative defense mechanism. While I have validated these target genes *in vitro*, a *in vivo* analysis is needed to substanciate these genes as true genes for PITX2. Using animal model, such as zebrafish or mouse, the expression and the role in eye development of these gene could be indicated. The model proposed in Chapter four, five and the present chapter could be tested in an animal model, such as wild-type PITX2 and knock-out PITX2 mouse model. The ROS production in trabecular meshwork tissue from wild-type PITX2 and knock-out PITX2 mouse models could be measured and compared to determine the involvement of PITX2 in ocular cellular stress pathway *in* vivo. Neverless, it will be interesting to see if *PDP2* and *SLC13A3* are causative gene disease for ARS and/ or glaucoma.

Analysis of other genes regulated by PITX2

Other PITX2 genes identified by microarray and northern blot or semi-quantitative RT-PCR look promising as their functions have been shown to be

related to glaucoma pathology. For example, *High Density Lipoprotein Binding Protein/ vigilin* (*HDLBP*) plays a role in recognition of extracellular molecules such as apolipoproteins and has been shown to be colocalized in the cells with apolipoprotein E, which is considered a high risk factor for glaucoma [234]. The analysis of *HDLBP* was already started by our summer student, Ms Chi. She investigated the upstream transcriptional regulatory regions of *HDLBP* using luciferase reporter gene assays. Her results indicated that PITX2 significantly activated transcription from reporter plasmids containing *HDLBP* upstream elements, while mutated PITX2 significantly decreased transcription from reporter plasmids containing *HDLBP* upstream elements.

C20ORF133 has the chromosomal location within the glaucoma loci. While *C20ORF133* was not selected for further analysis because of unknown expression profile and unknown cellular function, it would be interesting to confirm *C20ORF133* as a bona fide gene of PITX2 and to see if *C20ORF133* is a cause of glaucoma.

Similar analysis to *SLC13A3* and *PDP2* could be conducted on the other PITX2 target genes giving insight in understanding of PITX2 role in ocular regulatory pathway. Comparison of the genes regulated by PITX2 and FOXC1 will give insight into the pathology of ARS which results from mutations of either PITX2 or FOXC1. Ultimately, understanding the involvement of PITX2 and FOXC1 in ARS and glaucoma will help in the development of better glaucoma treatments.

Postulated mechanism of pathogenesis of PITX2 leading to glaucoma

My postulated model of PITX2 role in glaucoma is shown in Figure 6-1 and suggests that defects of PITX2 could generate disruption of genes implicated in cellular stress producing accumulation of ROS. Accumulation of ROS induces either cellular death by caspase and mitochondrial cell death pathway activation or protein functional loss by modification of the structure and function. The modified proteins can have impact on proteosome function leading to amplification of the production of ROS. ROS may also have cytotoxic and mutagenic impact on DNA. ROS released from stressed cells into the extracellular environment may damage the extracellular matrix. The decreased number or cells and the degradation of the extracellular matrix produce an elevated IOP leading to clinical onset of the glaucoma. Elevated IOP cause a vicious cycle of progressively worsening accumulation of ROS with progression of glaucoma.

Figure 6-1. Postulated mechanism of pathogenesis of PITX2 leading to glaucoma. *On the left* of the figure, the mechanism of pathogenesis is presented at the cellular level, whereas *on the right* part of the figure, the mechanism is presented at tissue level. The explanation of the figure is provided in the text.

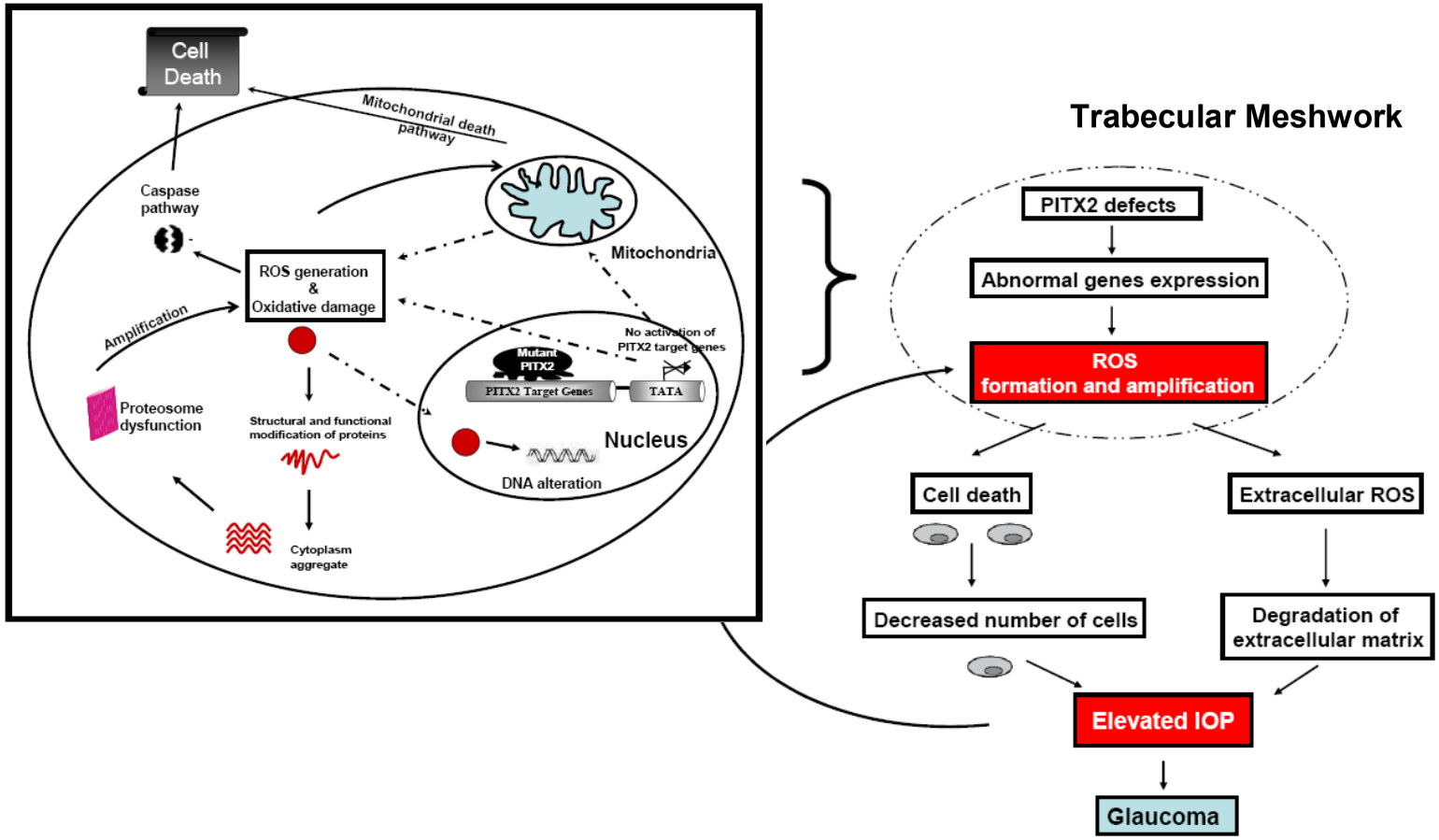
Cell Death
Mitochondrial death pathway
Caspase pathway
Mitochondria
ROS generation & Oxidative damage
Amplification
No activation of PITX2 target genes
Mutant PITX2
PITX2 Target Genes
TATA
Proteosome dysfunction
Structural and functional modification of proteins
Nucleus
DNA alteration
Cytoplasm aggregate
Trabecular Meshwork
PITX2 defects
Abnormal genes expression
ROS formation and amplification
Cell death
Extracellular ROS
Decreased number of cells
Degradation of extracellular matrix
Elevated IOP
Glaucoma

Table 6-1: Geographic distribution of patients included in prospective study										
	Canada	US	UK	Belgium	Germany	Ireland	Italy	New Zealand	Netherlands	**Total**
Probands	52	58	32	2	3	1	1	1	1	**151**
Patients	157	67	38	3	4	1	3	1	2	**276**

Table 6-2: Distribution of patients included in prospective study based on the genotype						
	FOXC1 mutation	FOXC1Duplication	Unaffected	PITX2 mutation	PITX2 deletion	**Unidentified**
Probands	16	14	1	5	3	**113**
Patients	36	61	1	19	9	**150**
% of Probands	10.60	9.27	0.66	3.31	1.99	74.83

References List

1. Strungaru, M.H., I. Dinu, and M.A. Walter, *Genotype-Phenotype Correlations in Axenfeld-Rieger Malformation and Glaucoma Patients with FOXC1 and PITX2 Mutations.* Invest Ophthalmol Vis Sci, 2007. **48**(1): p. 228.

2. Allingham, R.R., *An Overview of Glaucoma*, in *Shields' Textbook of Glaucoma*, R.R. Allingham, et al., Editors. 2005, Lippincott Willliams & Wilkins: Philadelphia. p. 1.

3. Mandal, A.K. and P.A. Netland, *Historical Perspective of Developmental Glaucomas*, in *The pediatric glaucomas*, A.K. Mandal and P.A. Netland, Editors. 2006, Elsevier Butterworth Heinemann: Philadelphia. p. 1.

4. Gupta, D., *Epidemiology*, in *Glaucoma Diagnosis and Management*, D. Gupta, Editor. 2005, Lippincott Williams & Wilkins: Philadelphia. p. 3.

5. Resnikoff, S., et al., *Global data on visual impairment in the year 2002.* Bull World Health Organ, 2004. **82**(11): p. 844.

6. Bartels, S., ed. *Aqueous Humor Formation*. The Glaucomas, ed. R. Ritch, M. Schields, and T. Krupin. Vol. 1. 1989, Mosby: St. Louis. 199.

7. Kaufman, P., ed. *Pressure-dependend Outflow*. The Glaucomas, ed. R. Ritch, M. Schields, and T. Krupin. Vol. 1. 1989, Mosby: St. Louis. 219.

8. Gordon, M.O., et al., *The Ocular Hypertension Treatment Study: baseline factors that predict the onset of primary open-angle glaucoma.* Arch Ophthalmol, 2002. **120**(6): p. 714.

9. Weih, L.M., et al., *Association of demographic, familial, medical, and ocular factors with intraocular pressure.* Arch Ophthalmol, 2001. **119**(6): p. 875.

10. Distelhorst, J.S. and G.M. Hughes, *Open-angle glaucoma.* Am Fam Physician, 2003. **67**(9): p. 1937.

11. Hewitt, A.W., J.E. Craig, and D.A. Mackey, *Complex genetics of complex traits: the case of primary open-angle glaucoma.* Clin Experiment Ophthalmol, 2006. **34**(5): p. 472.

12. Sheffield, V.C., et al., *Genetic linkage of familial open angle glaucoma to chromosome 1q21-q31.* Nat Genet, 1993. **4**(1): p. 47.

13. Wiggs, J.L., et al., *A genomewide scan identifies novel early-onset primary open-angle glaucoma loci on 9q22 and 20p12.* Am J Hum Genet, 2004. **74**(6): p. 1314.

14. Vogel, G., *Glaucoma gene provides light at the end of the tunnel.* Science, 1997. **275**(5300): p. 621.

15. Friedman, J.S. and M.A. Walter, *Biomedicine. Under pressure.* Science, 2002. **295**(5557): p. 983.

16. Monemi, S., et al., *Identification of a novel adult-onset primary open-angle glaucoma (POAG) gene on 5q22.1.* Hum Mol Genet, 2005. **14**(6): p. 725.

17. Stone, E.M., et al., *Identification of a gene that causes primary open angle glaucoma.* Science, 1997. **275**(5300): p. 668.

18. Karali, A., et al., *Localization of myocilin/trabecular meshwork--inducible glucocorticoid response protein in the human eye.* Invest Ophthalmol Vis Sci, 2000. **41**(3): p. 729.

19. Fingert, J.H., et al., *Myocilin glaucoma.* Surv Ophthalmol, 2002. **47**(6): p. 547.

20. Wiggs, J.L., et al., *Prevalence of mutations in TIGR/Myocilin in patients with adult and juvenile primary open-angle glaucoma.* Am J Hum Genet, 1998. **63**(5): p. 1549.

21. Fingert, J.H., et al., *Analysis of myocilin mutations in 1703 glaucoma patients from five different populations.* Hum Mol Genet, 1999. **8**(5): p. 899.

22. Aldred, M.A., et al., *Low prevalence of MYOC mutations in UK primary open-angle glaucoma patients limits the utility of genetic testing.* Hum Genet, 2004. **115**(5): p. 428.

23. Pang, C.P., et al., *TIGR/MYOC gene sequence alterations in individuals with and without primary open-angle glaucoma.* Invest Ophthalmol Vis Sci, 2002. **43**(10): p. 3231.

24. Ennis, S., et al., *Prevalence of myocilin gene mutations in a novel UK cohort of POAG patients.* Eye (Lond). **24**(2): p. 328.

25. Alward, W.L., et al., *Clinical features associated with mutations in the chromosome 1 open-angle glaucoma gene (GLC1A).* N Engl J Med, 1998. **338**(15): p. 1022.

26. Vincent, A.L., et al., *Digenic inheritance of early-onset glaucoma: CYP1B1, a potential modifier gene.* Am J Hum Genet, 2002. **70**(2): p. 448.

27. Lam, D.S., et al., *Truncations in the TIGR gene in individuals with and without primary open-angle glaucoma.* Invest Ophthalmol Vis Sci, 2000. **41**(6): p. 1386.

28. Wiggs, J.L. and D. Vollrath, *Molecular and clinical evaluation of a patient hemizygous for TIGR/MYOC.* Arch Ophthalmol, 2001. **119**(11): p. 1674.

29. Kim, B.S., et al., *Targeted Disruption of the Myocilin Gene (Myoc) Suggests that Human Glaucoma-Causing Mutations Are Gain of Function.* Mol Cell Biol, 2001. **21**(22): p. 7707.

30. Gobeil, S., et al., *Intracellular sequestration of hetero-oligomers formed by wild-type and glaucoma-causing myocilin mutants.* Invest Ophthalmol Vis Sci, 2004. **45**(10): p. 3560.

31. Rezaie, T., et al., *Adult-onset primary open-angle glaucoma caused by mutations in optineurin.* Science, 2002. **295**(5557): p. 1077.

32. Sahlender, D.A., et al., *Optineurin links myosin VI to the Golgi complex and is involved in Golgi organization and exocytosis.* J Cell Biol, 2005. **169**(2): p. 285.

33. Sarfarazi, M. and T. Rezaie, *Optineurin in primary open angle glaucoma.* Ophthalmol Clin North Am, 2003. **16**(4): p. 529.

34. Alward, W.L., et al., *Evaluation of optineurin sequence variations in 1,048 patients with open-angle glaucoma.* Am J Ophthalmol, 2003. **136**(5): p. 904.

35. Wiggs, J.L., et al., *Lack of association of mutations in optineurin with disease in patients with adult-onset primary open-angle glaucoma.* Arch Ophthalmol, 2003. **121**(8): p. 1181.

36. Tang, S., et al., *The association between Japanese primary open-angle glaucoma and normal tension glaucoma patients and the optineurin gene.* Hum Genet, 2003. **113**(3): p. 276.

37. Stoilova, D., et al., *Localization of a locus (GLC1B) for adult-onset primary open angle glaucoma to the 2cen-q13 region.* Genomics, 1996. **36**(1): p. 142.

38. Wirtz, M.K., et al., *Mapping a gene for adult-onset primary open-angle glaucoma to chromosome 3q.* Am J Hum Genet, 1997. **60**(2): p. 296.

39. Trifan, O.C., et al., *A third locus (GLC1D) for adult-onset primary open-angle glaucoma maps to the 8q23 region.* Am J Ophthalmol, 1998. **126**(1): p. 17.

40. Sarfarazi, M., et al., *Localization of the fourth locus (GLC1E) for adult-onset primary open-angle glaucoma to the 10p15-p14 region.* Am J Hum Genet, 1998. **62**(3): p. 641.

41. Wirtz, M.K., et al., *GLC1F, a new primary open-angle glaucoma locus, maps to 7q35-q36.* Arch Ophthalmol, 1999. **117**(2): p. 237.

42. Allingham, R.R., et al., *Early adult-onset POAG linked to 15q11-13 using ordered subset analysis.* Invest Ophthalmol Vis Sci, 2005. **46**(6): p. 2002.

43. Stoilov, I., A.N. Akarsu, and M. Sarfarazi, *Identification of three different truncating mutations in cytochrome P4501B1 (CYP1B1) as the principal cause of primary congenital glaucoma (Buphthalmos) in families linked to the GLC3A locus on chromosome 2p21.* Hum Mol Genet, 1997. **6**(4): p. 641.

44. Akarsu, A.N., et al., *A second locus (GLC3B) for primary congenital glaucoma (Buphthalmos) maps to the 1p36 region.* Hum Mol Genet, 1996. **5**(8): p. 1199.

45. Ali, M., et al., *Null mutations in LTBP2 cause primary congenital glaucoma.* Am J Hum Genet, 2009. **84**(5): p. 664.

46. Narooie-Nejad, M., et al., *Loss of function mutations in the gene encoding latent transforming growth factor beta binding protein 2, LTBP2, cause primary congenital glaucoma.* Hum Mol Genet, 2009. **18**(20): p. 3969.

47. Wiggs, J.L., et al., *Genome-wide scan for adult onset primary open angle glaucoma.* Hum Mol Genet, 2000. **9**(7): p. 1109.

48. Semina, E.V., et al., *Cloning and characterization of a novel bicoid-related homeobox transcription factor gene, RIEG, involved in Rieger syndrome.* Nat Genet, 1996. **14**(4): p. 392.

49. Mears, A.J., et al., *Mutations of the forkhead/winged-helix gene, FKHL7, in patients with Axenfeld-Rieger anomaly.* Am J Hum Genet, 1998. **63**(5): p. 1316.

50. Phillips, J.C., et al., *A second locus for Rieger syndrome maps to chromosome 13q14.* Am J Hum Genet, 1996. **59**(3): p. 613.

51. Werner, W., et al., *A small deletion of 16q23.1-->16q24.2 [del(16)(q23.1q24.2).ish del(16)(q23.1q24.2)(D16S395+, D16S348-, P5432+)] in a boy with iris coloboma and minor anomalies.* Am J Med Genet, 1997. **70**(4): p. 371.

52. Hauser, M.A., et al., *Distribution of WDR36 DNA sequence variants in patients with primary open-angle glaucoma.* Invest Ophthalmol Vis Sci, 2006. **47**(6): p. 2542.

53. Kramer, P.L., et al., *The role of the WDR36 gene on chromosome 5q22.1 in a large family with primary open-angle glaucoma mapped to this region.* Arch Ophthalmol, 2006. **124**(9): p. 1328.

54. Pang, C.P., et al., *A genome-wide scan maps a novel juvenile-onset primary open angle glaucoma locus to chromosome 5q.* Mol Vis, 2006. **12**: p. 85.

55. Rotimi, C.N., et al., *Genomewide scan and fine mapping of quantitative trait loci for intraocular pressure on 5q and 14q in West Africans.* Invest Ophthalmol Vis Sci, 2006. **47**(8): p. 3262.

56. Skarie, J.M. and B.A. Link, *The primary open-angle glaucoma gene WDR36 functions in ribosomal RNA processing and interacts with the p53 stress-response pathway.* Hum Mol Genet, 2008. **17**(16): p. 2474.

57. Footz, T.K., et al., *Glaucoma-associated WDR36 variants encode functional defects in a yeast model system.* Hum Mol Genet, 2009. **18**(7): p. 1276.

58. Stoilov, I., et al., *Sequence analysis and homology modeling suggest that primary congenital glaucoma on 2p21 results from mutations disrupting either the hinge region or the conserved core structures of cytochrome P4501B1.* Am J Hum Genet, 1998. **62**(3): p. 573.

59. Colomb, E., J. Kaplan, and H.J. Garchon, *Novel cytochrome P450 1B1 (CYP1B1) mutations in patients with primary congenital glaucoma in France.* Hum Mutat, 2003. **22**(6): p. 496.

60. Kakiuchi-Matsumoto, T., et al., *Cytochrome P450 1B1 gene mutations in Japanese patients with primary congenital glaucoma(1).* Am J Ophthalmol, 2001. **131**(3): p. 345.

61. Nemet, A.Y., et al., *Current concepts of ocular manifestations in Marfan syndrome.* Surv Ophthalmol, 2006. **51**(6): p. 561.

62. Ringvold, A., *Epidemiology of the pseudo-exfoliation syndrome.* Acta Ophthalmol Scand, 1999. **77**(4): p. 371.

63. Thorleifsson, G., et al., *Common sequence variants in the LOXL1 gene confer susceptibility to exfoliation glaucoma.* Science, 2007. **317**(5843): p. 1397.

64. Berry, F.B., et al., *Functional interactions between FOXC1 and PITX2 underlie the sensitivity to FOXC1 gene dose in Axenfeld-Rieger syndrome and anterior segment dysgenesis.* Hum Mol Genet, 2006. **15**(6): p. 905.

65. Evans, A.L. and P.J. Gage, *Expression of the homeobox gene Pitx2 in neural crest is required for optic stalk and ocular anterior segment development.* Hum Mol Genet, 2005. **14**(22): p. 3347.

66. Axenfeld, T.H., *Embryotoxon corneaposterius.* Klin.Monastbl. Augenheilkd, 1920(65): p. 381.

67. Rieger, H., *Dysgenesis mesodermalis corneae et iridis.* Z. Augenheilkd, 1935(86): p. 333.

68. Alward, W.L., *Axenfeld-Rieger syndrome in the age of molecular genetics.* Am J Ophthalmol, 2000. **130**(1): p. 107.

69. Burian, H.M., M.H. Rice, and L. Allen, *External visibility of the region of Schlemm's canal; report on a family with developmental anomalies of cornea, iris, and chamber angle.* AMA Arch Ophthalmol, 1957. **57**(5): p. 651.

70. Strungaru, M., I. Dinu, and M.A. Walter, *Genotype-Phenotype correlations in Axenfeld-Rieger Malformation and glaucoma patients with FOXC1 and PITX2 mutations.* Investigative ophthalmology and visual science, 2006.

71. Reese, A.B. and R.M. Ellsworth, *The anterior chamber cleavage syndrome.* Arch Ophthalmol, 1966. **75**(3): p. 307.

72. Fitch, N. and M. Kaback, *The Axenfeld syndrome and the Rieger syndrome.* J Med Genet, 1978. **15**(1): p. 30.

73. Alward, W.L., et al., *Autosomal dominant iris hypoplasia is caused by a mutation in the Rieger syndrome (RIEG/PITX2) gene.* Am J Ophthalmol, 1998. **125**(1): p. 98.

74. Nishimura, D.Y., et al., *The forkhead transcription factor gene FKHL7 is responsible for glaucoma phenotypes which map to 6p25.* Nat Genet, 1998. **19**(2): p. 140.

75. Gould, D.B., et al., *Autosomal dominant Axenfeld-Rieger anomaly maps to 6p25.* Am J Hum Genet, 1997. **61**(3): p. 765.

76. Lines, M.A., et al., *Characterization and prevalence of PITX2 microdeletions and mutations in Axenfeld-Rieger malformations.* Invest Ophthalmol Vis Sci, 2004. **45**(3): p. 828.

77. Riise, R., K. Storhaug, and K. Brondum-Nielsen, *Rieger syndrome is associated with PAX6 deletion.* Acta Ophthalmol Scand, 2001. **79**(2): p. 201.

78. Hjalt, T.A. and E.V. Semina, *Current molecular understanding of Axenfeld-Rieger syndrome.* Expert Rev Mol Med, 2005. **7**(25): p. 1.

79. Charles, M.A., et al., *PITX genes are required for cell survival and Lhx3 activation.* Mol Endocrinol, 2005. **19**(7): p. 1893.

80. Amendt, B.A., E.V. Semina, and W.L. Alward, *Rieger syndrome: a clinical, molecular, and biochemical analysis.* Cell Mol Life Sci, 2000. **57**(11): p. 1652.

81. Pierrou, S., et al., *Cloning and characterization of seven human forkhead proteins: binding site specificity and DNA bending.* Embo J, 1994. **13**(20): p. 5002.

82. Walter, M.A., *PITs and FOXes in ocular genetics: the Cogan lecture.* Invest Ophthalmol Vis Sci, 2003. **44**(4): p. 1402.

83. Lehmann, O.J., et al., *Fox's in development and disease.* Trends Genet, 2003. **19**(6): p. 339.

84. Carlsson, P. and M. Mahlapuu, *Forkhead transcription factors: key players in development and metabolism.* Dev Biol, 2002. **250**(1): p. 1.

85. Erickson, R.P., *Forkhead genes and human disease.* J Appl Genet, 2001. **42**(2): p. 211.

86. Berry, F.B., R.A. Saleem, and M.A. Walter, *FOXC1 transcriptional regulation is mediated by N- and C-terminal activation domains and contains a*

phosphorylated transcriptional inhibitory domain. J Biol Chem, 2002. **277**(12): p. 10292.

87. Mirzayans, F., et al., *Negative regulation of FOXC1 activity by the p44/42 MAP kinase pathway*. American Society for Human Genetics. Vol. 73 (Supp). 2003, Los Angeles. S988.

88. Nishimura, D.Y., et al., *A spectrum of FOXC1 mutations suggests gene dosage as a mechanism for developmental defects of the anterior chamber of the eye.* Am J Hum Genet, 2001. **68**(2): p. 364.

89. Ekong, R., et al., *Chromosomal anomalies on 6p25 in iris hypoplasia and Axenfeld-Rieger syndrome patients defined on a purpose-built genomic microarray.* Hum Mutat, 2004. **24**(1): p. 76.

90. Lehmann, O.J., et al., *Chromosomal duplication involving the forkhead transcription factor gene FOXC1 causes iris hypoplasia and glaucoma.* Am J Hum Genet, 2000. **67**(5): p. 1129.

91. Lines, M.A., K. Kozlowski, and M.A. Walter, *Molecular genetics of Axenfeld-Rieger malformations.* Hum Mol Genet, 2002. **11**(10): p. 1177.

92. Saleem, R.A., et al., *Structural and functional analyses of disease-causing missense mutations in the forkhead domain of FOXC1.* Hum Mol Genet, 2003. **12**(22): p. 2993.

93. Murphy, T.C., et al., *The wing 2 region of the FOXC1 forkhead domain is necessary for normal DNA-binding and transactivation functions.* Invest Ophthalmol Vis Sci, 2004. **45**(8): p. 2531.

94. Saleem, R.A., et al., *Identification and analysis of a novel mutation in the FOXC1 forkhead domain.* Invest Ophthalmol Vis Sci, 2003. **44**(11): p. 4608.

95. Kawase, C., et al., *Screening for mutations of Axenfeld-Rieger syndrome caused by FOXC1 gene in Japanese patients.* J Glaucoma, 2001. **10**(6): p. 477.

96. Suzuki, T., et al., *A novel (Pro79Thr) mutation in the FKHL7 gene in a Japanese family with Axenfeld-Rieger syndrome.* Am J Ophthalmol, 2001. **132**(4): p. 572.

97. Saleem, R.A., et al., *Analyses of the effects that disease-causing missense mutations have on the structure and function of the winged-helix protein FOXC1.* Am J Hum Genet, 2001. **68**(3): p. 627.

98. Mirzayans, F., et al., *Axenfeld-Rieger syndrome resulting from mutation of the FKHL7 gene on chromosome 6p25.* Eur J Hum Genet, 2000. **8**(1): p. 71.

99. Swiderski, R.E., et al., *Expression of the Mf1 gene in developing mouse hearts: implication in the development of human congenital heart defects.* Dev Dyn, 1999. **216**(1): p. 16.

100. Smith, R.S., et al., *Haploinsufficiency of the transcription factors FOXC1 and FOXC2 results in aberrant ocular development.* Hum Mol Genet, 2000. **9**(7): p. 1021.

101. Kume, T., et al., *The forkhead/winged helix gene Mf1 is disrupted in the pleiotropic mouse mutation congenital hydrocephalus.* Cell, 1998. **93**(6): p. 985.

102. Yamagishi, H., et al., *Tbx1 is regulated by tissue-specific forkhead proteins through a common Sonic hedgehog-responsive enhancer.* Genes Dev, 2003. **17**(2): p. 269.

103. Tamimi, Y., et al., *FGF19 is a target for FOXC1 regulation in ciliary body-derived cells.* Hum Mol Genet, 2006. **15**(21): p. 3229.

104. Berry, F.B., et al., *FOXC1 is required for cell viability and resistance to oxidative stress in the eye through the transcriptional regulation of FOXO1A.* Hum Mol Genet, 2008. **17**(4): p. 490.

105. Hayashi, H. and T. Kume, *Foxc transcription factors directly regulate Dll4 and Hey2 expression by interacting with the VEGF-Notch signaling pathways in endothelial cells.* PLoS One, 2008. **3**(6): p. e2401.

106. Rice, R., et al., *Progression of calvarial bone development requires Foxc1 regulation of Msx2 and Alx4.* Dev Biol, 2003. **262**(1): p. 75.

107. Tamimi, Y., et al., *Identification of target genes regulated by FOXC1 using nickel agarose-based chromatin enrichment.* Invest Ophthalmol Vis Sci, 2004. **45**(11): p. 3904.

108. Gage, P.J., H. Suh, and S.A. Camper, *Dosage requirement of Pitx2 for development of multiple organs.* Development, 1999. **126**(20): p. 4643.

109. Kitamura, K., et al., *Mouse Pitx2 deficiency leads to anomalies of the ventral body wall, heart, extra- and periocular mesoderm and right pulmonary isomerism.* Development, 1999. **126**(24): p. 5749.

110. Ganga, M., et al., *PITX2 isoform-specific regulation of atrial natriuretic factor expression: synergism and repression with Nkx2.5.* J Biol Chem, 2003. **278**(25): p. 22437.

111. Cox, C.J., et al., *Differential regulation of gene expression by PITX2 isoforms.* J Biol Chem, 2002. **277**(28): p. 25001.

112. Amendt, B.A., L.B. Sutherland, and A.F. Russo, *Multifunctional role of the Pitx2 homeodomain protein C-terminal tail.* Mol Cell Biol, 1999. **19**(10): p. 7001.

113. Espinoza, H.M., et al., *Protein kinase C phosphorylation modulates N- and C-terminal regulatory activities of the PITX2 homeodomain protein.* Biochemistry, 2005. **44**(10): p. 3942.

114. Furukawa, T., C.A. Kozak, and C.L. Cepko, *rax, a novel paired-type homeobox gene, shows expression in the anterior neural fold and developing retina.* Proc Natl Acad Sci U S A, 1997. **94**(7): p. 3088.

115. Galliot, B., C. de Vargas, and D. Miller, *Evolution of homeobox genes: Q50 Paired-like genes founded the Paired class.* Dev Genes Evol, 1999. **209**(3): p. 186.

116. Footz, T., et al., *Analysis of mutations of the PITX2 transcription factor found in patients with Axenfeld-Rieger syndrome.* Invest Ophthalmol Vis Sci, 2009. **50**(6): p. 2599.

117. Vaux, C., et al., *Evidence that Rieger syndrome maps to 4q25 or 4q27.* J Med Genet, 1992. **29**(4): p. 256.

118. Kulharya, A.S., et al., *Interstitial deletions 4q21.1q25 and 4q25q27: phenotypic variability and relation to Rieger anomaly.* Am J Med Genet, 1995. **55**(2): p. 165.

119. Makita, Y., et al., *Rieger syndrome with de novo reciprocal translocation t(1;4) (q23.1;q25).* Am J Med Genet, 1995. **57**(1): p. 19.

120. Flomen, R.H., et al., *Rieger syndrome locus: a new reciprocal translocation t(4;12)(q25;q15) and a deletion del(4)(q25q27) both break between markers D4S2945 and D4S193.* J Med Genet, 1997. **34**(3): p. 191.

121. Flomen, R.H., et al., *Construction and analysis of a sequence-ready map in 4q25: Rieger syndrome can be caused by haploinsufficiency of RIEG, but also by chromosome breaks approximately 90 kb upstream of this gene.* Genomics, 1998. **47**(3): p. 409.

122. Schinzel, A., et al., *Multiple congenital anomalies including the Rieger eye malformation in a boy with interstitial deletion of (4) (q25-->q27) secondary to a balanced insertion in his normal father: evidence for haplotype insufficiency causing the Rieger malformation.* J Med Genet, 1997. **34**(12): p. 1012.

123. Velinov, M., et al., *Hypoplastic left heart in a female infant with partial trisomy 4q due to de novo 4;21 translocation.* Am J Med Genet, 2002. **107**(4): p. 330.

124. Kulak, S.C., et al., *Mutation in the RIEG1 gene in patients with iridogoniodysgenesis syndrome.* Hum Mol Genet, 1998. **7**(7): p. 1113.

125. Saadi, I., et al., *Identification of a dominant negative homeodomain mutation in Rieger syndrome.* J Biol Chem, 2001. **276**(25): p. 23034.

126. Perveen, R., et al., *Phenotypic variability and asymmetry of Rieger syndrome associated with PITX2 mutations.* Invest Ophthalmol Vis Sci, 2000. **41**(9): p. 2456.

127. Priston, M., et al., *Functional analyses of two newly identified PITX2 mutants reveal a novel molecular mechanism for Axenfeld-Rieger syndrome.* Hum Mol Genet, 2001. **10**(16): p. 1631.

128. Phillips, J.C., *Four novel mutations in the PITX2 gene in patients with Axenfeld-Rieger syndrome.* Ophthalmic Res, 2002. **34**(5): p. 324.

129. Borges, A.S., et al., *Genetic analysis of PITX2 and FOXC1 in Rieger Syndrome patients from Brazil.* J Glaucoma, 2002. **11**(1): p. 51.

130. Kozlowski, K. and M.A. Walter, *Variation in residual PITX2 activity underlies the phenotypic spectrum of anterior segment developmental disorders.* Hum Mol Genet, 2000. **9**(14): p. 2131.

131. Hittner, H.M., et al., *Variable expressivity of autosomal dominant anterior segment mesenchymal dysgenesis in six generations.* Am J Ophthalmol, 1982. **93**(1): p. 57.

132. Doward, W., et al., *A mutation in the RIEG1 gene associated with Peters' anomaly.* J Med Genet, 1999. **36**(2): p. 152.

133. Xia, K., et al., *Mutation in PITX2 is associated with ring dermoid of the cornea.* J Med Genet, 2004. **41**(12): p. e129.

134. St Amand, T.R., et al., *Antagonistic signals between BMP4 and FGF8 define the expression of Pitx1 and Pitx2 in mouse tooth-forming anlage.* Dev Biol, 2000. **217**(2): p. 323.

135. Gage, P.J., et al., *Fate maps of neural crest and mesoderm in the mammalian eye.* Invest Ophthalmol Vis Sci, 2005. **46**(11): p. 4200.

136. Lu, M.F., et al., *Function of Rieger syndrome gene in left-right asymmetry and craniofacial development.* Nature, 1999. **401**(6750): p. 276.

137. Lin, C.R., et al., *Pitx2 regulates lung asymmetry, cardiac positioning and pituitary and tooth morphogenesis.* Nature, 1999. **401**(6750): p. 279.

138. Holmberg, J., C.Y. Liu, and T.A. Hjalt, *PITX2 gain-of-function in Rieger syndrome eye model.* Am J Pathol, 2004. **165**(5): p. 1633.

139. Gage, P.J., et al., *The canonical Wnt signaling antagonist DKK2 is an essential effector of PITX2 function during normal eye development.* Dev Biol, 2008. **317**(1): p. 310.

140. Shiratori, H., et al., *Two-step regulation of left-right asymmetric expression of Pitx2: initiation by nodal signaling and maintenance by Nkx2.* Mol Cell, 2001. **7**(1): p. 137.

141. Espinoza, H.M., et al., *A molecular basis for differential developmental anomalies in Axenfeld-Rieger syndrome.* Hum Mol Genet, 2002. **11**(7): p. 743.

142. Liu, W., et al., *Genetic dissection of Pitx2 in craniofacial development uncovers new functions in branchial arch morphogenesis, late aspects of tooth morphogenesis and cell migration.* Development, 2003. **130**(25): p. 6375.

143. Kioussi, C., et al., *Identification of a Wnt/Dvl/beta-Catenin --> Pitx2 pathway mediating cell-type-specific proliferation during development.* Cell, 2002. **111**(5): p. 673.

144. Szeto, D.P., et al., *Role of the Bicoid-related homeodomain factor Pitx1 in specifying hindlimb morphogenesis and pituitary development.* Genes Dev, 1999. **13**(4): p. 484.

145. Hjalt, T.A., B.A. Amendt, and J.C. Murray, *PITX2 regulates procollagen lysyl hydroxylase (PLOD) gene expression: implications for the pathology of Rieger syndrome.* J Cell Biol, 2001. **152**(3): p. 545.

146. Wei, Q. and R.S. Adelstein, *Pitx2a expression alters actin-myosin cytoskeleton and migration of HeLa cells through Rho GTPase signaling.* Mol Biol Cell, 2002. **13**(2): p. 683.

147. Shields, M.B., et al., *Axenfeld-Rieger syndrome. A spectrum of developmental disorders.* Surv Ophthalmol, 1985. **29**(6): p. 387.

148. Komatireddy, S., et al., *Mutation spectrum of FOXC1 and clinical genetic heterogeneity of Axenfeld-Rieger anomaly in India.* Mol Vis, 2003. **9**: p. 43.

149. Honkanen, R.A., et al., *A family with Axenfeld-Rieger syndrome and Peters Anomaly caused by a point mutation (Phe112Ser) in the FOXC1 gene.* Am J Ophthalmol, 2003. **135**(3): p. 368.

150. Ito, Y.A., et al., *Analyses of a novel L130F missense mutation in FOXC1.* Arch Ophthalmol, 2007. **125**(1): p. 128.

151. Walter, M.A., et al., *Autosomal-dominant iridogoniodysgenesis and Axenfeld-Rieger syndrome are genetically distinct.* Ophthalmology, 1996. **103**(11): p. 1907.

152. Zhou, Y., et al., *An altered phenotype in a conditional knockout of Pitx2 in extraocular muscle.* Invest Ophthalmol Vis Sci, 2009. **50**(10): p. 4531.

153. Hanes, S.D. and R. Brent, *DNA specificity of the bicoid activator protein is determined by homeodomain recognition helix residue 9.* Cell, 1989. **57**(7): p. 1275.

154. Treisman, J., et al., *A single amino acid can determine the DNA binding specificity of homeodomain proteins.* Cell, 1989. **59**(3): p. 553.

155. Saadi, I., et al., *Dominant negative dimerization of a mutant homeodomain protein in Axenfeld-Rieger syndrome.* Mol Cell Biol, 2003. **23**(6): p. 1968.

156. Qian, Z., Y.D. Cai, and Y. Li, *A novel computational method to predict transcription factor DNA binding preference.* Biochem Biophys Res Commun, 2006. **348**(3): p. 1034.

157. Moreno, M.C., et al., *Retinal oxidative stress induced by high intraocular pressure.* Free Radic Biol Med, 2004. **37**(6): p. 803.

158. Kerrigan, L.A., et al., *TUNEL-positive ganglion cells in human primary open-angle glaucoma.* Arch Ophthalmol, 1997. **115**(8): p. 1031.

159. Harman, D., *The free radical theory of aging.* Antioxid Redox Signal, 2003. **5**(5): p. 557.

160. Spector, A., W. Ma, and R.R. Wang, *The aqueous humor is capable of generating and degrading H2O2.* Invest Ophthalmol Vis Sci, 1998. **39**(7): p. 1188.

161. Garcia-Castineiras, S., et al., *Aqueous humor hydrogen peroxide analysis with dichlorophenol-indophenol.* Exp Eye Res, 1992. **55**(1): p. 9.

162. Gherghel, D., et al., *Systemic reduction in glutathione levels occurs in patients with primary open-angle glaucoma.* Invest Ophthalmol Vis Sci, 2005. **46**(3): p. 877.

163. Ferreira, S.M., et al., *Oxidative stress markers in aqueous humor of glaucoma patients.* Am J Ophthalmol, 2004. **137**(1): p. 62.

164. Sacca, S.C., et al., *Oxidative DNA damage in the human trabecular meshwork: clinical correlation in patients with primary open-angle glaucoma.* Arch Ophthalmol, 2005. **123**(4): p. 458.

165. Babizhayev, M.A. and A. Bunin, *Lipid peroxidation in open-angle glaucoma.* Acta Ophthalmol (Copenh), 1989. **67**(4): p. 371.

166. Kekuda, R., et al., *Primary structure and functional characteristics of a mammalian sodium-coupled high affinity dicarboxylate transporter.* J Biol Chem, 1999. **274**(6): p. 3422.

167. Wang, H., et al., *Structure, function, and genomic organization of human Na(+)-dependent high-affinity dicarboxylate transporter.* Am J Physiol Cell Physiol, 2000. **278**(5): p. C1019.

168. Pajor, A.M., B.A. Hirayama, and D.D. Loo, *Sodium and lithium interactions with the Na+/Dicarboxylate cotransporter.* J Biol Chem, 1998. **273**(30): p. 18923.

169. Steffgen, J., et al., *Expression cloning and characterization of a novel sodium-dicarboxylate cotransporter from winter flounder kidney.* J Biol Chem, 1999. **274**(29): p. 20191.

170. Chen, X., et al., *Molecular and functional analysis of SDCT2, a novel rat sodium-dependent dicarboxylate transporter.* J Clin Invest, 1999. **103**(8): p. 1159.

171. Huang, W., et al., *Transport of N-acetylaspartate by the Na(+)-dependent high-affinity dicarboxylate transporter NaDC3 and its relevance to the expression of the transporter in the brain.* J Pharmacol Exp Ther, 2000. **295**(1): p. 392.

172. George, R.L., et al., *Transport of N-acetylaspartate via murine sodium/dicarboxylate cotransporter NaDC3 and expression of this transporter and aspartoacylase II in ocular tissues in mouse.* Biochim Biophys Acta, 2004. **1690**(1): p. 63.

173. Chen, X.Z., et al., *Characterization of a rat Na+-dicarboxylate cotransporter.* J Biol Chem, 1998. **273**(33): p. 20972.

174. Hentschel, H., et al., *Basolateral localization of flounder Na+-dicarboxylate cotransporter (fNaDC-3) in the kidney of Pleuronectes americanus.* Pflugers Arch, 2003. **446**(5): p. 578.

175. Burckhardt, B.C. and G. Burckhardt, *Transport of organic anions across the basolateral membrane of proximal tubule cells.* Rev Physiol Biochem Pharmacol, 2003. **146**: p. 95.

176. Lash, L.H., *Role of glutathione transport processes in kidney function.* Toxicol Appl Pharmacol, 2005. **204**(3): p. 329.

177. Wada, M., A. Shimada, and T. Fujita, *Functional characterization of Na+-coupled citrate transporter NaC2/NaCT expressed in primary cultures of neurons from mouse cerebral cortex.* Brain Res, 2006. **1081**(1): p. 92.

178. Baslow, M.H. and S. Yamada, *Identification of N-acetylaspartate in the lens of the vertebrate eye: a new model for the investigation of the function of N-acetylated amino acids in vertebrates.* Exp Eye Res, 1997. **64**(2): p. 283.

179. Benuck, M. and A.F. D'Adamo, Jr., *Acetyl transport mechanisms. Metabolism of N-acetyl-L-aspartic acid in the non-nervous tissues of the rat.* Biochim Biophys Acta, 1968. **152**(3): p. 611.

180. Burri, R., C. Steffen, and N. Herschkowitz, *N-acetyl-L-aspartate is a major source of acetyl groups for lipid synthesis during rat brain development.* Dev Neurosci, 1991. **13**(6): p. 403.

181. Sager, T.N., A. Fink-Jensen, and A.J. Hansen, *Transient elevation of interstitial N-acetylaspartate in reversible global brain ischemia.* J Neurochem, 1997. **68**(2): p. 675.

182. Clark, J.B., *N-acetyl aspartate: a marker for neuronal loss or mitochondrial dysfunction.* Dev Neurosci, 1998. **20**(4-5): p. 271.

183. Taylor, D.L., et al., *Investigation into the role of N-acetylaspartate in cerebral osmoregulation.* J Neurochem, 1995. **65**(1): p. 275.

184. Matalon, R. and K. Michals-Matalon, *Biochemistry and molecular biology of Canavan disease.* Neurochem Res, 1999. **24**(4): p. 507.

185. Tezel, G., *Oxidative stress in glaucomatous neurodegeneration: mechanisms and consequences.* Prog Retin Eye Res, 2006. **25**(5): p. 490.

186. Yu, A.L., et al., *Effects of oxidative stress in trabecular meshwork cells are reduced by prostaglandin analogues.* Invest Ophthalmol Vis Sci, 2008. **49**(11): p. 4872.

187. Finkel, T. and N.J. Holbrook, *Oxidants, oxidative stress and the biology of ageing.* Nature, 2000. **408**(6809): p. 239.

188. Starkov, A.A., et al., *Mitochondrial alpha-ketoglutarate dehydrogenase complex generates reactive oxygen species.* J Neurosci, 2004. **24**(36): p. 7779.

189. Zhou, L., Y. Li, and B.Y. Yue, *Oxidative stress affects cytoskeletal structure and cell-matrix interactions in cells from an ocular tissue: the trabecular meshwork.* J Cell Physiol, 1999. **180**(2): p. 182.

190. Kahn, M.G., F.J. Giblin, and D.L. Epstein, *Glutathione in calf trabecular meshwork and its relation to aqueous humor outflow facility.* Invest Ophthalmol Vis Sci, 1983. **24**(9): p. 1283.

191. Izzotti, A., et al., *Oxidative deoxyribonucleic acid damage in the eyes of glaucoma patients.* Am J Med, 2003. **114**(8): p. 638.

192. Giblin, F.J. and J.P. McCready, *The effect of inhibition of glutathione reductase on the detoxification of H2O2 by rabbit lens.* Invest Ophthalmol Vis Sci, 1983. **24**(1): p. 113.

193. Richer, S.P. and R.C. Rose, *Water soluble antioxidants in mammalian aqueous humor: interaction with UV B and hydrogen peroxide.* Vision Res, 1998. **38**(19): p. 2881.

194. Hanashima, C. and H. Namiki, *Reduced viability of vascular endothelial cells by high concentration of ascorbic acid in vitreous humor.* Cell Biol Int, 1999. **23**(4): p. 287.

195. Brubaker, R.F., et al., *Ascorbic acid content of human corneal epithelium.* Invest Ophthalmol Vis Sci, 2000. **41**(7): p. 1681.

196. Ballatori, N. and W.J. Dutczak, *Identification and characterization of high and low affinity transport systems for reduced glutathione in liver cell canalicular membranes.* J Biol Chem, 1994. **269**(31): p. 19731.

197. Lash, L.H. and D.P. Jones, *Uptake of the glutathione conjugate S-(1,2-dichlorovinyl)glutathione by renal basal-lateral membrane vesicles and isolated kidney cells.* Mol Pharmacol, 1985. **28**(3): p. 278.

198. Inoue, M., S. Shinozuka, and Y. Morino, *Mechanism of renal peritubular extraction of plasma glutathione. The catalytic activity of contralumenal gamma-glutamyltransferase is prerequisite to the apparent peritubular extraction of plasma glutathione.* Eur J Biochem, 1986. **157**(3): p. 605.

199. Pajor, A.M., *Sodium-coupled transporters for Krebs cycle intermediates.* Annu Rev Physiol, 1999. **61**: p. 663.

200. Soga, T., et al., *Differential metabolomics reveals ophthalmic acid as an oxidative stress biomarker indicating hepatic glutathione consumption.* J Biol Chem, 2006. **281**(24): p. 16768.

201. Orlowski, M. and S. Wilk, *Synthesis of ophthalmic acid in liver and kidney in vivo.* Biochem J, 1978. **170**(2): p. 415.

202. Ferguson, J.G., Jr. and E.L. Hicks, *Rieger's anomaly and glaucoma associated with partial trisomy 16q. Case report.* Arch Ophthalmol, 1987. **105**(3): p. 323.

203. Pal, B., et al., *A new phenotype of recessively inherited foveal hypoplasia and anterior segment dysgenesis maps to a locus on chromosome 16q23.2-24.2.* J Med Genet, 2004. **41**(10): p. 772.

204. Chen, H.B., et al., *Identification of phosphatases for Smad in the BMP/DPP pathway.* Genes Dev, 2006. **20**(6): p. 648.

205. Huang, B., et al., *Isoenzymes of pyruvate dehydrogenase phosphatase. DNA-derived amino acid sequences, expression, and regulation.* J Biol Chem, 1998. **273**(28): p. 17680.

206. Teague, W.M., et al., *Purification and properties of pyruvate dehydrogenase phosphatase from bovine heart and kidney.* Biochemistry, 1982. **21**(22): p. 5585.

207. Pettit, F.H., T.E. Roche, and L.J. Reed, *Function of calcium ions in pyruvate dehydrogenase phosphatase activity.* Biochem Biophys Res Commun, 1972. **49**(2): p. 563.

208. Linn, T.C., F.H. Pettit, and L.J. Reed, *Alpha-keto acid dehydrogenase complexes. X. Regulation of the activity of the pyruvate dehydrogenase complex from beef kidney mitochondria by phosphorylation and dephosphorylation.* Proc Natl Acad Sci U S A, 1969. **62**(1): p. 234.

209. Korotchkina, L.G. and M.S. Patel, *Mutagenesis studies of the phosphorylation sites of recombinant human pyruvate dehydrogenase. Site-specific regulation.* J Biol Chem, 1995. **270**(24): p. 14297.

210. Sugden, P.H. and P.J. Randle, *Regulation of pig heart pyruvate dehydrogenase by phosphorylation. Studies on the subunit and phosphorylation stoicheiometries.* Biochem J, 1978. **173**(2): p. 659.

211. Willcox, P., *Secretion of beta-N-acetylglucosaminidase isoenzymes by normal human fibroblasts.* Biochem J, 1978. **173**(2): p. 433.

212. Wu, P., et al., *Mechanism responsible for inactivation of skeletal muscle pyruvate dehydrogenase complex in starvation and diabetes.* Diabetes, 1999. **48**(8): p. 1593.

213. Wu, P., et al., *Starvation and diabetes increase the amount of pyruvate dehydrogenase kinase isoenzyme 4 in rat heart.* Biochem J, 1998. **329 (Pt 1)**: p. 197.

214. Wu, P., et al., *Starvation increases the amount of pyruvate dehydrogenase kinase in several mammalian tissues.* Arch Biochem Biophys, 2000. **381**(1): p. 1.

215. Sugden, M.C., et al., *Fibre-type specific modification of the activity and regulation of skeletal muscle pyruvate dehydrogenase kinase (PDK) by prolonged starvation and refeeding is associated with targeted regulation of PDK isoenzyme 4 expression.* Biochem J, 2000. **346 Pt 3**: p. 651.

216. Huang, B., et al., *Starvation and diabetes reduce the amount of pyruvate dehydrogenase phosphatase in rat heart and kidney.* Diabetes, 2003. **52**(6): p. 1371.

217. Galkin, A. and U. Brandt, *Superoxide radical formation by pure complex I (NADH:ubiquinone oxidoreductase) from Yarrowia lipolytica.* J Biol Chem, 2005. **280**(34): p. 30129.

218. Martens, G.A., et al., *Glucose suppresses superoxide generation in metabolically responsive pancreatic beta cells.* J Biol Chem, 2005. **280**(21): p. 20389.

219. Liu, Y., G. Fiskum, and D. Schubert, *Generation of reactive oxygen species by the mitochondrial electron transport chain.* J Neurochem, 2002. **80**(5): p. 780.

220. Kudin, A.P., et al., *Characterization of superoxide-producing sites in isolated brain mitochondria.* J Biol Chem, 2004. **279**(6): p. 4127.

221. Green, K., *Free radicals and aging of anterior segment tissues of the eye: a hypothesis.* Ophthalmic Res, 1995. **27 Suppl 1**: p. 143.

222. Ringvold, A., E. Anderssen, and I. Kjonniksen, *Distribution of ascorbate in the anterior bovine eye.* Invest Ophthalmol Vis Sci, 2000. **41**(1): p. 20.

223. Costarides, A.P., M.V. Riley, and K. Green, *Roles of catalase and the glutathione redox cycle in the regulation of anterior-chamber hydrogen peroxide.* Ophthalmic Res, 1991. **23**(5): p. 284.

224. Kamata, H. and H. Hirata, *Redox regulation of cellular signalling.* Cell Signal, 1999. **11**(1): p. 1.

225. Mittag, T.W., et al., *Retinal damage after 3 to 4 months of elevated intraocular pressure in a rat glaucoma model.* Invest Ophthalmol Vis Sci, 2000. **41**(11): p. 3451.

226. Tatton, W.G., et al., *Maintaining mitochondrial membrane impermeability. an opportunity for new therapy in glaucoma?* Surv Ophthalmol, 2001. **45 Suppl 3**: p. S277.

227. Chen, J.Z. and F.F. Kadlubar, *A new clue to glaucoma pathogenesis.* Am J Med, 2003. **114**(8): p. 697.

228. Davies, K.J., *Degradation of oxidized proteins by the 20S proteasome.* Biochimie, 2001. **83**(3-4): p. 301.

229. Poppek, D. and T. Grune, *Proteasomal defense of oxidative protein modifications.* Antioxid Redox Signal, 2006. **8**(1-2): p. 173.

230. Berlett, B.S. and E.R. Stadtman, *Protein oxidation in aging, disease, and oxidative stress.* J Biol Chem, 1997. **272**(33): p. 20313.

231. Dean, R.T., et al., *Biochemistry and pathology of radical-mediated protein oxidation.* Biochem J, 1997. **324 (Pt 1)**: p. 1.

232. Bonne, C., A. Muller, and M. Villain, *Free radicals in retinal ischemia.* Gen Pharmacol, 1998. **30**(3): p. 275.

233. Aslan, M., et al., *Nitrotyrosine formation and apoptosis in rat models of ocular injury.* Free Radic Res, 2006. **40**(2): p. 147.

234. Chiu, D.S., et al., *High-density lipoprotein-binding protein (HBP)/vigilin is expressed in human atherosclerotic lesions and colocalizes with apolipoprotein E.* Arterioscler Thromb Vasc Biol, 1997. **17**(11): p. 2350.

Appendix A: Composition of reagents used

Morpholinopropanesulfonic acid (10x MOPS)
- 0.22M MOPS
- 3.0M NaOAc
- 0.5M EDTA
- Adjust the pH to 7.0 (with NaOH).

PBS (Phosphate-Buffered Saline)
- 9.1mM Na_2PO_4
- 1.7mM NaH_2PO_4
- 150mM NaCl
- Raise pH to 7.4 with 5N NaOH

Tris-buffered saline, tween (TBST)
- 10mM Tris pH 7.5
- 0.9% NaCl (75mM)
- 0.05% Tween 20

Lysis Buffer A
- 1M HEPES, pH 7.9
- 1M MgCl2
- 1M KCl
- 1M DTT
- 0.1M PMSF

Lysis Buffer C
- 1M HEPES, pH 7.9
- 25% glycerol
- 5M NaCl
- 1M MgCl2
- 0.5M EDTA
- 1M DTT
- 0.1M PMSF